A STUDY OF FIBERGLASS-REINFORCED PLASTIC FOR REINFORCING CONCRETE BRIDGE DECKS

by

Peter A. Allen

Thesis submitted to the Faculty of the

Virginia Polytechnic Institute and State University

in partial fulfillment of the requirements for the degree of

MASTER OF SCIENCE

in

Civil Engineering

APPROVED:

Richard M. Barker, Chairman

Thomas M. Murray

Don A. Garst

April, 1995
Blacksburg, VA

Keywords: FRP, Fiberglass-reinforced plastic, reinforced concrete, bridges

.2

A STUDY OF FIBERGLASS-REINFORCED PLASTIC FOR REINFORCING CONCRETE BRIDGE DECKS

by

Peter A. Allen

Richard M. Barker, Chairman

Civil Engineering

(ABSTRACT)

Deterioration of reinforced concrete bridge decks has gained widespread public attention and concern in recent years. Much of the damage can be attributed to corrosion of steel reinforcing bars. Numerous solutions have been suggested, one of which is the replacement of steel with a non-corroding reinforcement, such as fiberglass-reinforced plastic materials.

Much of the current research focuses on the applicability of FRP as the main tensile reinforcement in the slab. The nature of FRP presents many obstacles to its use in this capacity. This investigation aims to capitalize on the strengths of both steel and FRP by combining them. Traditional steel rebar should be used where it will provide strength and ductility to the deck--in the bottom layer of reinforcement. The FRP is placed where it will provide strength and non-corroding reinforcement where it is needed: the top layer. Recent research has shown that minimal negative moment is created over supports in bridge decks, suggesting that the use of the non-ductile FRP as the top reinforcement would not be detrimental.

A review of prior and current research in this area was conducted. Based on this information, four different FRP reinforcing materials were obtained. Simple-beam test specimens were designed and built. The procedure is described, and experimental results are presented and analyzed. Conclusions are drawn and recommendations for future work are outlined. This investigation provides first-hand data on the behavior of FRP reinforced concrete and will serve as the basis for future work.

ACKNOWLEDGMENTS

I would like to thank Dr. Richard Barker for providing the initiative for this study, as well as for his support and guidance. I thank Dr. Thomas Murray and Prof. Don Garst for serving on my thesis committee.

I give credit to Dr. Richard Weyers for formulating the steel-and-FRP deck concept, the basis for this work.

I am grateful to Dr. David Kibler, Dr. William Knocke, and the Charles Edward Via, Jr. Department of Civil Engineering for funding this project.

I owe special thanks to lab technicians Brett Farmer and Dennis Huffman for going out of their way to lend a hand, as well as to all the graduate students who helped with the project, especially Jeff Borgsmiller, Keith Grubb, Brandon Rossetti and Emmett Sumner, for their help, humor and friendship.

Finally, I am forever indebted to my parents and family. Without their unwavering love, support and encouragement, none of this would be possible.

CONTENTS

LIST OF FIGURES

LIST OF TABLES

NOTATION

A_b	=	area of reinforcing bar
A_f	=	area of fiberglass strands
A_s	=	area of steel reinforcement
A_r	=	total area of reinforcement
A_{rb}	=	area of reinforcement causing balanced failure
a	=	depth of equivalent rectangular stress block
a_1	=	distance from load point to support
b_1	=	distance between load points
b_w	=	width of beam
d	=	distance from extreme compression fiber to centroid of reinforcement
E_c	=	concrete modulus of elasticity
E_r	=	reinforcement modulus of elasticity
F	=	applied tensile force for calibration
f_c'	=	compressive strength of concrete
f_r	=	modulus of rupture of concrete
f_{ult}	=	ultimate strength of reinforcing
f_y	=	yield strength of reinforcing
I	=	moment of inertia
I_{cr}	=	moment of inertia, cracked transformed section
I_{eff}	=	effective moment of inertia
I_g	=	moment of inertia, gross section
L	=	span of test beam
M	=	moment in beam
M_a	=	applied moment at stage deflection being calculated
M_{cr}	=	moment causing first cracking
M_n	=	nominal moment capacity of section

P	=	applied load on test beam
P_{cr}	=	applied load causing first cracking
P_{ult}	=	ultimate applied load
V_c	=	shear strength provided by concrete
y_t	=	distance from centroidal axis of section to extreme tension fiber
Δ	=	centerline vertical displacement of beam
Δ_{max}	=	centerline deflection at ultimate load
β_1	=	compression block factor
ε	=	measured strain
ε_{cu}	=	ultimate strain in concrete
ε_{ry}	=	yield strain in reinforcement
σ	=	stress

CHAPTER 1

INTRODUCTION

1.1 Background

In recent years it has become more evident that reinforcing bars in concrete bridge decks are subjected to extremely corrosive conditions. Corrosion of the steel reinforcement causes damage to the surrounding concrete, which results in spalling and damage to the road surface, and eventually weakens the structure. There has been increasing public and professional awareness and concern over the condition of bridges in this country, spurring investigators to find solutions.

Epoxy-coated steel had been thought to provide a non-corrosive reinforcement with the same strength properties as normal steel. However, recent experience indicates that the epoxy might not be as ideal a protection as once thought. This has forced engineers to continue working on new methods of solving the corrosion problem.

Some engineers suggest that bridge deck slabs rarely generate any significant negative moment over the girders. This is based on the realization that the girders deflect and do not provide the rigid support assumed in conventional design. As a result, a reduction in top steel--the reinforcement most susceptible to corrosion and damage--is possible. A three-span reinforced concrete bridge constructed recently in Colorado contains no top steel in one span (ENR 1994).

Removing the top steel is one way to prevent corrosion damage. A less drastic method is to replace the steel with a reinforcing material that will not corrode, such as fiberglass-reinforced plastic (FRP). The FRP would provide reinforcement in the event negative moment is produced, in addition to serving as shrinkage and temperature crack control. Because the risk of the bottom steel corroding is minimal, it may be left as normal. This steel-FRP combination provides the two properties required in a bridge deck. The steel contributes the strength, ductility and stiffness needed to make the

structure work, while the FRP provides some strength and prevents damage to the concrete. Figure 1.1 shows a proposed reinforcing plan for such a deck.

Research is progressing into the use of FRP materials as reinforcement for concrete. Results to date indicate that the technology holds promise, though much needs to be done before it is widely accepted. Studies are focusing on two aspects of FRP reinforcing: its corrosion resistance and its physical performance in concrete. Investigation into physical behavior as a reinforcement includes examination of ductility, bond and anchorage, crack control, failure mechanisms and design procedures.

1.2 Objectives

Investigating the behavior of fiberglass-reinforced plastic materials as reinforcement for concrete is the primary focus of this study, with two main objectives within this focus.

The first goal is to investigate several different FRP materials as reinforcement. Performance criteria examined include their performance in terms of load-deflection response, cracking behavior, failure modes and ultimate load capacity.

The second objective is to provide a basis for future work at Virginia Tech. This study intends to determine which, if any, of the materials demonstrate promise and warrant further investigation. Recommendations for future work in this area are offered.

1.3 Scope

The first objective of this study is to investigate the behavior of several different FRP materials as reinforcement for concrete. To accomplish this, concrete beams with four different FRP reinforcing arrangements were constructed and tested. Investigation and comparison were based on several criteria, including load-deflection response, cracking behavior, failure modes and ultimate load capacity.

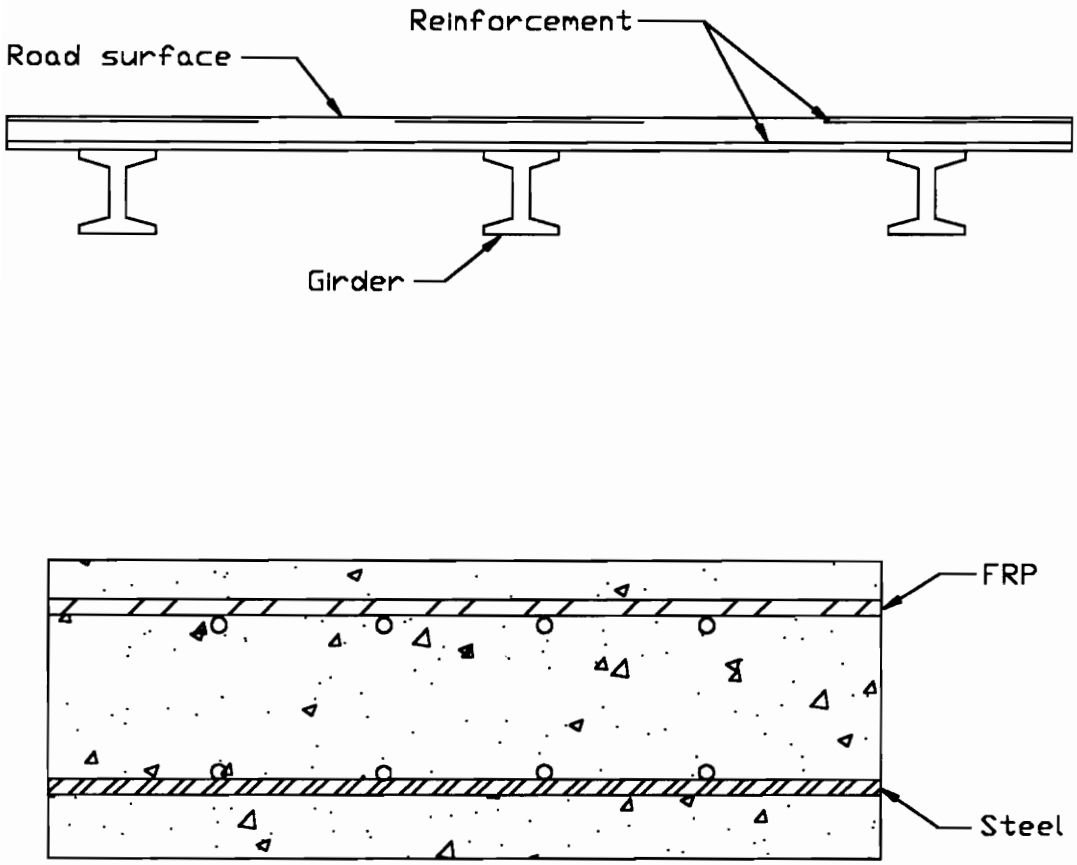

Figure 1.1 Bridge Deck Incorporating Steel and FRP Reinforcement

The reinforcements used in this investigation are described in detail in Chapter 3. They are: mild steel bars, FRP bars, Duragrid pultruded FRP grating (two different bar spacings), and Multigrid molded FRP grid.

Presented in Chapter 4 is information on the construction and testing of ten rectangular concrete beams, 7.25 in. by 12 in. by 4 ft. A single layer of tensile reinforcement was used in each specimen, with two specimens built for each type of reinforcement. One set of specimens was tested under monotonic load, the second set was loaded cyclically.

Data and observations from the experiments are presented in Chapter 5. These results are compared in Chapter 6 with prediction methods developed by others for the design of reinforced concrete: ACI 318-89 for steel reinforcement, GangaRao and Faza (1991) for FRP bars, and Bank (1993) for pultruded gratings.

Comparisons between each type of reinforcement are also made in Chapter 6. The performance of the steel reinforced beams is considered the standard against which the others are measured. Qualitative comparisons are made with the work of others. General trends and observations are noted and compared.

Conclusions, based on the test observations and comparisons with others, are made in Chapter 7. The project is summarized and recommendations for future work are presented.

CHAPTER 2

BACKGROUND INFORMATION

Much previous work has been done into the use of fiberglass materials for the reinforcement of concrete. The research has been diverse, with projects focusing on several aspects of this new application. In this chapter, some brief background information about the technology is provided, along with a brief summary and description of the work that most influenced this project.

2.1 Historical Background

Investigation into the use of fiberglass-reinforced plastic materials as reinforcement for concrete began mainly because of FRP's high tensile strength and resistance to corrosion. In recent years, there has been renewed interest in this alternative material, primarily due to increasing awareness of the fallibility of steel reinforcing bars, specifically in bridge decks and other damaging environments.

At first, researchers concentrated on finding better methods for protecting the steel bars from corrosive elements, using sealers, membranes, epoxy-coating and increased concrete cover. Recently, however, more investigation has been done into fixing the root of the corrosion problem--the steel itself (Bedard 1992).

Among the first to test concrete reinforced with FRP bars was Edward Nawy, at Rutgers University. In flexure tests, he found that, due to the low modulus of elasticity of FRP, failure was governed by crushing of the concrete. The FRP reinforced beams also tended to deflect several times more than similar steel-reinforced beams (Nawy et al. 1971). These findings demonstrate two of the major drawbacks of FRP reinforcement--lack of ductility and excessive deflections.

In 1991, researchers at West Virginia University completed an extensive investigation into the use of FRP reinforcing bars in concrete bridge decks. They

examined both the flexural behavior and the bond strength of the bars. Their objectives were to study the feasibility of FRP bar reinforcement and develop design equations (GangaRao and Faza 1991).

FRP bars are primarily an attempt to replace steel bars with non-corroding look-alike bars. This may not, however, represent the optimal use of fiberglass materials as reinforcement. A better idea might be a configuration which capitalizes on the material and manufacturing characteristics of fiberglass-plastic composites (Tarricone 1993). The use of molded and pultruded fiberglass gratings has been the result of this thinking. The gratings are typically manufactured for walkways and platforms, but are easily adapted for use as reinforcing.

The gratings are arranged as a grid of bars, providing reinforcement in both directions and eliminating the need for on-site arranging and tying of bars. Tests have shown that the grid provides a mechanical bond with the concrete. The grating bars can be formed in engineered shapes, such as an I or T shape, which improves their flexural strength.

Lawrence Bank (1991, 1992, 1993) and Charles Goodspeed (1990, 1991) are leaders in research into the use of FRP gratings as reinforcement. They have experimented with numerous types, sizes and arrangements of gratings. Goodspeed, at the University of New Hampshire, has concentrated on the use of NEFMAC, an FRP composite grid made of layers of fiber and resin laminated together. Bank, working at Catholic University, experimented mainly with FRP gratings manufactured as walkways and platforms. Both started with preliminary small-scale projects and then moved to larger full-scale experiments.

The sections which follow describe previous research performed on the two types of FRP reinforcement--bars and grids. The literature review focuses on the work of the researchers mentioned above, especially those investigations which applied directly to this study or assisted in the formulation of this project.

2.2 Fiberglass-Reinforced Plastic Bars

Fiberglass-reinforced plastic bars have an appearance and shape similar to steel reinforcing bars. They are made of fiberglass strands imbedded in a vinylester or isophthalic resin. The bars are formed by pultrusion (pulling through a die), with an additional band of fiberglass wrapped helically around the bar to deform the surface and provide better bond when placed in concrete. High tensile strength (at least 100 ksi), low elastic modulus (7000 ksi), light weight, chemical resistance and non-conductivity are typical characteristics of FRP materials (GangaRao and Faza 1991).

Nawy's research into the use of FRP reinforcement, as previously stated, revealed some of the weaknesses of the technology, but showed some promise as well. He found that the first cracking load, the ultimate load, and load-deflection behavior could all be accurately predicted for FRP reinforced beams. Therefore, members could be designed so the working load did not exceed the cracking load, and any cracks that developed would be acceptable in width and number. In addition, allowable crack widths for the FRP could be higher, since corrosion should not be of concern (Nawy and Neuwerth 1977).

In general, forces in the FRP bars were well below the bars' ultimate strength when the beams failed, typically due to crushing of the concrete. Deflections were higher than in steel-reinforced beams for a given load, although the fiberglass reinforced beams were capable of larger deflections before failure. As expected, the deflection service limit state was found to control the design of FRP reinforced members.

GangaRao and Faza (1991) explored several aspects of the performance of FRP bars as concrete reinforcement. Of primary concern was the bending and bond behavior, as well as the development of simple, yet practical, design equations. Their investigation reflected many of the same trends found by others.

In addition to those findings, they concluded that the use of high strength concrete (7-10 ksi) is "essential" to taking full advantage of the high strength of FRP materials. With normal strength concrete (4-6 ksi), the concrete tends to crush long before the FRP

bars reach their ultimate capacity. To reduce the limiting effect of the concrete and utilize more of the available FRP capacity, high strength concrete is needed.

GangaRao and Faza (1991) worked to develop equations to assist in the design of FRP bar reinforced concrete members. They recognized that current deflection prediction equations, developed for steel reinforced members and based on an effective moment of inertia, did not properly account for the behavior of the fiberglass materials. A modified equation was proposed, combining the cracked and effective moments of inertia. Further details on this equation and its application are discussed in Section 4.5.3 of this paper.

2.3 Fiberglass-Reinforced Plastic Gratings

Molded and pultruded gratings are another form of fiberglass-reinforced plastic for the reinforcement of concrete. These gratings, manufactured for use as walkways, have been tested as an alternative to reinforcing bars. The gratings are readily available from several sources, can have variable bar spacings, and are easy to handle. They are lightweight and provide reinforcement in both longitudinal and transverse directions, reducing on-site labor (Bank 1991). Disadvantages include price, FRP's general lack of ductility, and a shortage of performance data.

Some general trends can be observed from the work of Bank (1992, 1993) and Goodspeed (1991). Failure of test members was typically caused by either concrete crushing or flexural shear. In most of the tests, horizontal cracking and delamination along the level of the grating was noted. Bank reported that deflections of grating reinforced slabs tended to be about than twice those of steel reinforced slabs, but still close to calculated values. Ultimate load capacities were significantly more than the service load and greater than the load which caused yielding in the steel, the typical limit state for reinforced concrete.

Goodspeed performed a preliminary investigation of the flexure strength of concrete beams reinforced with a fiberglass grid material called NEFMAC. Though this grid material is somewhat different than the pultruded and molded gratings used by Bank,

the results followed the same general trends: failure was controlled by crushing of the concrete, the beams showed little ductility, and predictions were close, but not conservative (Goodspeed 1990).

To investigate the effect of repetitive loading on the FRP reinforced beams, Goodspeed (1991) performed "cyclic" loading tests, in which beams were loaded repetitively to several load levels. The performance of the FRP reinforced members was comparable to similarly loaded steel reinforced beams. The propagation of cracks stopped after "relatively few" cycles, and the amount of increased deflection tended to decrease asymptotically with each additional load cycle. Overall, Goodspeed reported that the performance of the cyclically loaded beams varied only slightly from monotonically loaded beams.

Bank (1991) performed pilot tests on slabs reinforced with several different grid types, both molded and pultruded. As expected with FRP materials, Bank concluded that slabs reinforced with the gratings tended to achieve the same strength as steel reinforced slabs, though the stiffness was less. To equal the stiffness of steel, gratings with deeper bars and closer bar spacing would be needed.

Bank (1992) continued his research with simple-span slabs designed to meet 1989 AASHTO specifications. Reinforcement was provided by a single pultruded grating. Several slabs were loaded cyclically, and verified that deflection growth slowed with repeated cycles, as reported previously by Goodspeed (1991). Little change in the ultimate strength or stiffness due to the cyclic loading was reported.

The behavior of doubly-reinforced, two-span slabs was investigated by Bank (1993). The objectives of the study included the investigation of the performance of such slabs in double curvature, the performance of the gratings in compression areas, post-peak load capacity, and the feasibility of fabrication of slabs reinforced with two grating layers.

Shear failures controlled for all the test slabs. Bank compared the shear crack patterns and the post-peak behavior of the grating reinforced slabs to steel reinforced slabs. The steel reinforced slab failed suddenly, and was a "typical flexural-shear failure"

with a large crack extending from a load point to a support. At failure, the slab lost all load carrying capacity.

The grating reinforced slab failures, though also in shear, were foreshadowed by cracking noises as the load neared ultimate. Cracking at failure was concentrated in the space between the grating layers, and propagated horizontally along the level of the gratings. After this failure, the slabs continued to support about half of the ultimate load, though deflections increased significantly.

Experimental results were close to the predicted failure loads, while observed shear capacities exceeded calculated values. Bank concluded that the fiberglass gratings contributed to the shear strength of the slabs and that the stiffness of the slab depended largely on the flexure modulus of the grating. In these tests, the total depth of grating (4 in.) was nearly one-half the depth of the slab (8.5 in.).

An accurate determination of the modulus is important because slabs with fiberglass gratings need to be designed to meet deflection requirements. Bank (1993) performed flexural and tensile tests on the gratings in order to determine a modulus. In the flexure tests, the gratings are subjected to both tension and compression, while the tensile specimens are only in tension. The two tests usually give different results for the elastic modulus. When the gratings are used as reinforcement, however, they may be completely in tension, completely in compression, or a combination of the two. Therefore, the selection of the proper modulus is difficult.

Goodspeed (1990) noted a difference in bond behavior between steel bars and fiberglass gratings. Steel reinforced members typically transfer force from the concrete to the steel through a continuous, uniformly developed bond along the entire length of the bar, due to the bar's surface deformations. The gratings have no such surface deformations through which to interlock with the concrete and allow transfer of force. As a result, the grids must transfer force through bearing on a series of transverse bars. This may explain why crack locations in grating reinforced members tend to correspond with the locations of transverse bars.

CHAPTER 3

MATERIAL PROPERTIES

In this study, five different reinforcements were examined. Two concrete beams were constructed with each reinforcing material, for a total of ten test specimens. Traditional mild steel reinforcing bars were used as the control. Four different configurations of fiberglass reinforcement were used: fiberglass-reinforced plastic bars, pultruded fiberglass gratings (two different bar spacings) and a molded fiberglass grid.

The sections below describe each reinforcement in detail. Material properties, obtained either from laboratory tests or from manufacturer's data, are summarized in Table 3.1. Details on the data source for each material are found in the corresponding section. Properties of the concrete used are also presented.

Table 3.1 Reinforcement Properties

Material	f_y (ksi)	f_{ult} (ksi)	E - tension (ksi)	Bar area (in^2)	I (in^4)
#4 Steel	92	147	29000	0.20	--
#4 FRP	86	107	6500	0.20	--
Duragrid 1" I-bar	--	70	5000	0.31	0.041
Multigrid	--	17	2000	0.12	0.0031

3.1 Steel Bars

The mild steel bars (not epoxy coated) were acquired from a local hardware store. The four-foot long pieces for the test specimens were all cut from the same 20 ft bar. Tensile tests were performed on two full-section samples of the bar, as per ASTM A370, A9.2.1. Table 3.1 lists the average yield and ultimate strengths of the samples. Although the steel bars were expected to be Grade 60, with a yield strength of 60 ksi, the tensile tests showed them to be 50% stronger, with the yield point (0.2 percent offset) above 90

ksi. In addition, the observed stress-strain curve for the bars was not consistent with expected steel behavior. The curve was not bilinear with a well-defined yield point, but instead resembled the curve of high-strength prestressing steel. A stress-strain curve from these tensile tests is provided in Appendix A.

In the test specimens, the main bars were #4 (0.5 in. nominal diameter) at 8 in. with #3 (0.375 in. nominal diameter) transverse bars at approximately 10 in. spacing. Each beam contained two #4 bars (0.4 in^2 total cross-sectional area) and four #3 bars. Figure 3.1 shows the bar layout for the steel reinforced beams.

3.2 Fiberglass-Reinforced Plastic Bars

Two tests were run with fiberglass-reinforced plastic (FRP) reinforcing bars. These bars were the same nominal size and were arranged the same as the steel bars, allowing for a direct performance comparison between the two materials. Figure 3.2 shows the bar layouts for the FRP bar reinforced beams.

The FRP bars--product name Kodiak--were purchased from International Grating, Inc., Houston, Texas. The bars arrived pre-cut in four-foot lengths, so it was not possible to determine if they were cut from the same main bar. They all varied in appearance, suggesting they were cut from different bars.

The tensile strength of the FRP bars is based on previous research on Kodiak bars by GangaRao and Faza (1991). They recommend testing at least six bar samples to determine the ultimate tensile strength. In the event this is not possible, they provide the results of numerous tensile tests for use in design. These are the numbers presented in Table 3.1. These values were used mainly because only one 4 ft bar was available for tensile tests (no tensile tests were performed). The yield strength is an "effective" yield strength used for design and equal to 80 percent of ultimate, as suggested by GangaRao and Faza. This reduction factor is used to account for variations in manufacturing and to provide a margin of safety because of FRP's lack of a yield plateau.

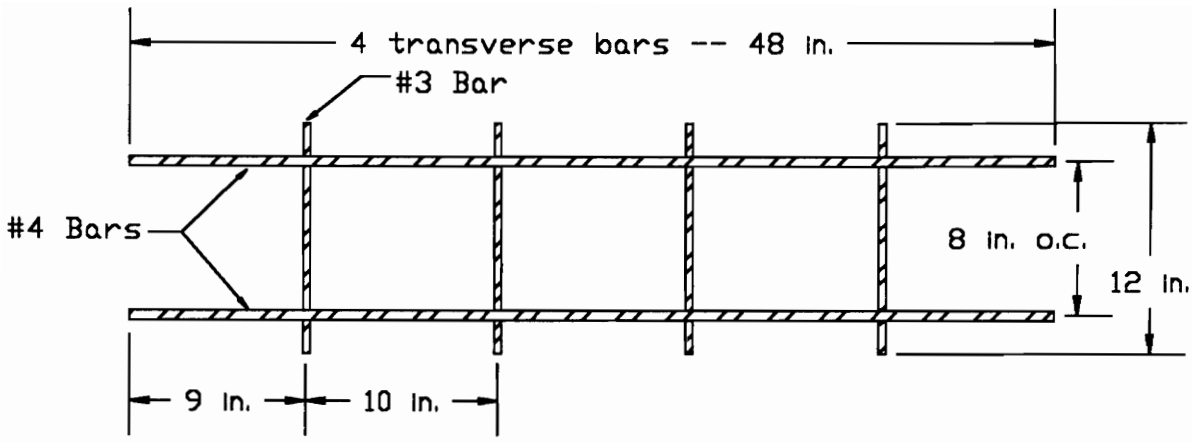

Figure 3.1 Bar Layout for Steel Bar Reinforced Beams

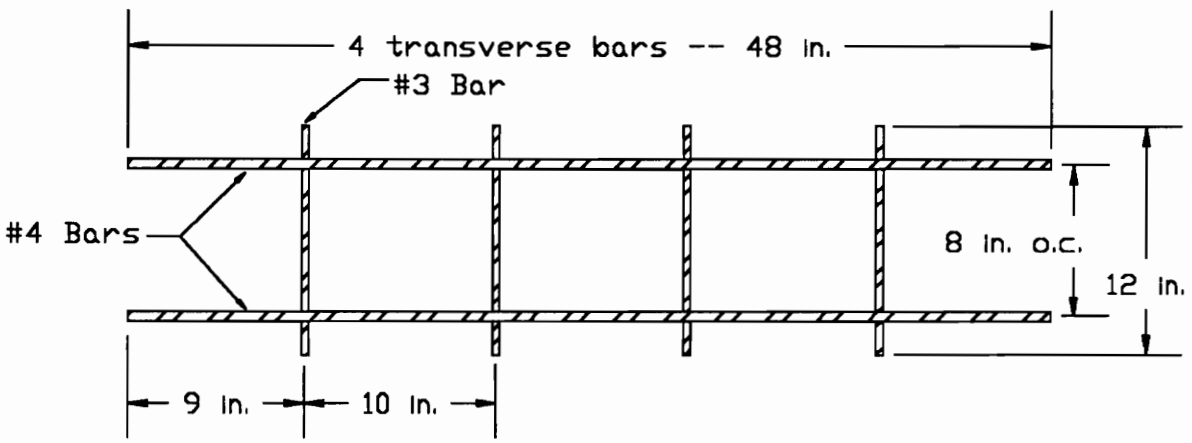

Figure 3.2 Bar Layout for FRP Bar Reinforced Beams

3.3 Pultruded Fiberglass Grating

Pultruded grids are made from individual bars. The resin and glass fibers are pulled through a die which shapes the bars. This allows for different size transverse and main bars. The main bars are typically I- or T-shaped, which adds to their flexural strength. Pultruded gratings have flexible bar spacing, as each bar is formed individually and then built into a grid with the interlocking transverse bars.

Duragrid is a high-strength fiberglass grating produced by the Morrison Molded Fiber Glass (MMFG) Company and purchased from Aligned Fiber Composites, Chatfield, Minnesota. It is designed primarily for use as walkway grating, and is available in a range of sizes and bar arrangements.

Two samples of Duragrid were purchased, one with the main bars at 4.5 in. spacing, the other with the bars at 6 in. Both consisted of 1 in. deep longitudinal I-shaped bearing bars connected into a grid by transverse bars spaced at 6 in., as shown in Fig. 3.3. The grids were cut into 1 ft by 4 ft pieces, with several bars left over for calibration and tensile testing. All of the main bars appeared to be identical.

The beams with the bars spaced at 4.5 in. contained three longitudinal bars (0.93 in^2 total cross-sectional area), while the 6 in. spacing provided two longitudinal bars per beam (0.62 in^2). Both arrangements had eight cross-bars. The bar layouts are shown in Figs. 3.4 and 3.5.

A main-bar tensile strength of 70 ksi was assumed. The modulus of elasticity for the Duragrid bars was calculated by three different methods. Table 3.2 lists the results of these calculations.

Table 3.2 Duragrid Modulus of Elasticity

Source	E (ksi)
Tensile calibration	5000
MMFG Catalog	4880
Flexure test	4500

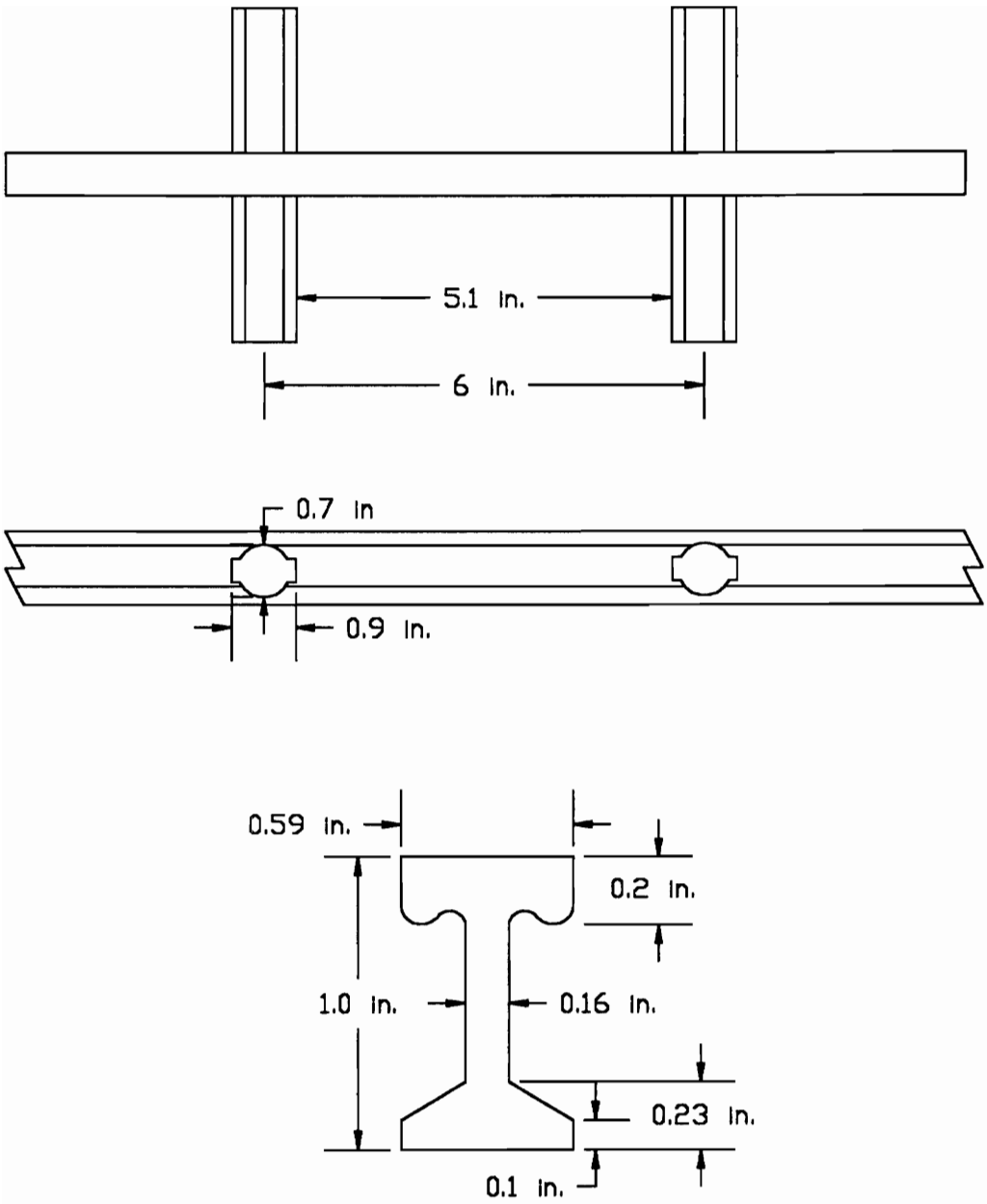

Figure 3.3 Duragrid Grating Dimensions

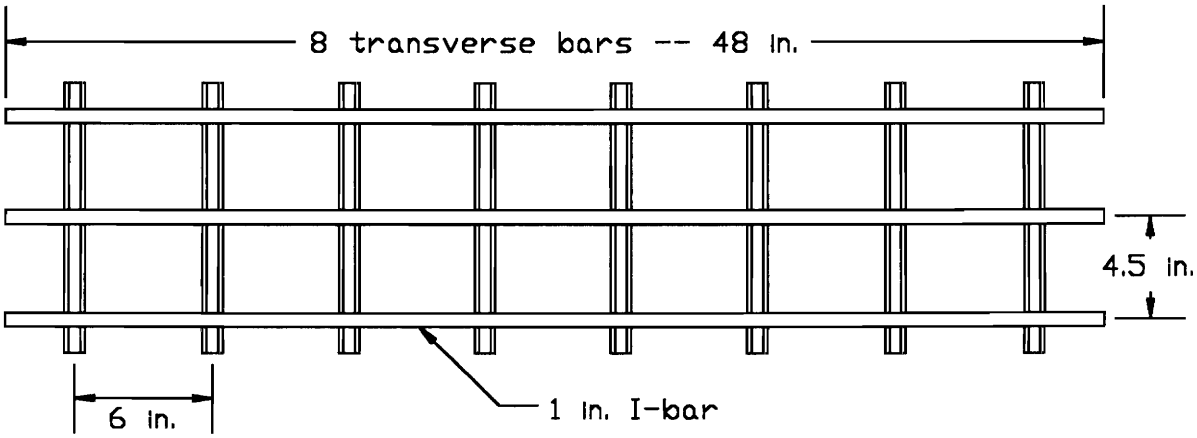

Figure 3.4 Bar Layout for Duragrid (4.5 in.) Reinforced Beams

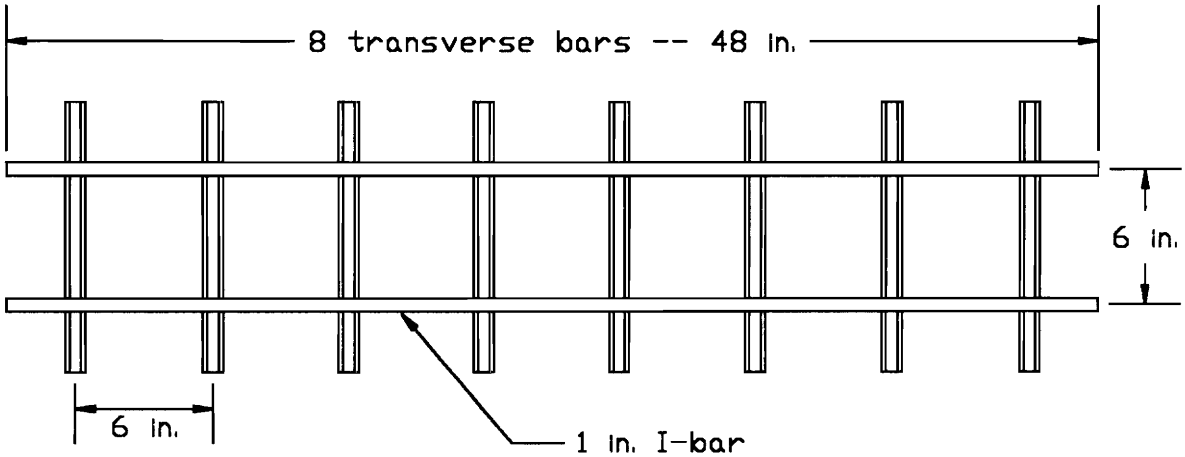

Figure 3.5 Bar Layout for Duragrid (6 in.) Reinforced Beams

First, a modulus was calculated from the load-strain data of the tensile calibrations, as follows:

$$E_r = \frac{\sigma}{\varepsilon} = \frac{F/A_b}{\varepsilon} = \frac{F}{0.31\varepsilon} \tag{3-1}$$

where,

σ = stress = F/A_b

ε = measured strain

E_r = bar modulus of elasticity

F = applied tensile force

A_b = cross-sectional area of bar = 0.31 in^2

Second, MMFG's Duragrid catalog lists values of the modulus of elasticity for various span lengths. The manual states that the modulus is a function of the span length because of the bars' non-homogeneous composition.

Finally, a flexure test was performed on a sample of the grating. MMFG's Design Manual (1989) recommends performing a flexure test to determine the modulus of elasticity of the section, rather than calculating a value from tensile coupons. For the flexure test, a 1 ft by 4 ft piece of Duragrid with two bars at 6 in. spacing was tested in flexure to failure. The span was 42 in., as in the beam tests. Applied load and centerline deflection were measured and a modulus of elasticity calculated. Figure 3.6 shows the flexure test setup.

Because of their I-shape, it is believed that the Duragrid bars act as more than just tensile reinforcing. They may act in bending and tension, thus the behavior of a concrete section reinforced with these bars may not be accurately predicted by normal reinforced concrete equations, which ignore the flexural stiffness of the reinforcement.

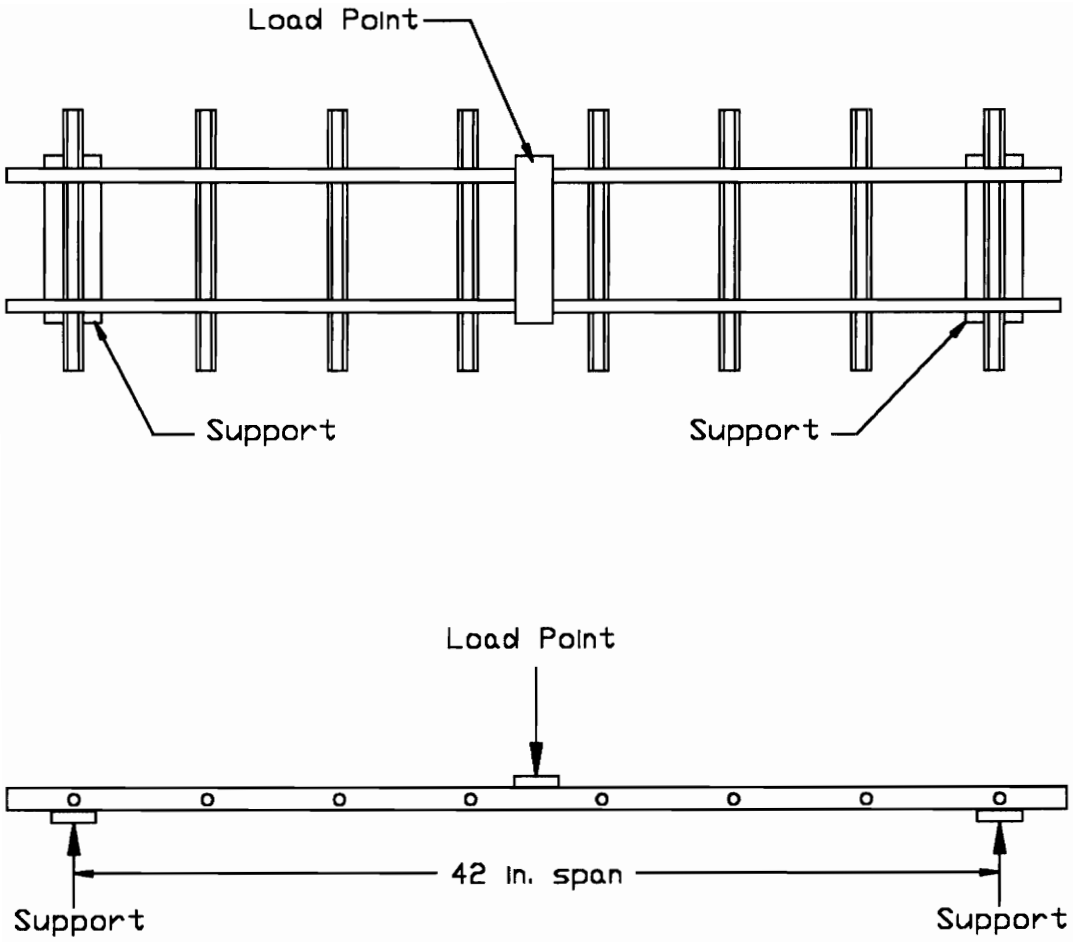

Figure 3.6 Flexure Test Setup for Gratings

3.4 Molded Fiberglass Grid

Molded grids are formed by pouring resin over glass fibers which have been laid out in a mold. Molded grids typically have a pre-set bar size and spacing (based on the mold). Transverse bars and main bars are typically the same size and shape.

McNichols Co., Tampa, Florida, manufactures a "multipurpose all fiberglass screening material" called Multigrid. A single 4 ft by 12 ft panel was purchased from Energy Equipment, Inc. Midlothian, Virginia.

Multigrid is a molded fiberglass-reinforced plastic grid, so it was assumed that all the bars in the grid had the same properties. The material appeared to be uniform in both directions. The manufacturer advertised dimensions of 0.5 in. deep, 0.25 in. wide bars, with a 2 in. square mesh (McNichols 1993). Measured dimensions are shown in Fig. 3.7. The two test beams each contained a single 1 ft by 4 ft piece of the material, as shown in Fig. 3.8. The sections were cut across the width of the 4 ft by 12 ft panel, and provided six longitudinal bars per beam (0.72 in^2 total cross-sectional area).

Molded gratings are formed with the fiberglass strands placed in interlocking layers, as shown in Fig. 3.9. Therefore, the area of strands in tension is not necessarily equal to the total cross-sectional area of the bar. Examination of the tensile specimens indicated that only about 40 percent of the total cross-sectional area contains glass fibers. The remaining area is simply a plastic resin forming the shape of the bars and not contributing any strength. Furthermore, the area of fibers visible is actually a fiber and resin matrix. According to McNichols' description of their molded gratings, this fiber-resin matrix consists of from 35 percent to 65 percent fibers. As a result, only about a quarter of the total cross-sectional area is fiberglass and capable of resisting significant tensile force.

This reasoning was supported by tensile tests of individual bars. The tensile strength of a bar was determined to be 2000 lb, as shown in Table 3.1. Assuming the tensile strength of fiberglass is 100 ksi, the amount of fiberglass (A_f) in a single Multigrid bar can be approximated as:

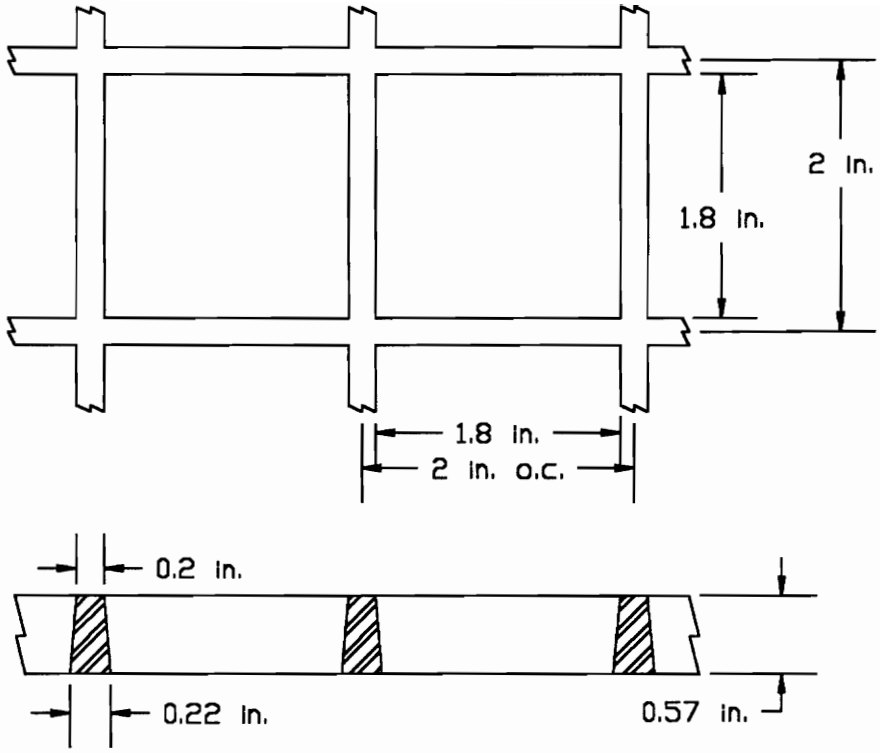

Figure 3.7 Multigrid Grating Dimensions

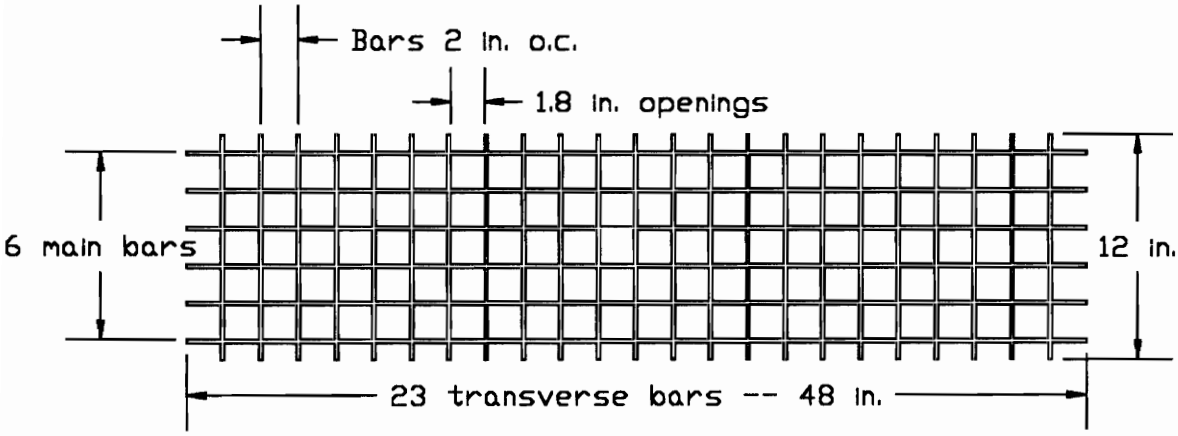

Figure 3.8 Bar Layout for Multigrid Reinforced Beams

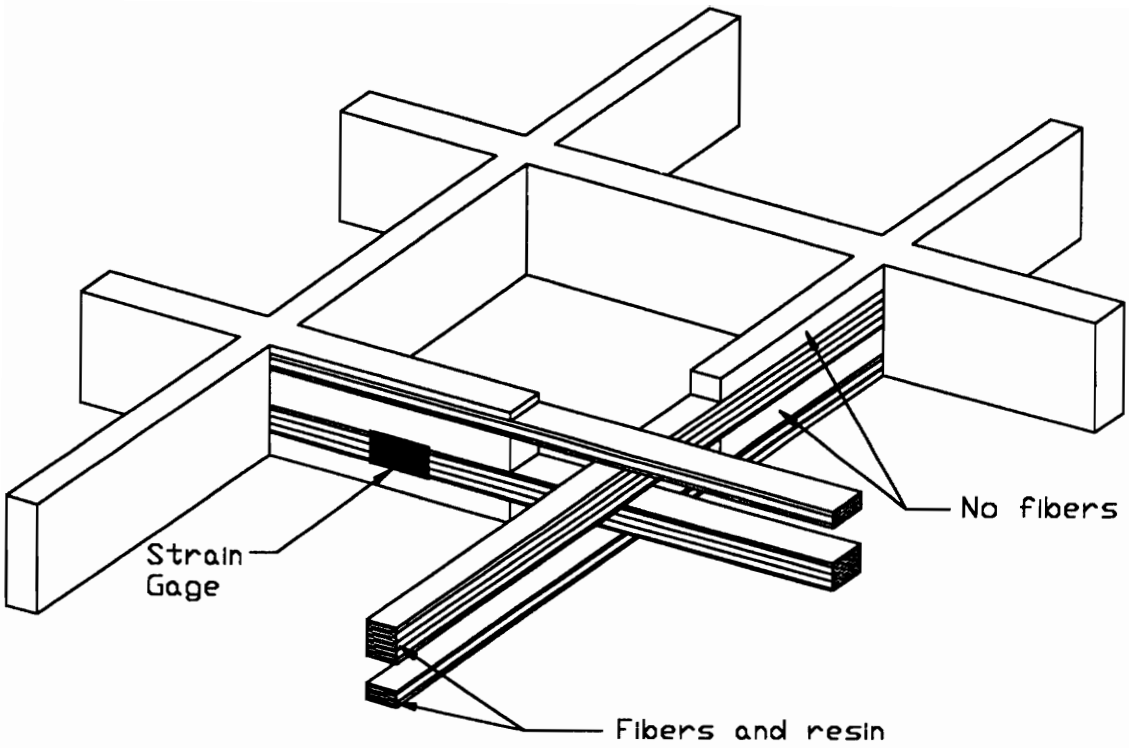

Figure 3.9 Fiberglass Layout in Multigrid Grating

$$A_f = \frac{2 \text{ kips}}{100 \text{ ksi}} = 0.02 \text{ in}^2 \qquad (3\text{-}2)$$

which is about 20 percent of the total cross-sectional area. Tensile specimens were taken from bars in both directions (main and transverse). The tensile tests confirmed the assumption that all of the bars had the same properties and strength.

A modulus of elasticity for the Multigrid was calculated with methods similar to the Duragrid modulus calculations. First, load-strain data from the strain gage calibration was used to determine a modulus value, using Eq. 3.1. A modulus was also determined from a flexure test, performed with the same parameters as the Duragrid test (Fig. 3.6). Table 3.3 lists the results of these tests.

Table 3.3 Multigrid Modulus of Elasticity

Source	E (ksi)
Tensile calibration	2000
Flexure test	1900

3.5 Weight and Cost Analysis

An important consideration for any new reinforcing material is its weight and cost relative to existing reinforcements. Table 3.4 lists the weight and cost for each of the reinforcing materials used in this project. Cost information is based on the price paid for the samples used. Because only small amounts of the materials were purchased, the costs may be inflated relative to the bulk price of the material. Weight information was provided by the manufacturers, except for the steel bars, whose weight data was obtained from ACI 318-89 *Building Code Requirements* (1989). In this section, the materials are compared and discussed with respect to their weight and cost.

Table 3.4 Weight and Cost Comparison of Reinforcing Materials

Material	Weight	Weight per beam	Cost ($/lb)	Cost ($/beam)
Steel Bars	0.668 plf (#4 bar)	7.22 lb	0.31	2.25
FRP Bars	0.172 plf (#4 bar)	1.86 lb	3.47	6.48
Multigrid	0.8 psf	3.20 lb	6.25	20.00
Duragrid 4.5	0.253 plf (1" I-bar)	5.45 lb	5.15	28.00
Duragrid 6	0.253 plf (1" I-bar)	4.44 lb	6.31	28.00

In Table 3.4, the per-beam values include the weight and cost of the transverse bars. The steel reinforced beams use #3 bars, which weigh 0.376 lb/ft and cost $0.13/ft. The FRP bar reinforced beams use #3 bars at 0.096 lb/ft and $0.40/ft. The Multigrid weight and cost are per-square-foot. The Duragrid transverse bars weigh 0.302 lb/ft, while the material is priced per-square-foot.

Fiberglass-reinforced plastic materials offer significant savings in weight over steel bars. An arrangement of FRP bars weighs slightly more than 25 percent of an identical steel bar setup. Low weight is advantageous for transportation and delivery of the reinforcement to the site. Handling and placement of large pieces of fiberglass material by construction workers is more feasible than steel because of the weight difference.

The Duradek and Multigrid reinforcing grids provide an additional advantage in placement. Because they are purchased with both longitudinal and transverse bars already installed, placement on site is quick and easy. There is no need to measure, cut and attach cross bars on site. The grid is simply cut to the desired size and laid in place. The grids are intended as walkways, so with proper support they may withstand human traffic before concrete is placed.

The price of the fiberglass materials is a problem, however. The FRP bars are somewhat comparable to steel bars in price, while the Multigrid and Duragrid materials are significantly more expensive. Because initial cost is typically of primary concern to the construction industry, the use of fiberglass reinforcing may be discouraged.

The materials may make up some of the difference in immediate cost by saving over the long term. Because the fiberglass will not deteriorate and corrode like steel, there is a reduced chance of future repair and replacement being necessary. Studies into the long-term performance of fiberglass reinforcing under corrosive conditions are currently being conducted by several researchers.

3.6 Concrete Properties

All test specimens were cast from the same batch of normal weight concrete. The initial design concrete strength was 4500 psi. Two test cylinders were made from the concrete batch as it was being placed in the beam forms. One was broken the day after the first test (54 days after placement), the second on the day after the last test (89 days). The cylinder strengths were 5300 psi and 6000 psi, respectively. A linear variation of strength was assumed: the concrete strength for each test was interpolated from the cylinder test values. Table 3.5 lists the calculated concrete strength and modulus of elasticity for each test. The concrete modulus of elasticity was calculated following ACI 318-89, Section 8.5, simplified for normal weight concrete, as:

$$E_c = 57{,}000\sqrt{f_c'} \qquad (3\text{-}3)$$

where,

E_c = concrete modulus of elasticity, psi

f_c' = concrete compressive strength, psi

Table 3.5 Concrete Strength and Modulus for each test

Test	Day #	f_c' (psi)	E (ksi)
ST-1	53	5300	4100
FR-1	57	5400	4200
D4-1	62	5500	4200
D6-1	67	5600	4300
MG-1	69	5600	4300
ST-2	74	5700	4300
D4-2	77	5800	4300
D6-2	81	5900	4400
FR-2	84	5900	4400
MG-2	88	6000	4400

CHAPTER 4

EXPERIMENTAL PROGRAM

The experimental program proceeded in several stages. First, the test beams were designed and the reinforcing materials obtained. The reinforcements were then instrumented and calibrated. Third, the concrete test beams were cast and cured. The testing frame was then constructed and the test procedure developed. Finally, the beams were tested, half under monotonic load, the remainder under cyclic load. The following sections describe each of these stages in detail.

4.1 Calibration of Reinforcing Bars

Strain gages were applied to each reinforcing bar placed in concrete (in the case of the Duragrid and Multigrid, with multiple bars, two longitudinal bars were gaged). Because each bar type was made of a different material (with a different modulus of elasticity), it was necessary to determine how the strain gages behaved on each. Therefore, the bars were calibrated--pulled in tension so that a load-to-strain relationship could be recorded. Then, during the beam tests, the indicated strains in the bars can be related to the force in the bars. This indicates when, and if, the bars are near yield or failure. Additionally, from the strain in the bars and strain in concrete (indicated by a strain gage on the top surface), a strain distribution through the depth of the specimen can be determined.

The following sections describe the calibration procedure, in general and then in detail for each reinforcement. A full summary of the calibration data is found in Appendix A.

4.1.1 Calibration Procedure

4.1.1.1 Strain Gage Application

Two locations on each bar, on opposite faces at the midpoint, were prepared for strain gage application. This involved removing enough material to form a flat spot large enough for a gage and a terminal. The intent was to remove a minimum amount of material. The gages were applied using the surface preparation techniques recommended by the gage manufacturer. The same type of general purpose strain gages, with a gage length of 0.125 in., were used on all of the reinforcing bars. Specific details for each type of reinforcement can be found in the corresponding section following these general comments. The bars were calibrated before any rubber protection material was applied to the gages (Section 4.3.1).

4.1.1.2 Calibration

The calibration was performed in a Satec Universal Testing Machine, located in the Structures and Materials Laboratory. Split-wedge grips with either a flat face or a V-notch were used to grip the calibration specimens. Details for each type of reinforcement are given under the heading for each material.

The strain gages were connected with wires to a digital strain indicator. The load was recorded from the Satec-Mats II computer terminal. Both the strains and the load were zeroed after the bars were secured in the grips, but before the test began.

The Satec machine was programmed to perform a "universal test" in which it loads to a certain level, then unloads to zero. The intent was to load the specimens at a constant rate, hold at the peak load, and then unload at the same rate. Each test was paused approximately ten times to allow for recording of load and strain data.

It should be noted that the Satec machine often loaded the specimens much quicker than programmed. The initial loading occurred very quickly, slowing to the programmed rate at about 3000 lb, depending on the material and programmed rate. The test was able to be paused, though the Satec machine continued to slowly apply load, even

though the computer indicated it was paused. This is how much of the loading data was obtained--reading load and strain data as the machine "coasted" slowly. Typically, a test was started, then paused when the load reached about 1000 lb. The load would then drop 500 lb or more, then slowly rise back up to 1000 lb and beyond. When the load finally held constant, the test was resumed and the machine behaved as programmed. Some drift was evident during unloading, but usually not as severe.

Using a spreadsheet program, a regression analysis of the data was performed to determine the linearity of the points. Primary output of the regression analysis is the slope of the best fit line for the data. This slope is the load-to-strain ratio, with units of lb/$\mu\varepsilon$, where $\mu\varepsilon$ = microstrain = in./in. x 10^{-6}. The indicated strains during the beam tests are multiplied by the slope to determine the force in the bar.

4.1.2 Steel Bars

4.1.2.1 Strain Gage Application

A compressed-air driven belt sander was used to remove the surface deformations on the bars and to grind off enough steel to form a flat spot large enough for a gage and a terminal. Measurements showed the remaining diameter to be approximately 0.43 in., down from 0.5 in. originally.

4.1.2.2 Grips

The Satec machine's V-notch grips were used to grip the steel bars. Care was taken to ensure that the bar deformations faced the grips, providing a good surface for gripping. The portions of the bars to be gripped, about 8 in. at each end, were cleaned and degreased prior to calibration.

4.1.2.3 Results

The steel bars were pulled to a peak load of 5000 lb. This corresponded to approximately one-half of the estimated yield strength (60 ksi), based on an estimate of the reduced cross-section at the gages (0.15 in^2 to 0.17 in^2).

All four bars calibrated well, with no problems encountered during testing. The two gages on each bar tended to differ from each other in actual strain readout (40 $\mu\varepsilon$ to 100 $\mu\varepsilon$), but the final regression result was good for all. The ratios ranged from 4.48 lb/$\mu\varepsilon$ to 5.33 lb/$\mu\varepsilon$, with the average close to 5.0 lb/$\mu\varepsilon$.

4.1.3 FRP Bars

4.1.3.1 Strain Gage Application

Sandpaper and files were used to remove the deformations on the bar and form a flat spot large enough for a gage and a terminal. Measurements showed the remaining diameter varied from 0.37 in. to 0.44 in., down from 0.5 in. originally.

4.1.3.2 Grips

Split-wedge grips with a V-notch were used to grip the FRP bars. Previous research by others into tension tests of FRP bars indicated that gripping is typically a problem. Although the FRP is strong in tension (in the direction of the glass fibers), it is weak transversely, and tends to crush when gripped. Therefore, some initial investigation and trials were needed to determine a good method for gripping the bars.

First, a one-foot test piece of FRP bar with an extensometer attached was placed in the Satec grips and loaded to 1 kip. The extensometer indicated little strain in the bar, suggesting that the bar was sliding in the grips. Upon removal of the bar, it could be seen that the grips had damaged the outer resin portion of the bars and had not been able to grip the fibers.

In an attempt to solve a similar problem, Porter and Barnes (1991) bonded a steel pipe to the end of the bar to be gripped. The testing machine would grip the steel pipe, transferring the force through an epoxy to the FRP bar. This method was tried, by this author, with a scrap copper pipe and a two-part "plastic welder" epoxy. The sample was pulled successfully to 1000 lb, but one end of pipe slid off, revealing that the epoxy had not completely set. To improve the bond, holes were drilled through the pipe and bar, and shear pins added. The first set of pins--pieces of nails--bent when loaded. A second attempt used 1/8 in. diameter cotter pins, which broke when loaded. The pipe also tended to bulge out at the sides between the grips, pulling away from the bar.

ASTM D3916 recommends "aluminum-alloy tab grip adapters", as shown in Fig. 4.1. This standard, combined with the results of a discussion with Bob Simonds, supervisor of the Engineering Science and Mechanics laboratory, led to the development of the next set of adapters--two half-pipes bonded to each end of the specimen, as shown in Fig. 4.2. The split allows the Satec machine grips to better squeeze down on the pipe and bar. A one-foot test piece bar was constructed, using 3 in. adapters at both ends. This was loaded to 3000 lb with no problems. An extensometer was attached and the bar pulled again. The extensometer indicated a linear stress-strain relation, with little slip apparent. The bar was then pulled to 6000 lb, with no problems encountered.

The performance of the trial adapters was then extrapolated to determine the length of pipe needed to reach 10,000 lb on a full length bar. Three-inch long adapters allowed 6000 lb, so it was estimated that 5 in. long adapters would be sufficient. As a factor of safety, the actual adapters were each made 5.75 in. long.

A steel pipe with an inside diameter of 0.5 in. was used to make the adapters. The pipe was first cut to length, then partially threaded inside with a pipe tap. The tapping was intended to provide some bond and friction for the epoxy by roughening the inside of the pipe. The pipe was then cut in half lengthwise, making two half-pipes. (The pieces were actually less than half, as the saw removed about 1/16 in. of material. This is desired, as the gap is needed to allow the pipe to squeeze down on the bar.)

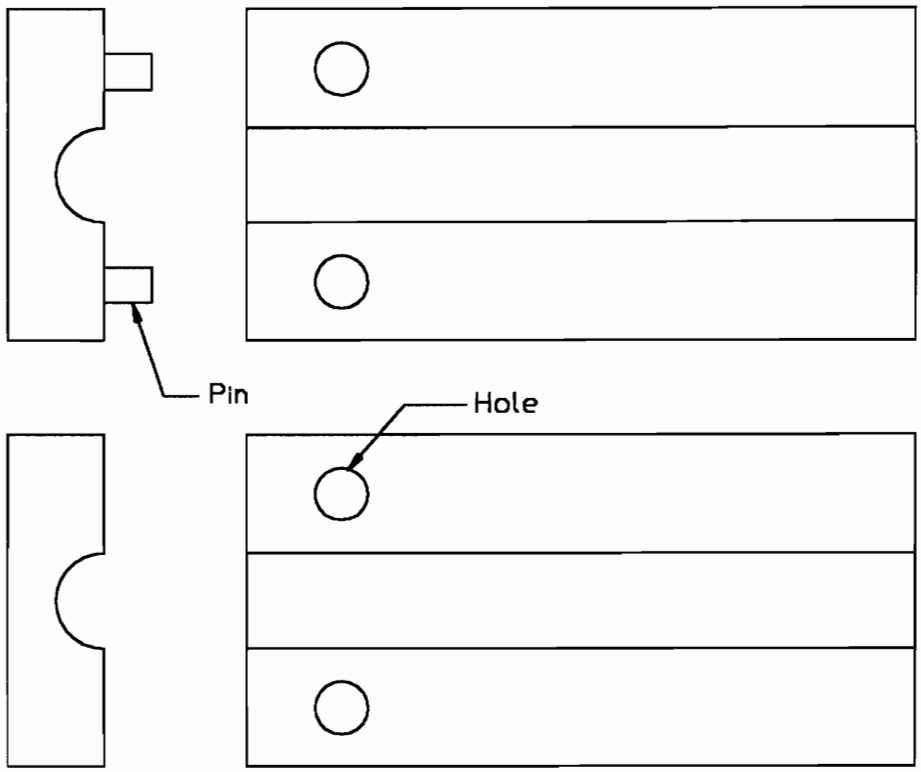

Figure 4.1 ASTM Grip Adapters for FRP Rods

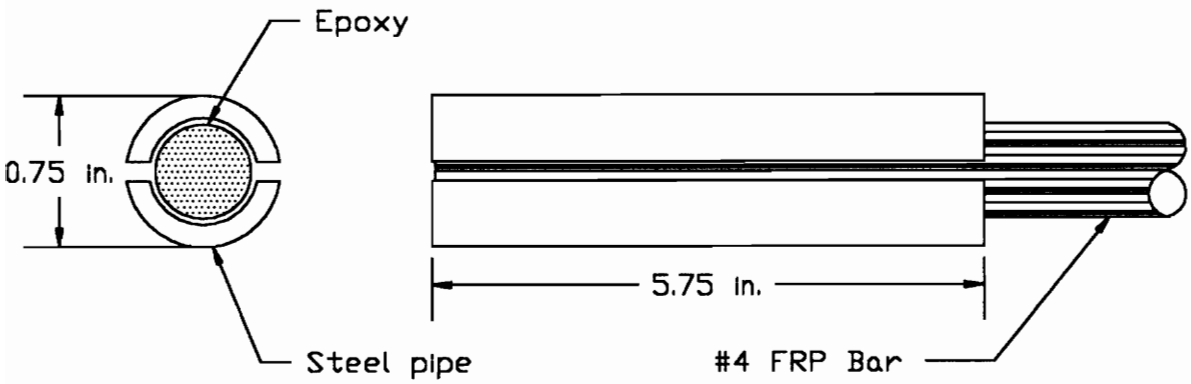

Figure 4.2 FRP Bar Grip Adapters

The FRP bars were slightly more than 0.5 in. in diameter. The section to be bonded to the adapters was filed down until the pipe fit snugly. The pipe pieces and bar were labeled to ensure a custom fit for each piece. The two-part epoxy was mixed and applied to the pipe. The pipe pieces were placed on the bar, clamped, and the epoxy allowed to cure for at least 48 hours before testing.

4.1.3.3 Results

Two bars (named Group I) were pulled to a maximum load of 10,000 lb, the other two (named Group II) to 5000 lb. This variation is due to problems encountered during calibration, as discussed below. The 10,000 lb load corresponds to approximately one-half of the estimated ultimate strength (107 ksi), based on an estimate of the reduced cross-section at the gages (0.17 in^2 to 0.19 in^2).

As expected, the strains in the FRP bars were much larger than in the steel bars. On average, the FRP indicated strains four to five times those of the steel. Considering that the modulus of elasticity of FRP is about one-fourth that of steel, this difference in measured strain is appropriate.

Group I, consisting of the bars labeled #2 and #4, calibrated well to 10,000 lb, with no problems encountered during testing. The two gages on each bar tended to differ from each other in actual strain readout (100 $\mu\varepsilon$ to 800 $\mu\varepsilon$), but the final regression results were good. The load-strain ratios ranged from 0.92 lb/$\mu\varepsilon$ to 1.02 lb/$\mu\varepsilon$, with an average of 0.95 lb/$\mu\varepsilon$.

The bars in Group II, labeled #1 and #3, did not calibrate well at first. Initial trials to 5000 lb on bar #1 showed a significant difference between the two gage readings (one gage indicated about one-half the strain of the other). This was attributed to the fact that the bar was initially bent, so that when the Satec machine pulled it straight, one side was more in tension due to bending than the other. Trials on bar #3 indicated the same trend, though the strains tended to increase rapidly, even when the applied load was not increasing.

It was presumed that the gages on these two bars must not have been in contact with the glass fibers. Instead, they were on the resin coating, which had no strength and simply deformed under load. To fix this, more material was removed and the gages reapplied. The remaining cross-sectional area was approximately 0.14 in^2.

To counteract the bending effects, the two gages were wired together in a half-bridge arrangement. This means the gages are wired in series, essentially adding the strain readings together. The gages are electrically balanced by another bar (at rest) with two gages also wired in series. The strain indicator uses a Wheatstone bridge which allows this arrangement. The gages work together and cancel out the bending effects. This wiring arrangement produces a single load-strain relation for each bar.

The bars in Group II were calibrated to only 5000 lb. This lower load was used to avoid any further problems with the strain gages at high loads. These modified bars calibrated satisfactorily, with load-to-strain ratios of 0.69 lb/$\mu\varepsilon$ (bar #1) and 1.32 lb/$\mu\varepsilon$ (bar #3).

When the bars were arranged in grids for placement in the concrete, one bar from each group was placed in each beam. It was felt that Group I would perform well, while Group II (the reworked bars) might encounter problems at high tensile forces. Placing one Group I bar in each beam was done to ensure that at least one bar in each beam would produce good strain data. The grip adapters remained on the bars when they were placed in the concrete. It was felt that they would not significantly affect the bond behavior of the bars.

4.1.4 Duragrid Grating

Unlike the steel and FRP bars, the Duragrid bar that was calibrated was not later placed in concrete. This is because the bars are in a grid form that prevents gripping in the testing machine. It was assumed that all the main bars in the grids had the same properties. Therefore, one bar was removed from a grid, strain gaged, and pulled to produce a load-to-strain relation.

4.1.4.1 Strain Gage Application

Sandpaper was used to remove the coating on the bars to provide a good area for bonding of the gage. The gages were placed on the top and bottom flanges of the I-bars. Because the flanges were initially flat, little material was removed, thus the dimensions of the bar were not changed significantly.

4.1.4.2 Grips

Due to their I-shape, it was not immediately apparent how to grip the Duragrid bars for calibration. Several trials were made before a successful method was reached.

First, 7/16 in. square, 5 in. long steel bars were attached with epoxy to each side of the web at both ends of a trial bar. This method worked up to a load of about 3000 lb, above which the epoxy-Duragrid bond failed and the steel bars fell off.

The next attempt involved removing the flange material at each end of the bar. This left a rectangular section of Duragrid, 1 in. by 0.16 in., to which steel plates were bonded. This method worked up to a load of 4000 lb, when it became apparent that there was a stress concentration at the location where the flanges started again. This occurred near a transverse bar, which is attached by a hole through the web of the main bar. Therefore, all the load had to be transferred from the web at the grips to the flanges at the hole.

The final trial was essentially the same as the second, though a transition area was created to allow load transfer between the web and the flanges. The grip adapter length was shortened to 3 in. and a 2 in. tapered section was made. Figure 4.3 shows the Duragrid bar and gripping arrangement used for calibration.

4.1.4.3 Results

Because the previous gripping methods had encountered problems above 4000 lb, the final calibration was done to 4000 lb. The bars were pulled twice to this load and

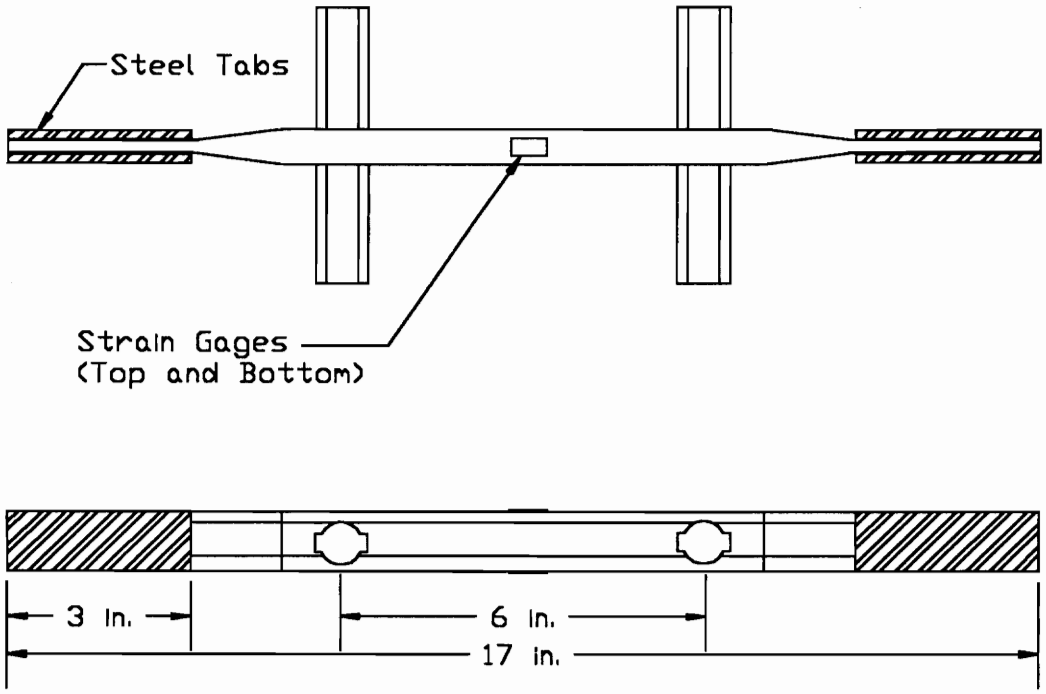

Figure 4.3 Duragrid Calibration Specimen

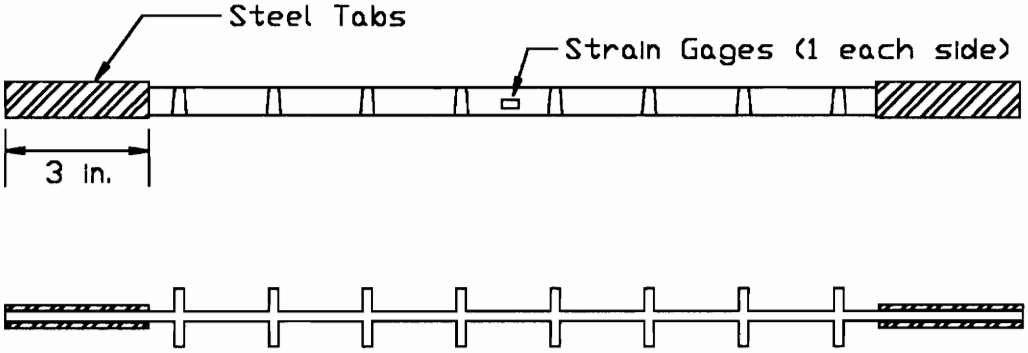

Figure 4.4 Multigrid Calibration Specimen

load-strain relations made for each gage. Each gage gave consistent results, although the relations differed significantly between the two gages. Gage A, on the top flange, had a ratio of 1.79 lb/με, while Gage B, on the bottom flange, had a ratio of 1.52 lb/με. The average ratio for the two gages was 1.66 lb/με.

It was unknown whether the difference was due to the gages themselves or to the difference between the top and bottom flanges. To investigate, the gages were next wired in series (half-bridge), and the sample re-pulled. Two calibration trials were made with this arrangement. The average load-strain relation was 1.65 lb/με.

Given the similarity of these two values, it was determined that the load-strain ratio for the Duragrid must be close to 1.65 lb/με. For the actual grids used in the tests, the gages were wired individually and a ratio of 1.65 lb/με was used for each gage.

4.1.5 Multigrid Grating

Unlike the steel and FRP bars (but like the Duragrid), the Multigrid bar that was calibrated was not the same one placed in concrete. Because the Multigrid is in a grid form, gripping it in the testing machine was not possible. Therefore, one bar was removed from the grid, gaged, and pulled to produce a load-strain relation. Figure 4.4 shows the sample used for calibration.

4.1.5.1 Strain Gage Application

Sandpaper was used to remove the coating on the bars to provide a good surface on which to bond the gages. The gages were applied to both sides of the bar, rather than top and bottom. This was necessary in order to ensure that the gages were in contact with the fibers, as described in Section 3.4.

The gages were wired in a half-bridge arrangement (Section 4.1.3.3) in order to eliminate any bending effects. Also, because the grid calibrated was different than the grid used in the beams, there would be no way to distinguish between the gages. That is, if a different load-strain relation were made for a gage A and a gage B, how would one know

whether a gage on the real grid was acting like A or B? With the gages wired in series, there is only one load-strain relation for each bar.

4.1.5.2 Grips

Some initial trials were performed in order to determine the best method for gripping the bars, as it was expected that the testing machine grips would damage a bare bar. First, a test piece of Multigrid, approximately 16 in. long, was cut. The last three crossbars at each end were removed to provide an area to attach steel plates to the grid for gripping. Steel plates about 1 in. by 6 in. were made and epoxied to the grid. The plan was to pull the grid to 5000 lb, corresponding to about one-half of the initial estimated ultimate strength, based on an assumed tensile strength of 100 ksi and cross-sectional area of 0.12 in^2. This test piece was not strain gaged and served only to test the steel plate grips.

The test sample was placed in the Satec machine, which was programmed to pull to 2000 lb and return to zero. Beginning at approximately 700 lb, a repeated cracking sound was observed. The test was stopped at 900 lb and the sample removed. Examination showed many faint lines, both on the top and sides of the material. They appeared to be similar to yield lines in steel. It was assumed that it was only the protective coating placed on the material that was cracking.

The specimen was reloaded to 1000 lb. There was a large amount of cracking noise heard, but the load reached 1000 lb. An attempt was then made to load the specimen to 2000 lb. Much more cracking was heard, and sounded more serious, so the test was stopped at 1800 lb. Some cracks appeared to be deeper than just a coating. The specimen was then reloaded to determine whether the cracks were serious or merely cosmetic. Upon reloading, the specimen failed just above the bottom grip at about 1600 lb. Both vertical and horizontal cracks appeared and the specimen pulled apart. This failure led to the determination of the actual fiber arrangement in the Multigrid (Section 3.4).

A new specimen was constructed with smaller (3 in. long) steel grip plates. To ensure that the specimen would not fail, it was calibrated to only 700 lb. The strain gages were placed where the fibers appeared to be, as shown in Fig. 3.9 and Fig. 4.4.

4.1.5.3 Results

The gaged sample was first pulled with the gages wired separately. This produced a load-strain ratio for each gage, with the average equal to 0.2047 lb/με. The gages were then rewired in series and the specimen re-pulled. The resultant ratio was 0.2031 lb/με. For the actual grids used in the tests, the gages were wired in series and a factor of 0.203 lb/με used.

Following completion of the beam tests, tensile tests were performed on samples of Multigrid. The strain-gaged sample used for calibration was pulled to failure, allowing the development of a load-strain curve up to failure, rather than only the 700 lb level of calibration. This test revealed that the Multigrid material is not linear elastic to failure, as shown in Fig. 4.5. A curve was fit to the data, providing a new load-strain equation. Use of the original equation,

$$F = 0.203 \times \varepsilon \qquad (4\text{-}1)$$

would result in an over-estimation of the force in the grid for a given strain reading. The new equation, used to calculate the force in the Multigrid during the beam tests, is:

$$F = (0.000005 \times \varepsilon^2) + 0.211\varepsilon \qquad (4\text{-}2)$$

where,

F = applied tensile force

ε = measured strain in bar.

4.2 Construction of Test Specimens

The formwork was constructed to allow all ten concrete beams to be cast at the same time. Formwork consisted of a quarter-inch plywood base with (nominal) two-by-eights forming the sides. The beams, 7.25 in. by 12 in. by 4 ft, were constructed as they

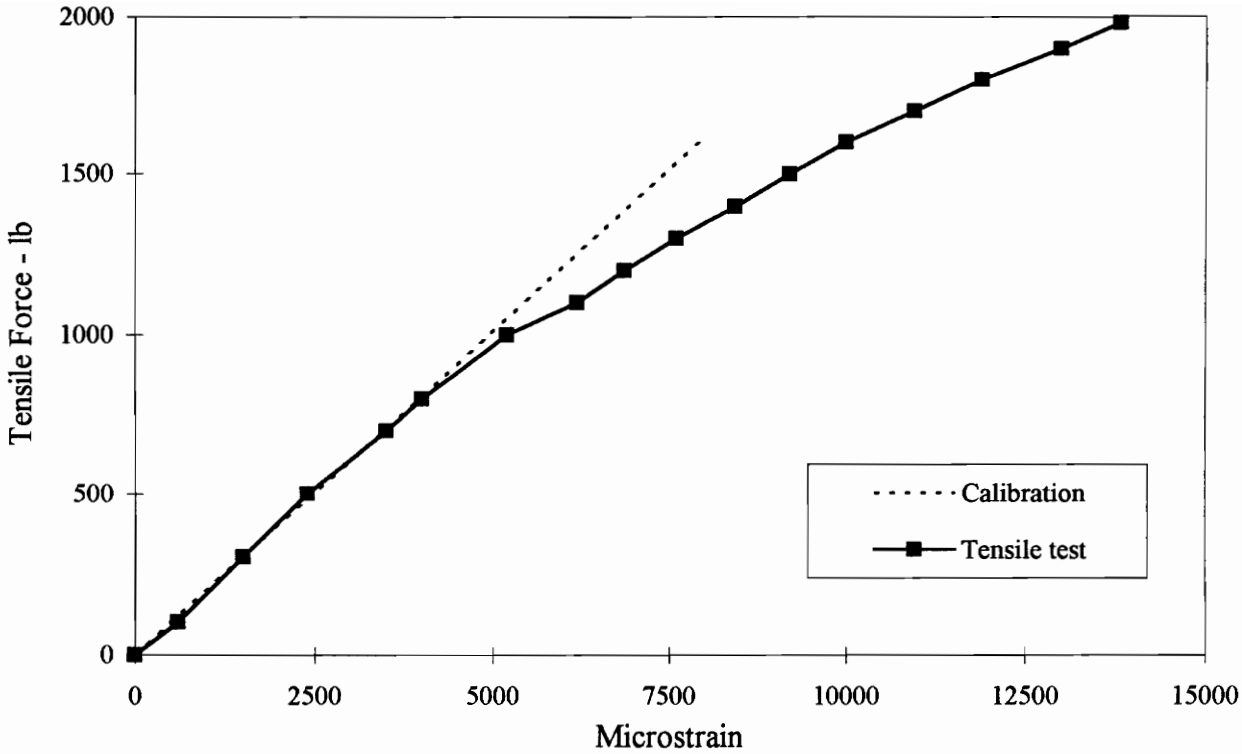

Figure 4.5 Multigrid Bar Tensile Force v. Strain

would be in a real deck, with the reinforcement placed in the top layer. (However, the beams were tested upside down from how they were cast.) Nails were placed in the formwork sides to support the reinforcements. The steel bars were tied to the nails with normal wire bar ties. The FRP bars and fiberglass grids were attached using plastic ties, in keeping with the "non-steel" concept.

The steel reinforced beams were designed with 2 in. of clear cover, as per ACI 345-82, *Standard for Bridge Deck Construction*, Section 2.4.1. Because of the corrosion resistance of fiberglass materials, it is expected that the required cover can be reduced. Therefore, for the fiberglass reinforced beams, the design clear cover was 1 in.

The beams were labeled according to the type of reinforcement used. The label consists of a two letter abbreviation for the reinforcement and a number. The "-1" label indicates the first series of tests, the "-2" indicates the second series. Table 4.1 lists the test designations and a description of the reinforcement.

Table 4.1 Test Designations and Reinforcement Description

	Reinforcement		
Beam Label	Type	Layout	Area
ST	Steel bars	2-#4 @ 8 in.	0.40 in^2
FR	FRP bars	2-#4 @ 8 in.	0.40 in^2
D4	Duragrid	3 bars @ 4.5 in.	0.93 in^2
D6	Duragrid	2 bars @ 6 in.	0.62 in^2
MG	Multigrid	6 bars @ 2 in.	0.72 in^2

Form oil was applied to the formwork immediately prior to concrete placement. All of the beams were constructed from the same batch of concrete. Only two test cylinders were made, due to an under-estimation of the concrete volume needed. It was also necessary to skim some concrete off of several beams to finish filling others. This led to slightly reduced depths on those beams, though the difference was only about 1/8 in.

Table 4.2 lists the depth of the beams and the actual cover provided, as measured after testing of all the beams.

Table 4.2 Actual Dimensions for Test Beams

Test	Depth (in.)	Cover (in.)
ST-1	7.25	1.75
ST-2	7.125	2
FR-1	7.25	0.75
FR-2	7.25	0.75
D4-1	7.25	1
D4-2	7.25	1
D6-1	7.25	1
D6-2	7.25	1
MG-1	7.125	0.875
MG-2	7.125	0.875

Following placement, the beams were covered with plastic and moist cured on the lab floor for seven days. The beams were removed from the forms about ten days after casting and stored in the lab until tested. The cylinders were kept with the beams at all times to ensure identical curing conditions.

With the exception of the Multigrid, the bars and gratings had enough open space to allow unobstructed concrete placement. The Multigrid, with openings only 1.8 in. square, inhibited easy placement. Although the largest nominal aggregate size was 0.75 in., the concrete mixture tended to get caught on the grating. The best method found for getting the concrete through was to hold the mechanical vibrator directly against the grating, thereby vibrating the grating and essentially sifting the concrete through. The vibrator fit through all of the reinforcing grids, allowing vibration of the full depth of concrete.

4.3 Test Setup

4.3.1 Instrumentation

Applied load was measured with a 50 kip load cell, which was calibrated for loads up to 20 kips--the expected maximum load for the tests. The load cell was placed between the hydraulic ram and the support frame. Figure 4.6 shows the instrumentation arrangement for the tests.

Vertical displacement of the beams was measured at midspan by two potentiometers, one on either side of the beam. The potentiometers were placed approximately under the reinforcement, 2.5 in. in from the beam edges.

Strain gages were placed on the reinforcement, as discussed in Section 4.1. Following calibration and prior to placement in the forms, the gages were sealed to protect them from the concrete, as shown in Fig. 4.7. The gage manufacturer provided the method and materials used. First, the gages and wires were coated with a liquid polyurethane and a rubber sealant. Next, Teflon tape and two layers of rubber sheets were placed on the gage. Finally, the entire area was sealed with aluminum tape to provide additional mechanical coverage. The protection of the gages was successful, as all the gages continued to function properly after concrete was placed.

One strain gage was placed on the top of the concrete, at midspan of the beam, between the load points. These gages had a gage length of 90 mm (3.5 in.), and were applied after the concrete had cured. The application procedure involved sanding an area for the gage, placing an epoxy coating to form a smooth surface, and then covering the gage with another epoxy coating.

The strain gages, potentiometers and load cell were all wired to the System 4000 data acquisition system.

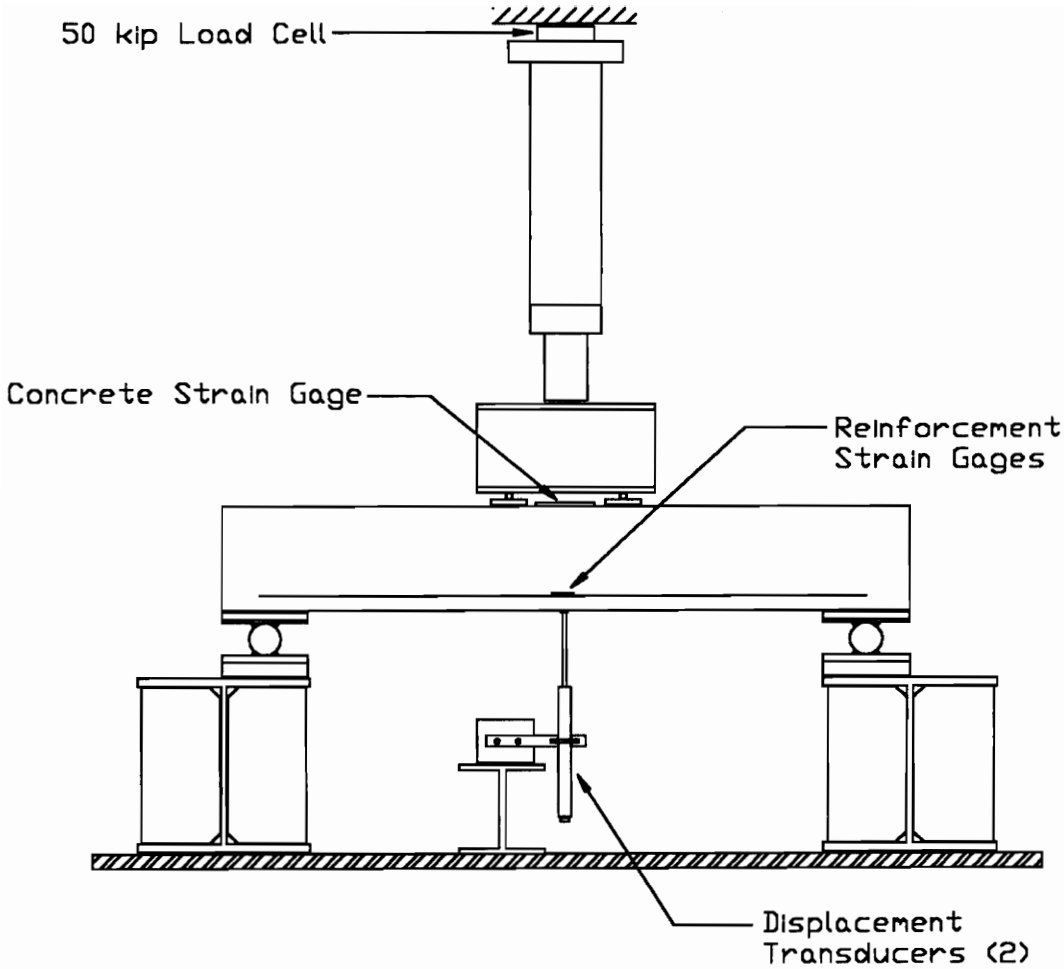

Figure 4.6 Instrumentation Arrangement

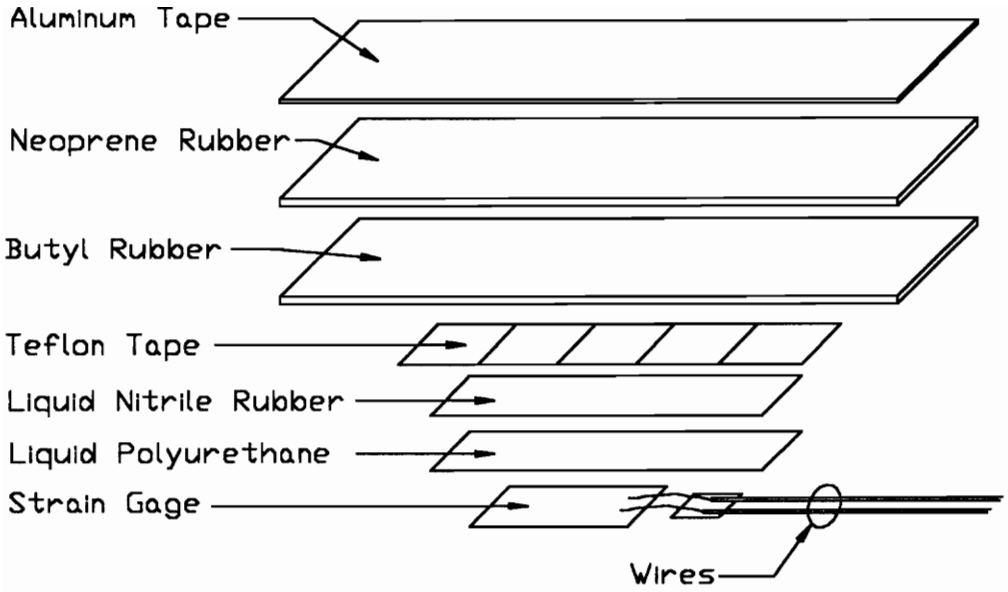

Figure 4.7 Strain Gage Protection

4.3.2 Beam Test Arrangement

Figure 4.8 shows the test frame setup and specimen supports. Two W12x65 beams placed on the reaction floor served as the supports. Two columns bolted to the reaction floor held the hydraulic ram setup.

A spacer plate (to provide proper clearance), a pin support (to allow rotation), and a support plate (to support the full width of the specimen) were placed on top of each support beam. The concrete test beam was then placed atop the support plate. The beams spanned 42 in. center-to-center of the pin supports.

A small spreader beam was used to distribute the single ram load into two applied loads. The spreader was placed on two rods to allow rotation. Two rectangular plates transferred the load to the concrete specimen. The load points were 8 in. center-to-center of the rods.

4.4 Testing Procedure

Load was applied at regular, typically 1 kip, intervals. Cracks were marked as they propagated and photographs were taken periodically. Where possible, the locations of the transverse reinforcing bars were marked prior to testing. This was done to facilitate comparison of their location to the location of the cracks. It has been reported by others that the cracks tended to align with the transverse bars of the gratings. Data was recorded by hand as well as on the System 4000. After each load point, deflection and strain data were plotted using a computer spreadsheet. Following each additional increment of load, five minutes were allowed to pass before data was recorded. This wait was necessary in order to allow the indicated load to stabilize.

Before each test began, a pre-load of about 2 kips was applied to check that all instruments were functioning properly. The beam was then unloaded and all readings reset to zero.

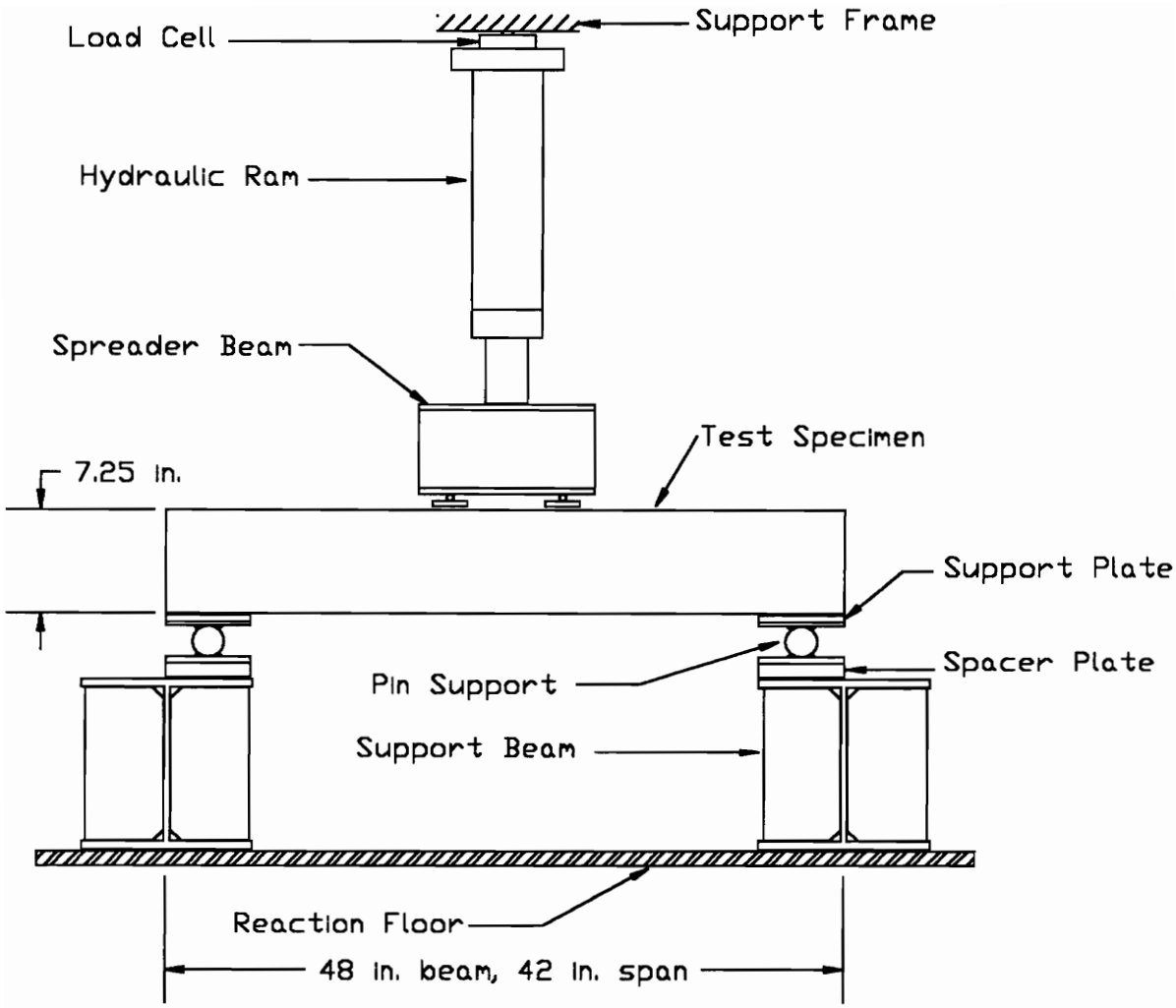

Figure 4.8 Test Frame Setup

4.4.1 Monotonic Tests

The first series of tests (labeled "-1") were loaded monotonically to failure. Load was applied in approximately 1 kip intervals.

4.4.2 Cyclic Tests

The second series of tests ("-2") were cyclic in nature, going from zero load to a certain level, and then returning to zero. Each level was based on a percentage of the ultimate load observed in the monotonic series of tests. Table 4.3 lists each load level and number of cycles the load level was repeated. A plot of the loading history is shown in Fig. 4.9.

Table 4.3 Load steps for cyclic tests

Percent of ultimate monotonic load	Number of times load repeated
20	7
35	7
20	7
50	7
20	7
65	7
20	7
80	7

For the initial loading to a level, the load was increased in approximately 1 kip intervals up to that level. Successive cycles to that level were made by unloading directly to zero, waiting approximately three minutes for all readings to stabilize, then loading back to that level, with no intermediate load steps. The next higher level was reached by loading directly to the previously attained level, then in 1 kip increments to the new level.

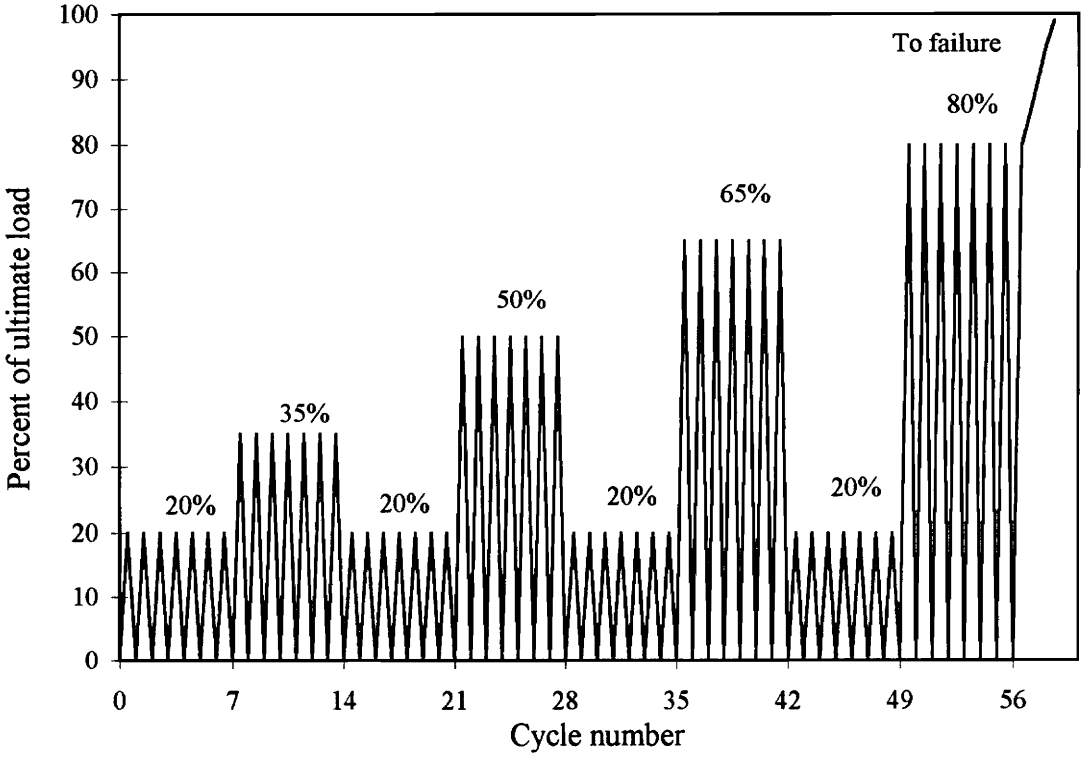

Figure 4.9 Loading History for Cyclic Tests

This load pattern was used previously by Goodspeed (1991), although he applied 10 cycles at each load step. According to Goodspeed, the behavior of his specimens "leveled out" after several cycles, suggesting that once a certain point was reached, the number of cycles was not important. This realization, coupled with time constraints, led to the reduction of cycles to seven at each load step.

4.5 Predictions

For each test, several prediction calculations were made. The moment causing first cracking, the shear capacity, the moment capacity and a load-displacement curve were all calculated. The following sections describe the prediction procedures used for each reinforcement type.

Calculation of shear capacity and cracking moment followed the same procedure for all beams. Moment capacity and load-displacement behavior varied by reinforcement type. For the FRP bars, the load-deflection calculations were made following GangaRao and Faza (1991).

Sample calculation results are given for each test for the cracking moment, the moment of inertia used for deflection calculations, and the predicted deflection under an applied load of 10 kips. Complete prediction results, including full plots of the load-deflection predictions and comparisons of ultimate loads, are found in Chapter 5.

4.5.1 General Calculations

Figure 4.10 shows a model of a loaded test beam and corresponding shear and moment diagrams. From statics, the moment at the center of the beam is calculated as:

$$M = Pa_1 \qquad (4\text{-}3)$$

where,

M = moment on section

P = concentrated load (one-half of total applied load)

a_1 = distance from load point to support

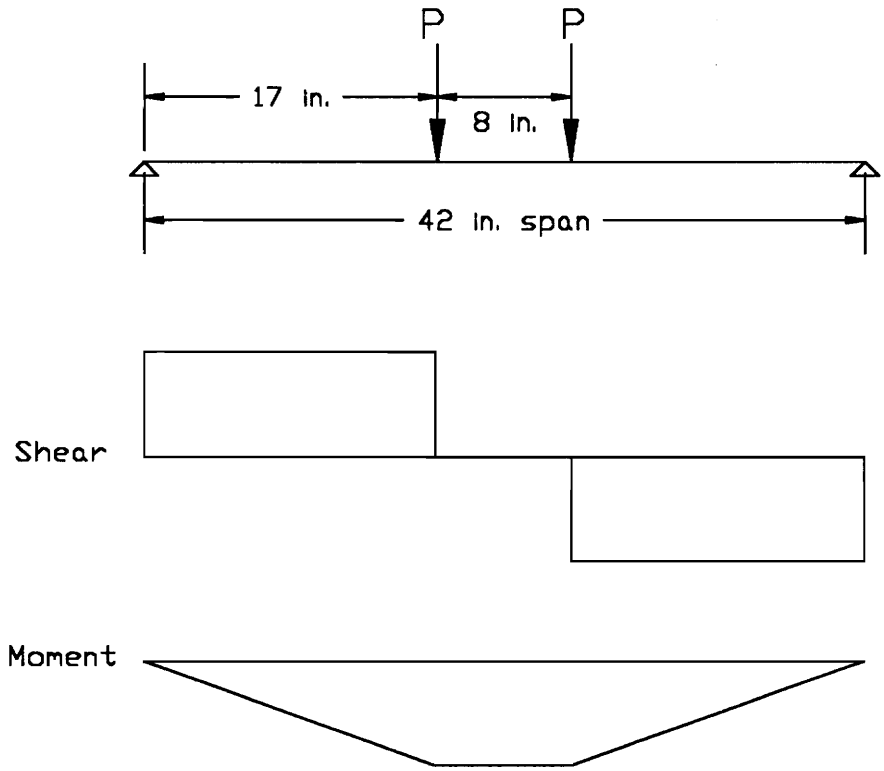

Figure 4.10 Model of Loaded Beam, with Shear and Moment Diagrams

The moment causing first cracking is based on the estimated tensile strength of the concrete, and is given by ACI Eq. 9-8 as:

$$M_{cr} = \frac{f_r I_g}{y_t} \tag{4-4}$$

where,

M_{cr} = moment causing first cracking

f_r = modulus of rupture of concrete = $7.5\sqrt{f_c'}$

I_g = moment of inertia, gross section

y_t = distance from centroidal axis of section to extreme tension fiber

The shear strength of each beam is calculated, following ACI Eq. 11-3, as:

$$V_c = 2\sqrt{f_c'}\, b_w d \tag{4-5}$$

where,

V_c = shear strength provided by concrete

b_w = width of beam

d = distance from extreme compression fiber to centroid of reinforcement

There are three flexure failure possibilities: concrete in compression, reinforcement in tension, or a balanced failure in which both the concrete and the reinforcement fail simultaneously. Based on the work of others, it was expected that the compressive strength of the concrete would control in some of the fiberglass reinforced beams. To determine which factor controls, the amount of reinforcement present is compared to the amount of reinforcement which would cause the balanced failure. A member is under-reinforced (bar failure controlling) if the area is less than the area for balanced failure, and over-reinforced (concrete failure controlling) if the area is greater.

The area of reinforcement resulting in a balanced failure in the concrete and reinforcement is defined as:

$$A_{rb} = \beta_1 b_w d \frac{0.85 f_c'}{f_y} \frac{\varepsilon_{cu}}{\varepsilon_{cu} + \varepsilon_{ry}} \tag{4-6}$$

where,

A_{rb} = area of reinforcement causing balanced failure

β_1 = compression block factor = $1.05 - 0.05\, f_c'/1000 \geq 0.65$

f_y = yield strength of reinforcement

ε_{cu} = ultimate strain in concrete = 0.003 in./in.

ε_{ry} = strain in reinforcement at yield

To ensure ductile behavior, ACI limits the amount of steel reinforcement which may be placed in a section to 75 percent of the area causing balanced failure. Results of these calculations for each beam are discussed in the following sections.

4.5.2 Steel Bar Reinforced Beams

The steel reinforced beams were considered under-reinforced, as the area of reinforcement provided was less than the maximum amount allowed. Therefore, flexure capacity was calculated using an equivalent rectangular stress block and summing the internal resisting moment:

$$a = \frac{A_s f_y}{0.85 f_c' b_w} \tag{4-7}$$

$$M_n = A_s f_y \left(d - \frac{a}{2} \right) \tag{4-8}$$

where,

a = depth of equivalent rectangular stress block

A_s = area of reinforcing

f_y = yield strength of reinforcing

M_n = nominal moment capacity of section

Load-displacement behavior was calculated using a linear elastic, cracked transformed section. The centerline deflection was calculated using the expression:

$$\Delta = \frac{Pa_1}{24E_cI_{eff}}\left(3L^2 - 4a_1^2\right) \tag{4-9}$$

where,

Δ = centerline vertical displacement of beam

L = span length

E_c = concrete modulus of elasticity

I_{eff} = effective moment of inertia for section (see below)

ACI (1989) recommends the use of an "effective" moment of inertia for calculation of post-cracking deflections of reinforced concrete beams. The effective moment of inertia provides a transition between the gross and cracked section moments of inertia, and is defined by ACI as:

$$I_{eff} = I_{cr} + \left(I_g - I_{cr}\right)\left[\frac{M_{cr}}{M_a}\right]^3 \tag{4-10}$$

where,

I_{cr} = moment of inertia, cracked section

M_a = applied moment at stage deflection being calculated

In addition to the above calculations, the computer program RESPONSE (Collins and Mitchell 1991) was used to predict the load-displacement behavior of the steel reinforced beams. The results of this prediction are given for each test in Figs. 6.6 and 6.7.

Table 4.4 lists typical calculation results for the steel reinforced beams with an applied load of 10 kips, based on the above equations. Values for ultimate load and deflection, as well as a full load-deflection prediction curve, are found in Chapter 6.

Table 4.4 Typical Prediction Calculation Results, Tests ST-1 and ST-2

Test	M_{cr} (in-kips)	I_{eff} (in^4)	Δ (in.)
ST-1	57	148	0.08
ST-2	59	159	0.08

4.5.3 FRP Bar Reinforced Beams

GangaRao and Faza (1991) found that deflection calculations based solely on the effective moment of inertia of a section, from Eq. 4-10, tended to underestimate the post-cracking deflection of FRP bar reinforced concrete beams. They attributed this difference to the "nature of crack pattern and propagation" and the small depth of the neutral axis in such beams.

To improve the deflection predictions, they formulated a new theory on the extent of cracking in a FRP reinforced beam. They assumed that between the applied loads, the section would be fully cracked and the moment of inertia for the cracked section would apply. The end sections, between load and support, were assumed to be only partially cracked and closer to the effective moment of inertia, as shown in Fig. 4.11.

GangaRao and Faza developed deflection equations, using the moment-area method, for three different load patterns: concentrated loads at the third points, one concentrated load at midspan, and a uniformly distributed load. Their experimental data confirmed that these "modified" deflection expressions better represented the actual behavior of FRP reinforced beams.

GangaRao and Faza's deflection equation for a beam with concentrated loads at the third points is given as:

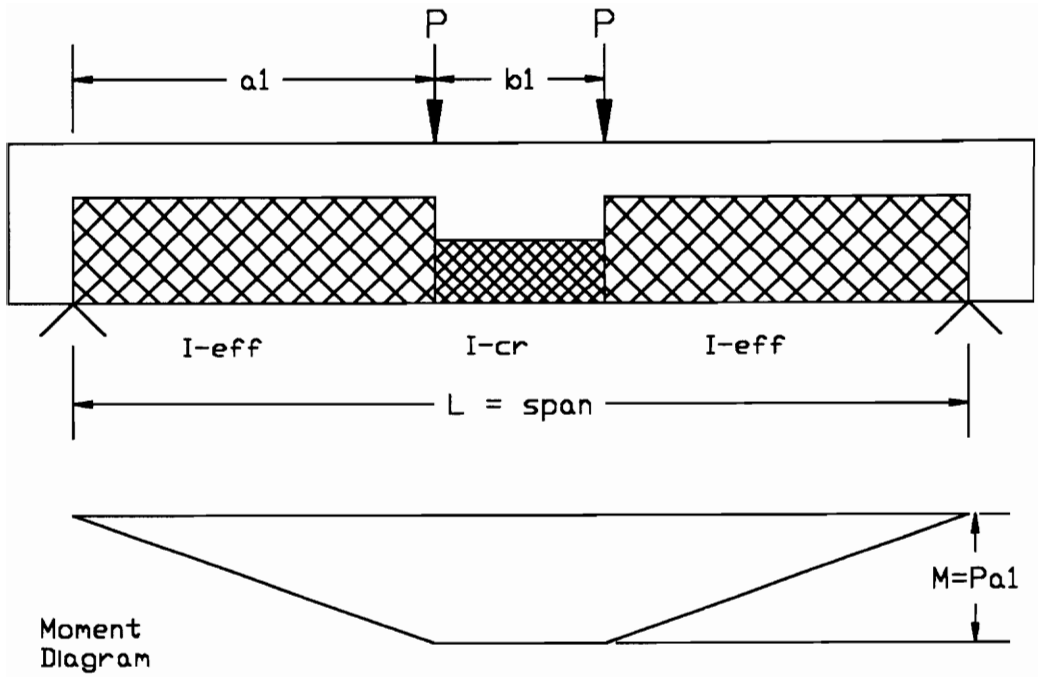

Figure 4.11 Assumed Cracking Pattern for Modified Deflection Equation

$$\Delta = \frac{8PL^3 I_{cr} + 15PL^3 I_{eff}}{648 E_c I_{cr} I_{eff}} \tag{4-11}$$

Following their example, an expression was developed for two concentrated loads at a variable spacing. This expression, Eq. 4-12, was used for prediction of the load-deflection behavior of tests FR-1 and FR-2.

$$\Delta = \frac{Pa_1^3}{3E_c I_{eff}} + \frac{2Pa_1 b_1}{E_c I_{cr}}\left(a_1 + \frac{b_1}{4}\right) \tag{4-12}$$

where,

b_1 = distance between load points

Table 4.5 lists typical calculation results for the FRP reinforced beams for an applied load of 10 kips, based on the above equations. Values for ultimate load and deflection, as well as a full load-deflection prediction curve, are found in Chapter 6.

Table 4.5 Typical Prediction Calculation Results, Tests FR-1 and FR-2

Test	M_{cr} (in-kips)	I_{eff} (in^4)	Δ (in.)
FR-1	58	133	0.10
FR-2	60	146	0.09

4.5.4 Duragrid Reinforced Beams

The Duragrid (4.5 in.) reinforced beams contained the largest area of reinforcement, 0.93 in^2. These beams were the only ones to be considered over-reinforced based on the balanced area of reinforcement. This suggests that concrete compression failure would occur before bar tension failure. Calculations of the moment capacity of the Duragrid (4.5 in.) beams confirmed that concrete compression failure would occur before bar tension failure. However, the shear capacity of the sections was determined to be the limiting factor.

The Duragrid (6 in.) beams were calculated to be under-reinforced, though shear capacity was again the limiting factor. Load-deflection behavior for all of the Duragrid reinforced beams was calculated using the moment of inertia of the cracked, transformed section.

Tables 4.6 and 4.7 list typical calculation results for the Duragrid reinforced beams for an applied load of 10 kips. Values for ultimate load and deflection, as well as a full load-deflection prediction curve, are found in Chapter 6.

Table 4.6 Typical Prediction Calculation Results, Tests D4-1 and D4-2

Test	M_{cr} (in.-kips)	I_{cr} (in^4)	Δ (in.)
D4-1	58	25	0.14
D4-2	60	25	0.14

Table 4.7 Typical Prediction Calculation Results, Tests D6-1 and D6-2

Test	M_{cr} (in.-kips)	I_{cr} (in^4)	Δ (in.)
D6-1	59	17	0.20
D6-2	60	17	0.20

4.5.5 Multigrid Reinforced Beams

Because of the demonstrated tensile weakness of the Multigrid (Section 3.4), it was assumed that tensile failure of the grid would control. Ultimate moment capacity based on bar failure was calculated following the steel reinforcing calculations (Section 4.5.2). An equivalent rectangular stress block was assumed and the flexure capacity calculated using Eqs. 4-7 and 4-8, replacing f_y with the ultimate tensile strength of a Multigrid bar (Table 3.1). The load-deflection behavior of the Multigrid reinforced beams was calculated following Eq. 4-9, using the moment of inertia of the cracked, transformed section.

Table 4.8 lists typical calculation results for the Multigrid reinforced beams, based on the above equations. The deflection value shown was calculated for an applied load of 8 kips (instead of 10 kips), because the ultimate load predicted for the Multigrid beams was only about 8 kips. Values for ultimate load and deflection, as well as a full load-deflection prediction curve, are found in Chapter 6.

Table 4.8 Typical Prediction Calculation Results, Tests MG-1 and MG-2

Test	M_{cr} (in.-kips)	I_{cr} (in^4)	Δ (in.)
MG-1	59	11	0.25
MG-2	61	11	0.25

CHAPTER 5

EXPERIMENTAL RESULTS

The results of each beam test are described in this chapter. Each section below contains observations made during the tests, as well as a description of load-deflection behavior, concrete strain and reinforcement strain. This chapter is limited to objective descriptions; analysis and comparison of the results is made in Chapter 6.

5.1 Summary of Test Results

Each test followed a similar pattern. The uncracked load-deflection behavior for each test was essentially the same. The first flexure crack typically appeared near midspan, extending up about two-thirds of the depth of the beam. The occurrence of all cracks could be clearly seen on the data plots by a drop in load and an increase in deflection.

Additional cracks appeared at different load intervals for each beam. These cracks were typically evenly spaced on both sides of the first. Failure occurred in one of three modes: concrete crushing in compression, bar failure in tension, or concrete failure in shear. Tables 5.1 and 5.2 list some important results for each test. In these tables, Δ_{max} is the maximum measured deflection at ultimate load (P_{ult}), and P_{cr} represents the load causing first cracking.

The tests were halted after a failure had occurred and the specimen exhibited no further load carrying capacity. Typically, once load capacity had decreased (but not to zero), the loading ram was extended further to investigate the post-peak flexibility of the beam. Ultimate load was taken as the maximum load recorded on the System 4000, regardless of whether this load was sustained or not.

The sections that follow contain observations and a description of each test. In these descriptions, the labels "right" and "left" are taken looking at the front of the test

specimen, from the data acquisition system. The crack pattern figures show the front of the beam. On these figures, the cracks are labeled in order of their occurrence.

Table 5.1 Monotonic Test Results

Test	Failure Mode	P_{ult} (kips)	P_{cr} (kips)	Δ_{max} (in.)
ST-1	Shear	20.8	4.8	0.38
FR-1	Flexure-concrete	18.8	6.0	0.75
D4-1	Flexure and shear	28.8	5.0	0.67
D6-1	Flexure and shear	19.9	4.5	0.77
MG-1	Flexure-bars	8.6	5.0	0.42

Table 5.2 Cyclic Test Results

Test	Failure Mode	P_{ult} (kips)	P_{cr} (kips)	Δ_{max} (in.)
ST-2	Bar yield, shear	26.8	6.0	0.57
FR-2	Flexure-concrete	21.3	6.5	0.66
D4-2	Flexure-concrete	23	5.5	0.73
D6-2	Flexure-concrete	19.6	6.0	0.70
MG-2	Flexure - bars	8.2	5.3	0.43

5.2 Monotonic Tests

The first series of tests were loaded monotonically to failure.

5.2.1 Test ST-1

Beam ST-1 was reinforced with two #4 steel reinforcing bars. First cracking occurred at the center line of the beam. The cracking load of 4.8 kips was less than the calculated cracking load of 6.7 kips (by Eq. 4-4). A second crack appeared 8 in. to the left of the first at about 10 kips. A third crack occurred, at the same distance, on the right side of center at about 12 kips. The crack locations did not correspond to the location of the transverse bars. Figure 5.1 shows the cracking pattern. The cracks continued to propagate as additional load was applied.

The beam failed suddenly and unexpectedly in shear at the left end. Maximum applied load was 20.8 kips. Centerline deflection at ultimate load was 0.38 in. Immediately after failure, the load dropped to about 7 kips. Further extension of the ram simply caused the beam to deflect and increased the size of the shear crack, with no additional load capacity. Figure 5.2 shows the load-deflection behavior for ST-1.

Maximum indicated concrete strain was about 0.0014 in./in. Crushing of the concrete due to flexure was not evident. Indicated bar strains were on the order of 0.004 in./in. at ultimate. Based on the calibration and tensile tests, this indicates a stress just beyond the bar yield point of 93 ksi. Plots of concrete and reinforcement strain are shown in Fig. 5.3 and Fig. 5.4, respectively.

5.2.2 Test FR-1

Beam FR-1 was reinforced with two #4 FRP bars. First cracking occurred at 6 kips, and was more violent and sudden than ST-1. The crack caused a significant drop in load, to 2.6 kips. Second cracking occurred at about 10 kips, dropping the load to 8.3 kips. Cracking was less violent than the first time. The first crack was located at midspan, the second about 8 in. to the left of center. The cracking pattern is shown in Fig. 5.5.

No further cracks developed during this test. At a load of 16.9 kips, it was observed that the top surface of concrete had begun crushing. Indicated strain in the concrete was 0.0037 in./in. at this point. Further loading increased the distress in the concrete. Once the concrete began crushing, the specimen continued to deflect, although the applied load dropped slowly. Frequent cracking noises were heard during this time. The specimen settled violently when it was attempted to apply further load. Ultimate load of 18.8 kips was reached, then capacity dropped to 10 kips. Deflection at ultimate was 0.75 in. Figure 5.6 shows the load-deflection plot for this test.

The ram was extended further in an attempt to achieve one inch of deflection, which was reached at a post-peak load capacity of 12 kips. Upon further extension, the concrete cracked completely through at the location of the first crack and the load

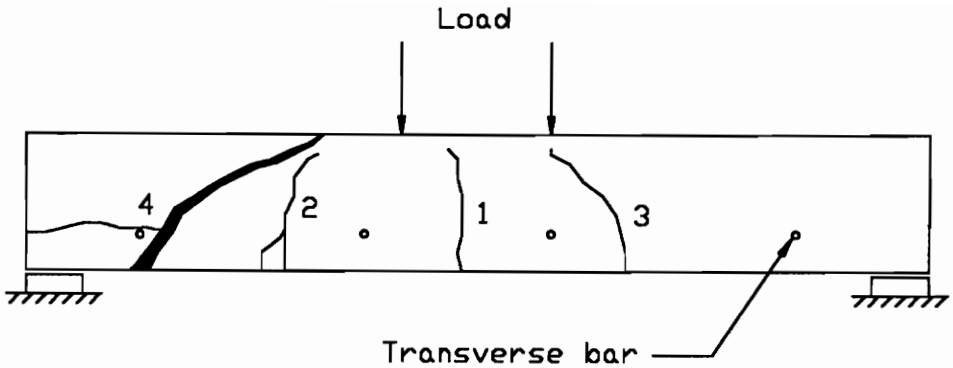

Figure 5.1 Cracking Pattern for Test ST-1

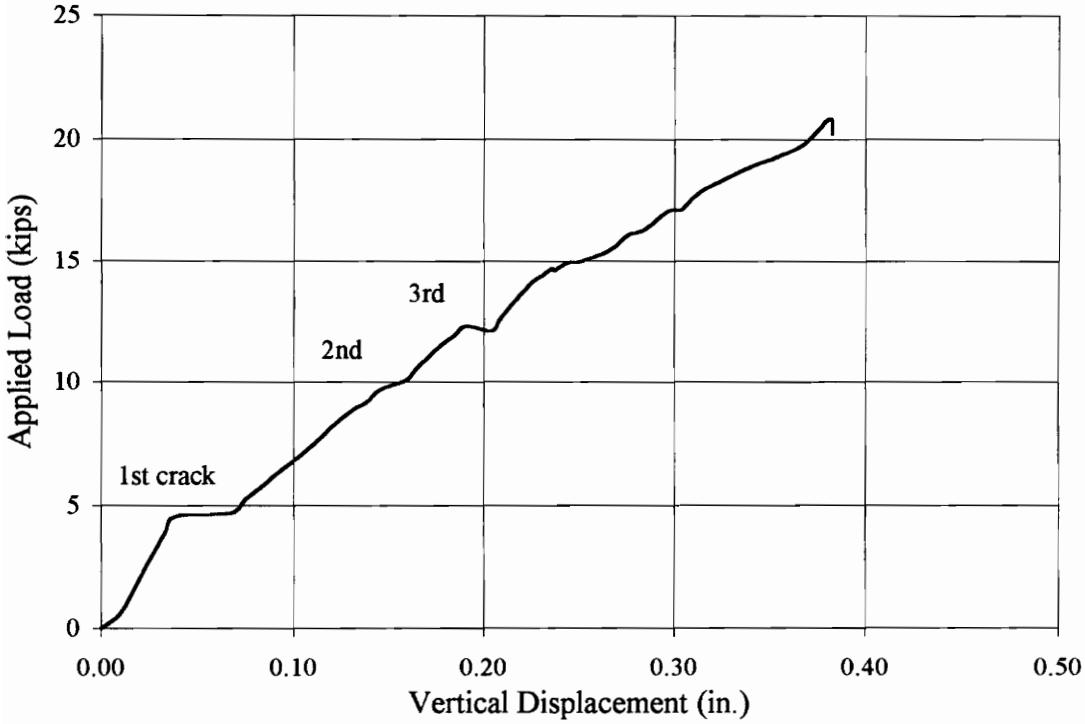

Figure 5.2 Load v. Vertical Displacement, Test ST-1

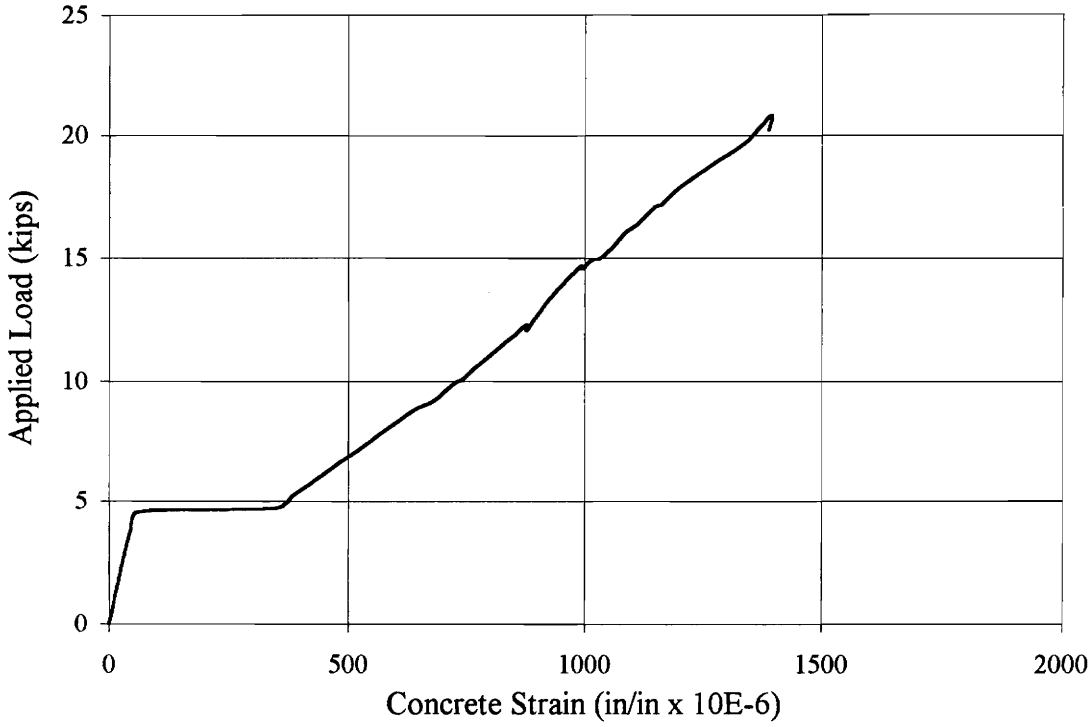

Figure 5.3 Load v. Concrete Strain, Test ST-1

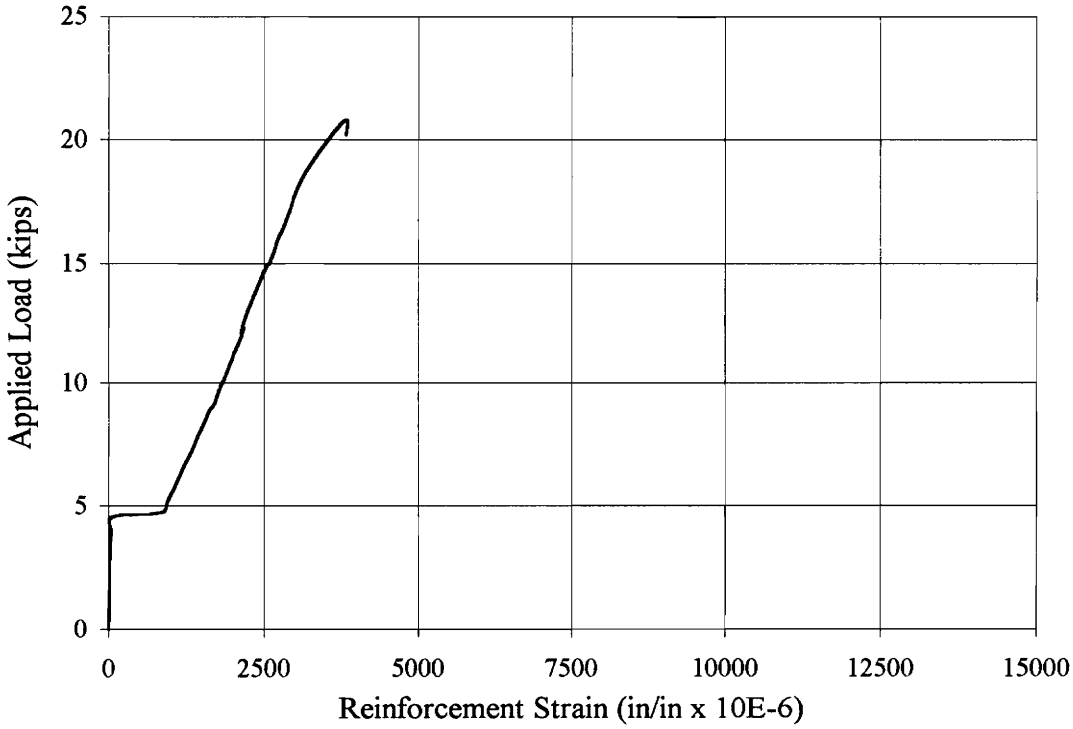

Figure 5.4 Load v. Reinforcement Strain, Test ST-1

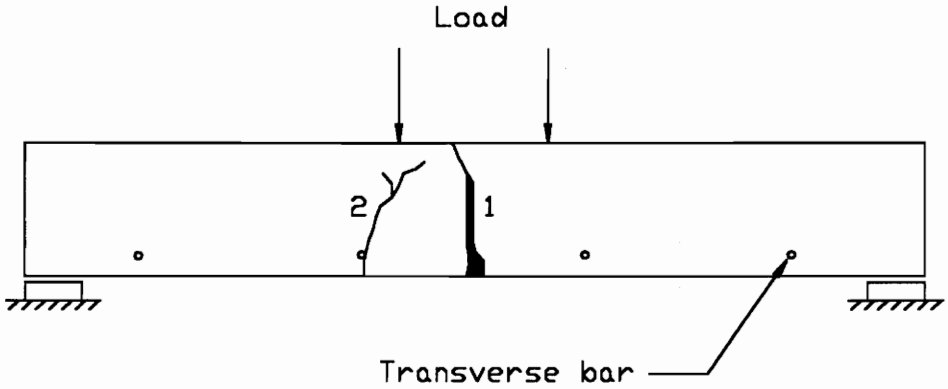

Figure 5.5 Cracking Pattern for Test FR-1

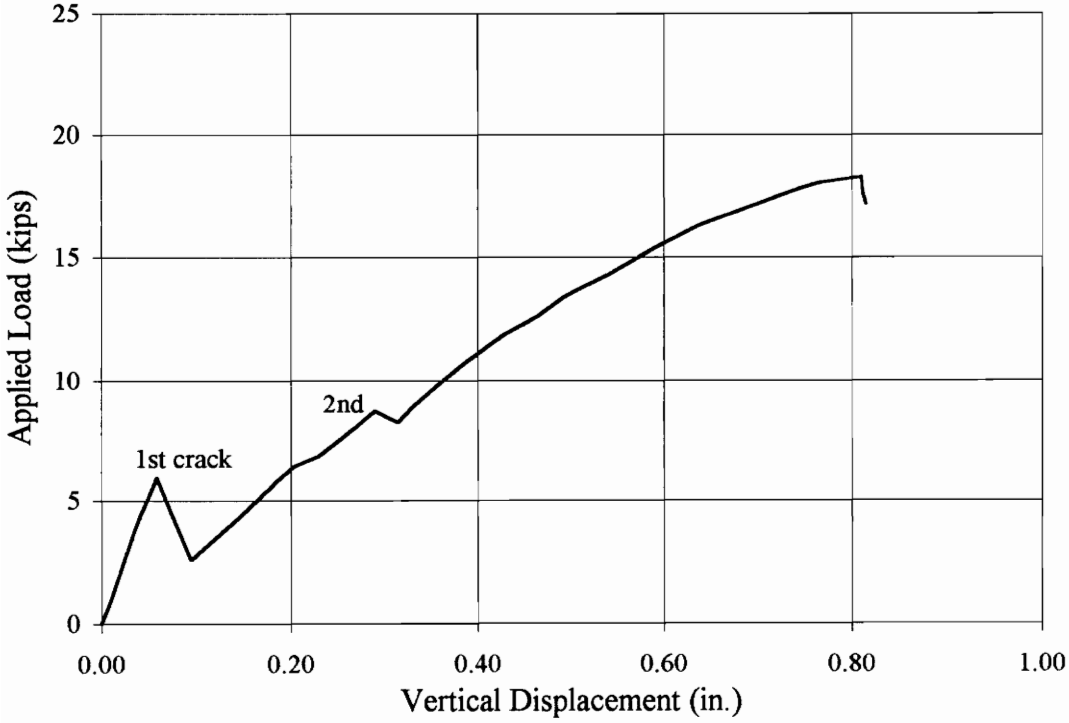

Figure 5.6 Load v. Vertical Displacement, Test FR-1

capacity dropped to zero. The deflection increased to nearly 1.4 in., and remained at that level even after the specimen was completely unloaded.

The concrete gage functioned well until the concrete began crushing. After crushing set in, the gage indicated a decrease in strain. The concrete directly under the gage was crushing, causing the gage to deform and not indicate a true strain in the concrete. Figure 5.7 shows the concrete strain data for this test.

Several problems were encountered with the strain gages on the bars. Bar #1 (part of Group II with the two gages wired in series) indicated an "offscale" reading immediately after first cracking. This meant that the strain went beyond the range of the gages. It was not known if this was because the gage was at the crack and overstrained, if the cracking damaged the gage or wiring, or if the gages simply malfunctioned. As a result of this failure, there is no strain data from bar #1.

Bar #2, with the two gages wired individually, functioned well until indicated strains increased above 15000 microstrains (0.015 in./in.), at an applied load of about 17 kips. Stress in the bar, calculated from the load-strain relation acquired during calibration, was about 70 ksi at that time. A plot of the strain data from bar #2 is in Fig. 5.8.

5.2.3 Test D4-1

Test specimen D4-1 was reinforced with a Duragrid grating with three longitudinal 1 in. I-bars spaced 4.5 in. on center. First cracking occurred at 5 kips, under the right load point. The second crack occurred at 8 kips, about 6 in. to the left of the first. A third crack occurred at 10 kips, 6 in. to the left of the second. The fourth crack occurred at about 14 kips, to the right of the first. All flexure cracks lined up with the location of transverse bars. Figure 5.9 shows the crack pattern for test D4-1.

The outermost cracks (2nd and 4th) began branching as the load increased, similar to test ST-1, indicating that a shear failure would eventually take place. The shear crack became apparent at about 28 kips. The beam was loaded starting from 27 kips, but upon reaching about 28.8 kips, the load began dropping quickly, in about a minute it had

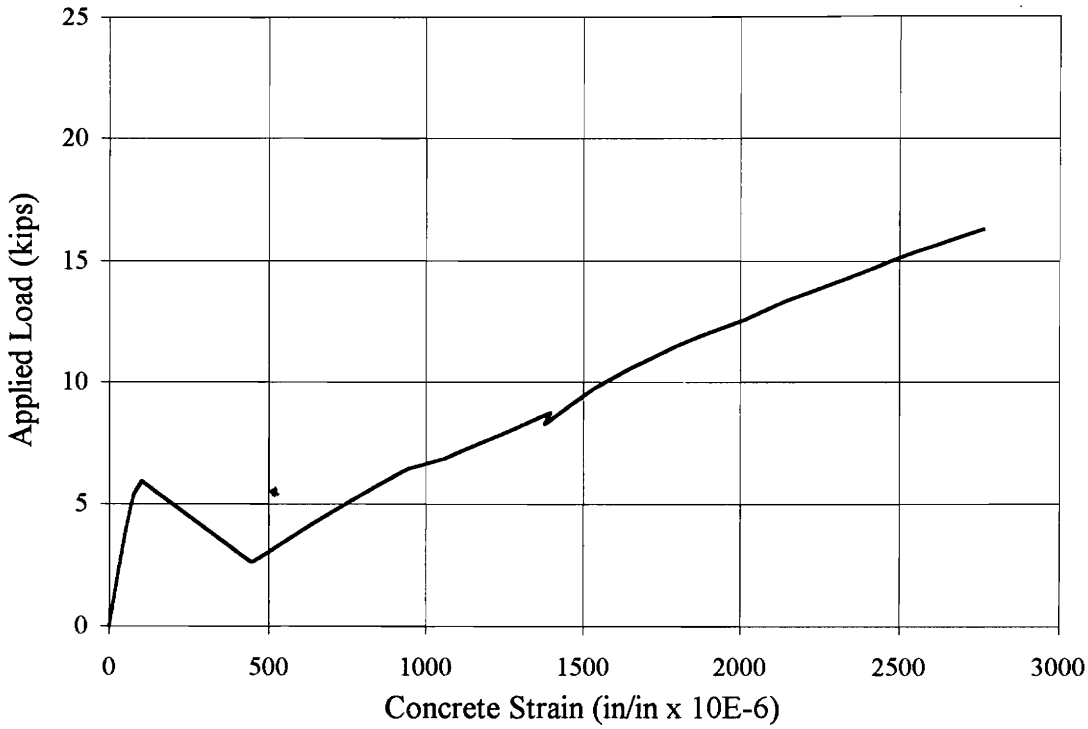

Figure 5.7 Load v. Concrete Strain, Test FR-1

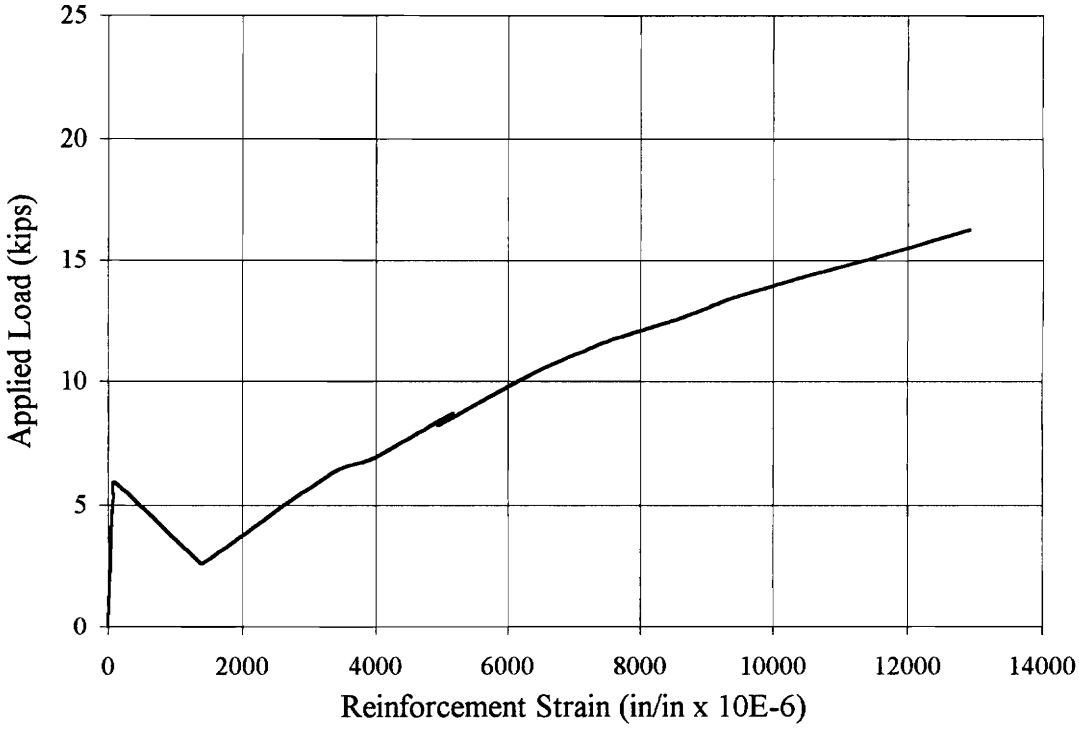

Figure 5.8 Load v. Reinforcement Strain, Test FR-1

returned to just over 27 kips, where it eventually stabilized. Examination of the specimen at that point revealed the shear crack. Ultimate load proved to be 28.8 kips, although it was not sustained. Deflection at ultimate was 0.67 in.

Upon further extension of the ram, the shear crack opened up and it was apparent that the concrete was crushing at the location of the right-side load point. Load capacity quickly dropped to 23 kips. Further extension only increased the shear cracking, the concrete distress and the deflection. Several loud sounds were heard during this extension. It was attempted to deform the beam further to reach one inch of displacement, which was reached with a final load of 8.5 kips. Extension was stopped at this point and all load removed. The beam did not rebound much, with a permanent deflection of one inch. A load-deflection plot is given in Fig. 5.10.

Following the test, the beam was examined. It was apparent that the Duragrid bars had broken in the area of the shear crack. Between two transverse bars, the I-bar was split in two through the web, the flanges pulling away from each other, as shown in Fig. 5.11. On one of the bars, it was apparent that the grid had bent at a transverse bar, almost forming a hinge. It is assumed that the bars broke during the post-peak loading, after the shear failure of the beam.

The indicated concrete strain at midspan remained very low throughout the test, peaking at about 0.001 in./in. However, since crushing did occur at a point away from the gage, this is not a completely accurate picture of the concrete's behavior. From statics, the bending moment in the beam is constant between the two loads. Crushing of the concrete can occur anywhere between these loads, depending on where the section is weakest, not necessarily at midspan where the gage is located. Figure 5.12 shows the load versus concrete strain behavior for this test.

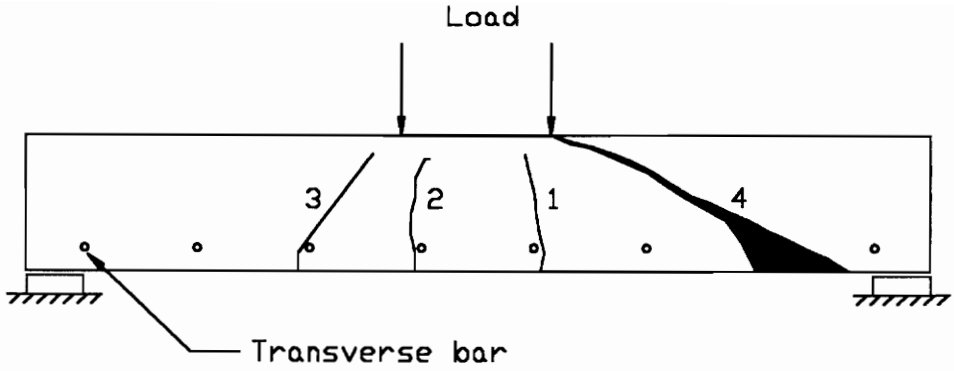

Figure 5.9 Cracking Pattern for Test D4-1

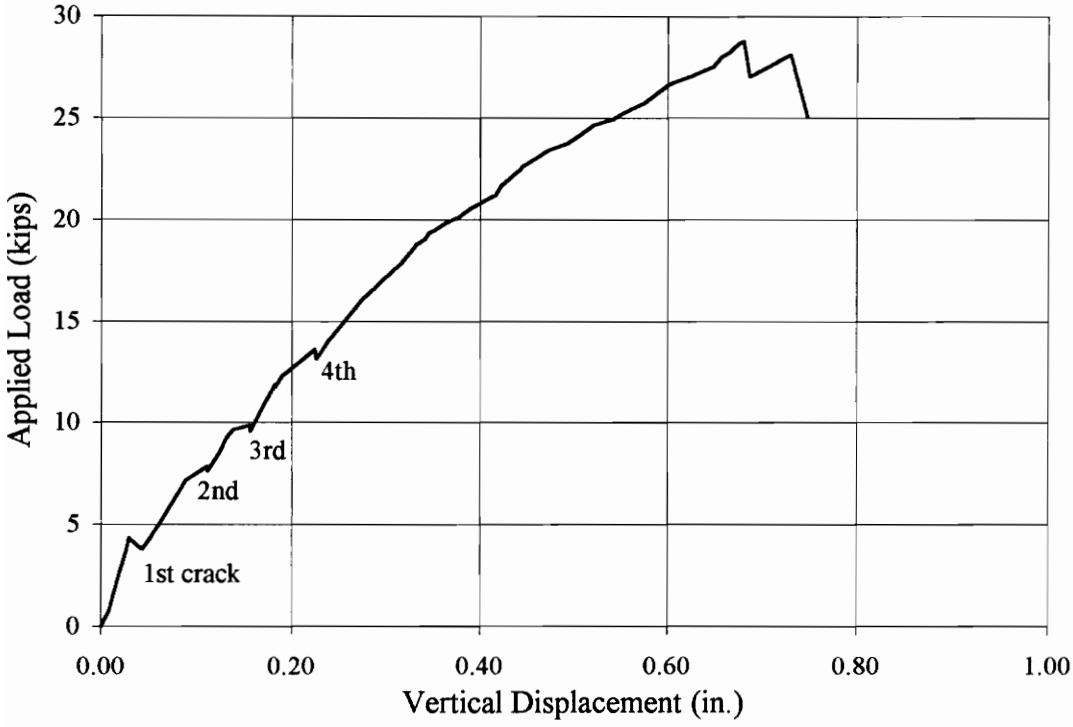

Figure 5.10 Load v. Vertical Displacement, Test D4-1

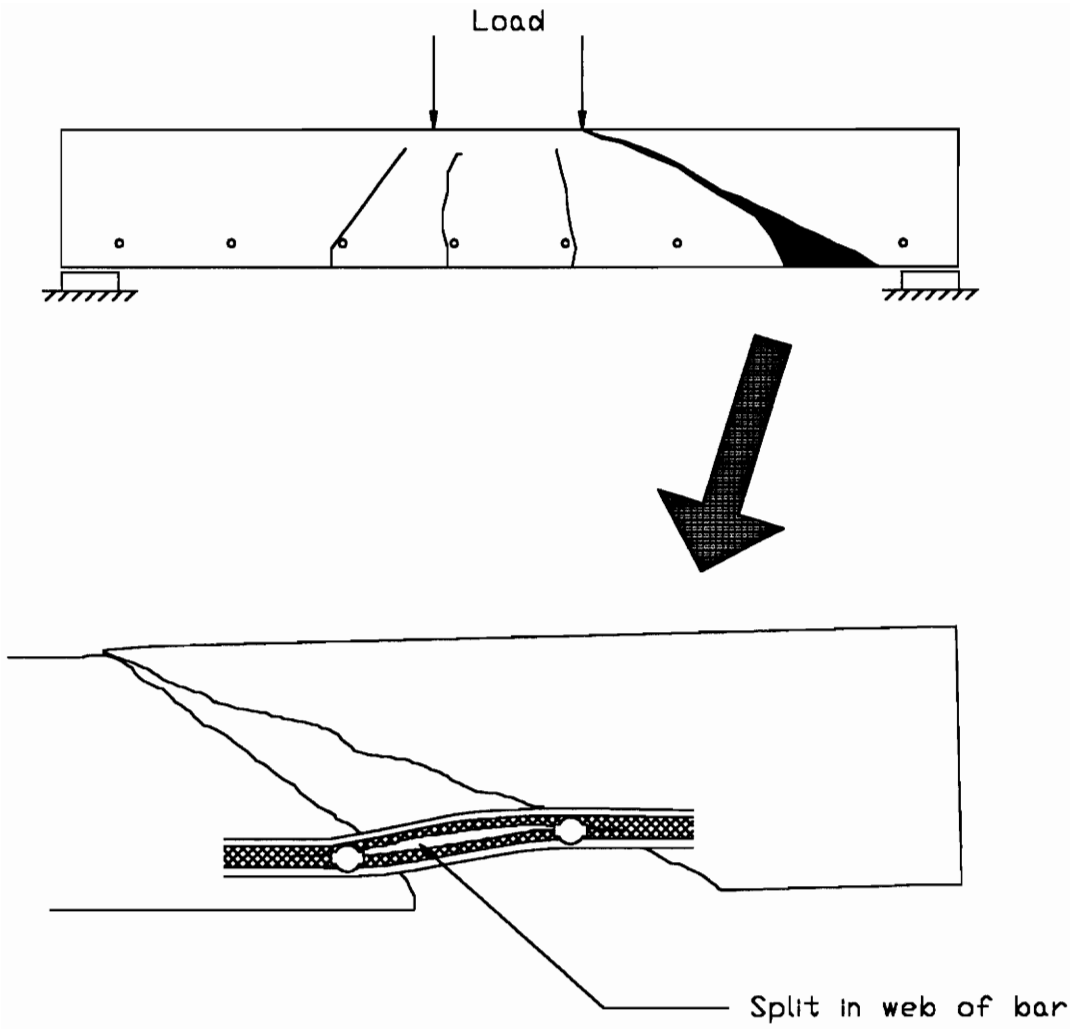

Figure 5.11 Failure of Duragrid Bar, Test D4-1

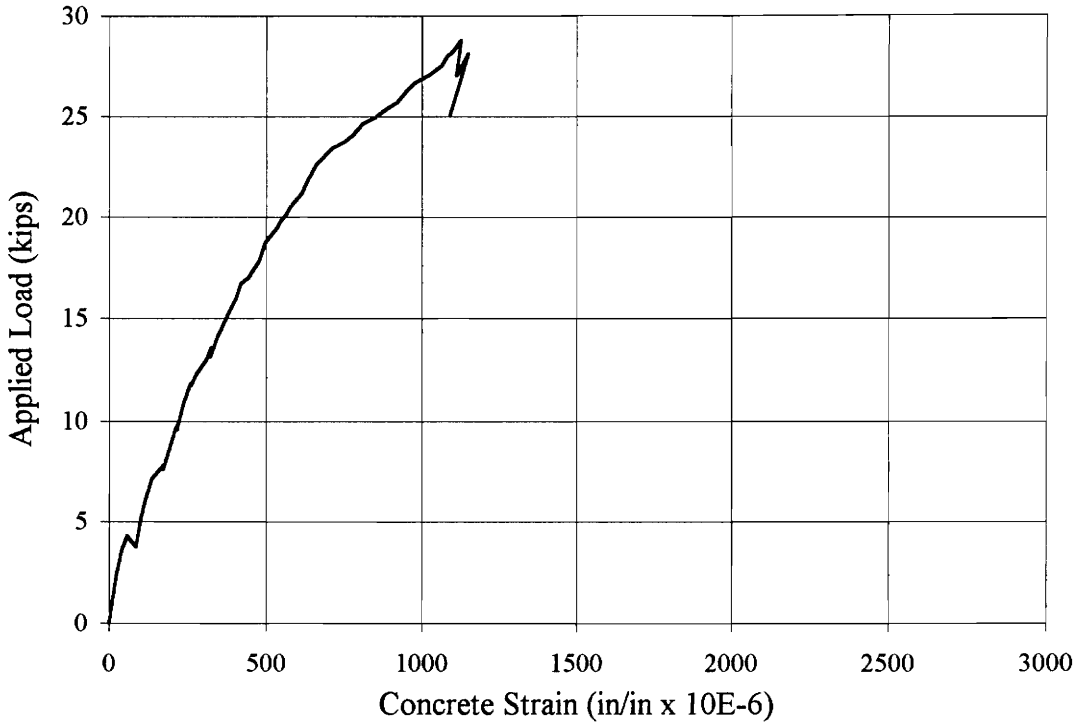

Figure 5.12 Load v. Concrete Strain, Test D4-1

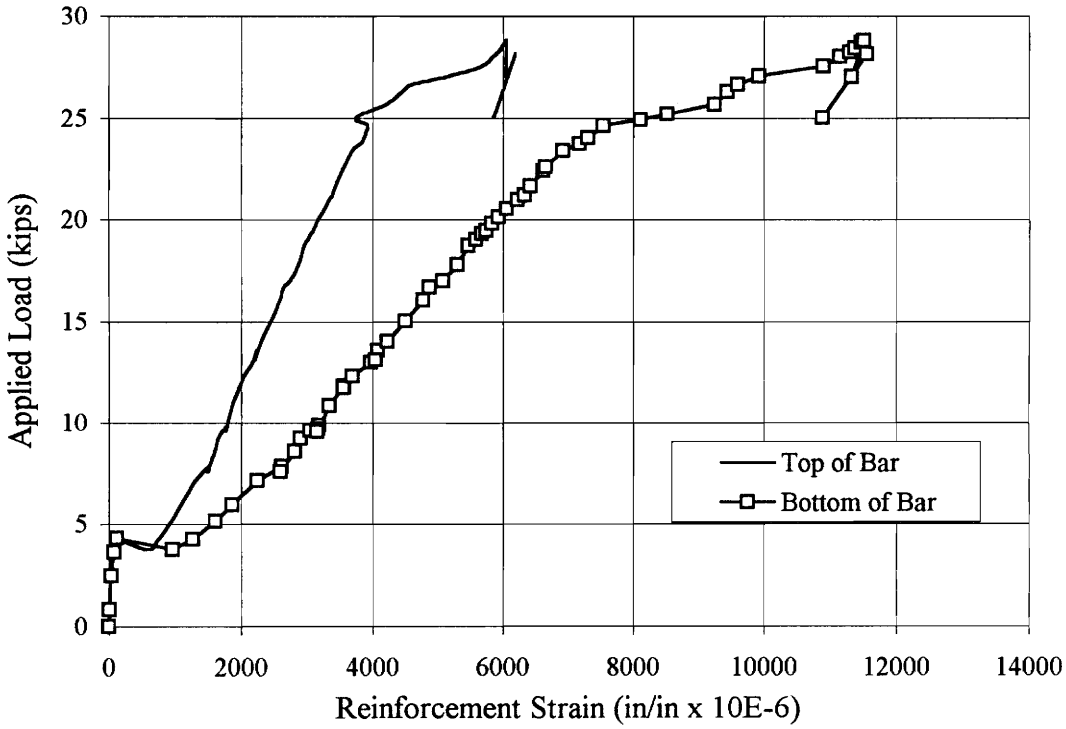

Figure 5.13 Load v. Reinforcement Strain, Test D4-1

The bar strain gages indicated a significant difference in strain between the top and bottom flanges of the bars. At ultimate, the gages on the top reported a strain of about 0.006 in./in., while those on the bottom indicated a strain of 0.011 in./in. The calculated stresses were 32 ksi and 59 ksi, respectively. A plot of load versus bar strains is shown in Fig. 5.13.

5.2.4 Test D6-1

Beam D6-1 contained Duragrid reinforcing with two bars 6 in. on center. First cracking occurred at 4.5 kips, located at the transverse bar just to the left of center. Second cracking occurred at 7.7 kips, 12 in. to the right of the first. A third main crack appeared at about 17 kips, 6 in. to the left of the first. Figure 5.14 shows the crack pattern. As with test D4-1, the crack locations corresponded to the location of the transverse bars.

Some crushing of the concrete under the back right load point was first observed at 18.7 kips. The beam was then loaded to 19.9 kips (ultimate load), when loading was stopped as several loud cracking noises were heard. A shear crack opened up and the load dropped quickly to about 14 kips. The beam held this load for about three minutes, then all of the indicated strains began dropping, loud cracking sounds were heard and the beam suddenly collapsed. Displacement increased from 0.87 in. to 1.04 in. and load capacity dropped to about 1 kip. At this point, all load was removed and the test concluded. Figure 5.15 shows the load-deflection behavior for this test.

Indicated concrete strain at ultimate load was only 0.00083 in./in., although crushing of the concrete was observed. The concrete strain data is plotted in Fig. 5.16. As with test D4-1, the bar strain gages indicated a difference between the top and bottom of the bar, although not as extreme. At ultimate, the strains were 0.011 in./in. (equivalent to a stress of 59 ksi) and 0.013 in./in. (69 ksi), respectively. Figure 5.17 provides a plot of load versus bar strain.

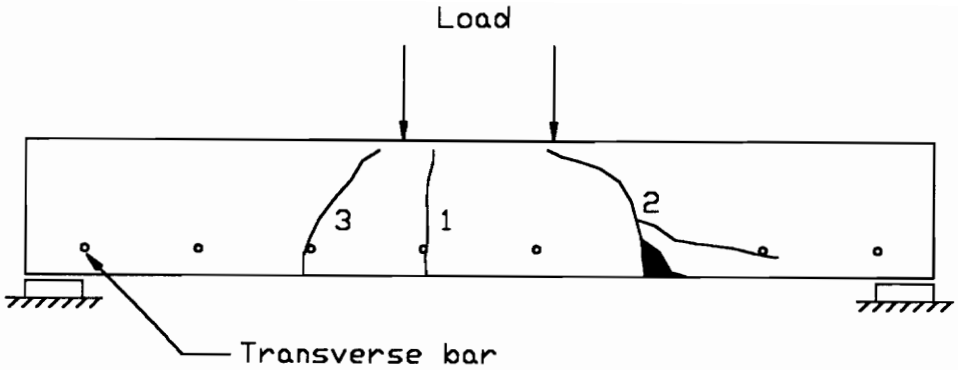

Figure 5.14 Cracking Pattern for Test D6-1

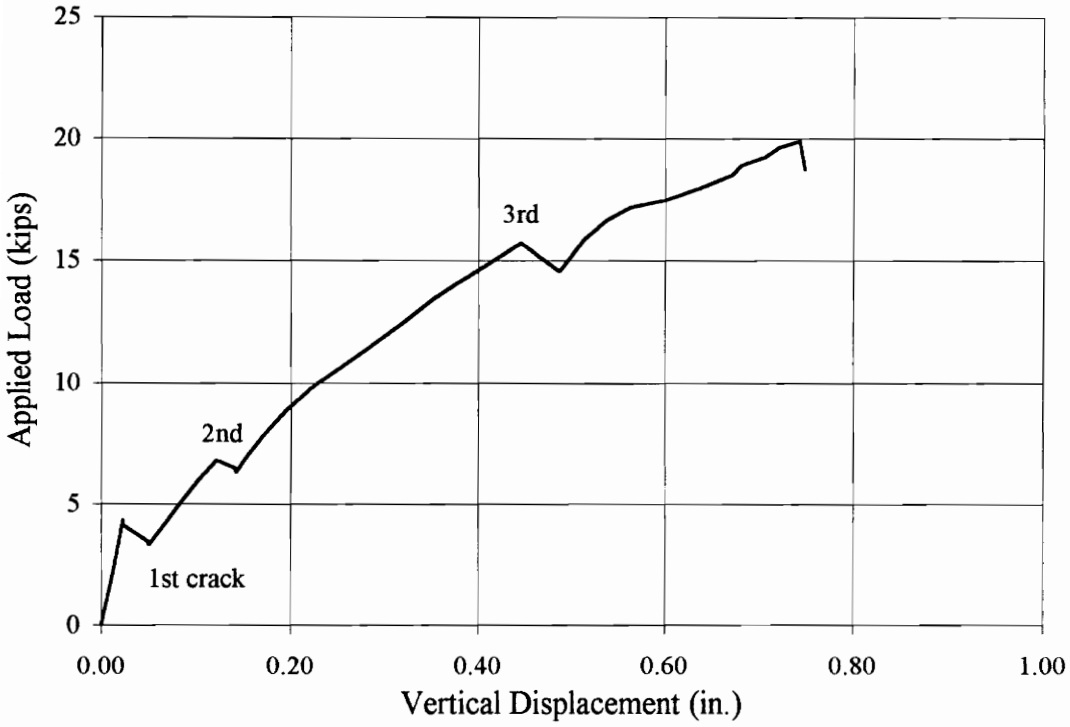

Figure 5.15 Load v. Vertical Displacement, Test D6-1

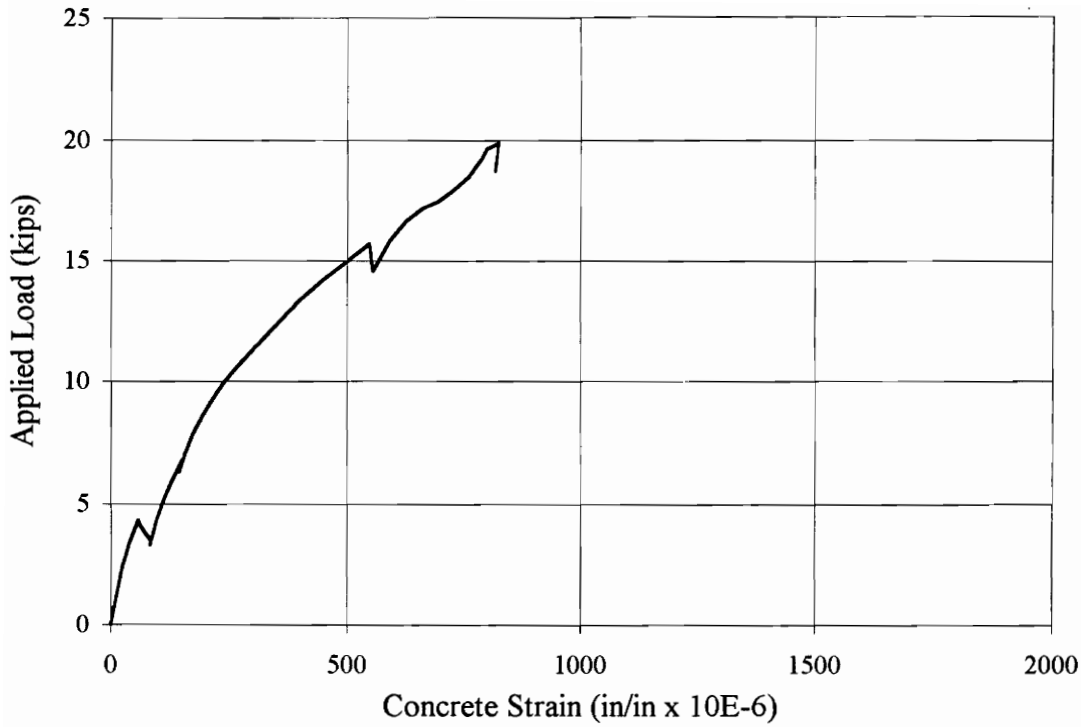

Figure 5.16 Load v. Concrete Strain, Test D6-1

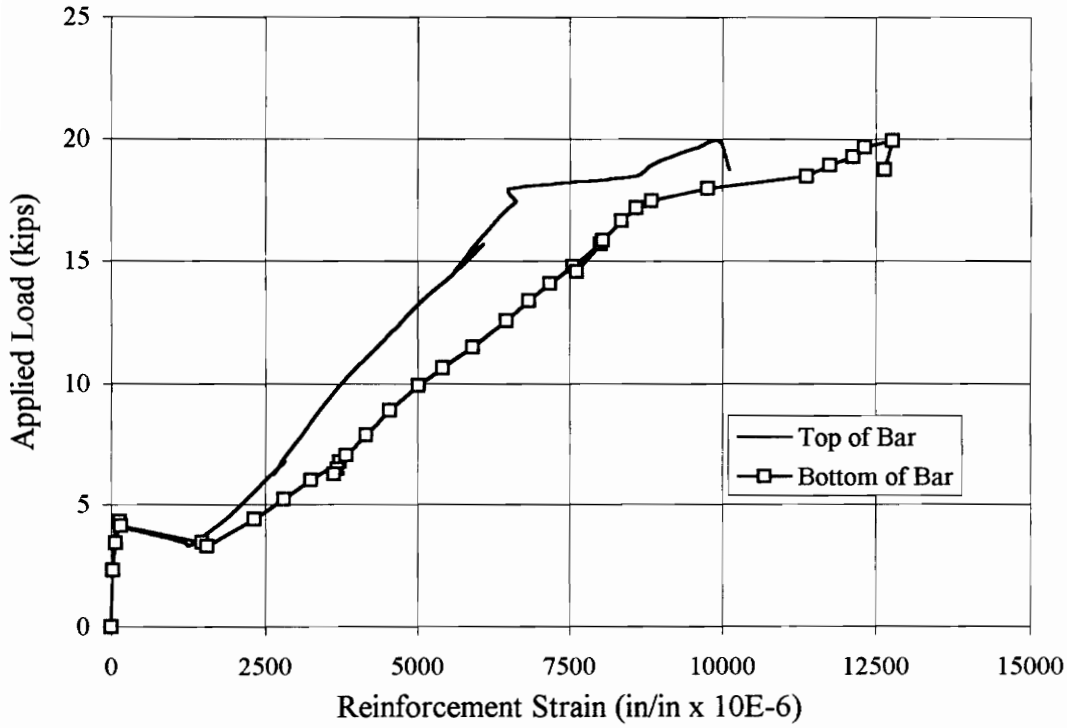

Figure 5.17 Load v. Reinforcement Strain, Test D6-1

5.2.5 Test MG-1

Test beam MG-1 was reinforced with a 1 ft by 4 ft sheet of Multigrid grating. More cracks developed on MG-1 than on any of the previous tests. A first crack occurred just left of midspan at about 5 kips. The second crack occurred to the right of midspan at 6.3 kips. A third crack appeared at 7.5 kips, 2 in. to the right of the second, but was visible only on the front. A fourth crack formed during the next load step (only 7 kips, as the load had dropped following the third crack) to the left of the first. A fifth crack appeared at the centerline when the load again reached 7.5 kips. Figure 5.18 shows the cracking pattern.

After the fifth crack, deflections increased with little increase in load capacity. Failure occurred as the centerline crack opened up and the bars fractured. Loading was stopped at 8.6 kips (ultimate load), from which the load slowly dropped to about 8 kips, accompanied by cracking noises. Then several louder cracks were heard and the capacity dropped to 6 kips and then 4.9 kips. Several moments later, more loud cracking occurred and the load dropped to 1.4 kips. Further ram extension only increased deflection, while the load decreased to zero. A load-deflection plot for the test is shown in Fig. 5.19.

The cracks occurred at the locations of the transverse bars. The cracks were spaced at increments of 2 in., equal to the grid spacing. The grid was visible in the center crack. The bars appeared stressed, with some cracks in them, though no tensile failure was immediately apparent. At one intersection of bars, it appeared that the transverse bar had been sheared off from the longitudinal bar. This is not surprising, given that fiberglass-reinforced plastics are typically weak when loaded transverse to the fibers. No delamination of concrete at the level of the grid was visible.

The concrete strains were closer to those measured in test FR-1 than to the other tests. At peak load, indicated concrete strain was about 0.001 in./in. No distress to the concrete was visible, even at maximum deflection. The concrete strain curve is shown in Fig. 5.20.

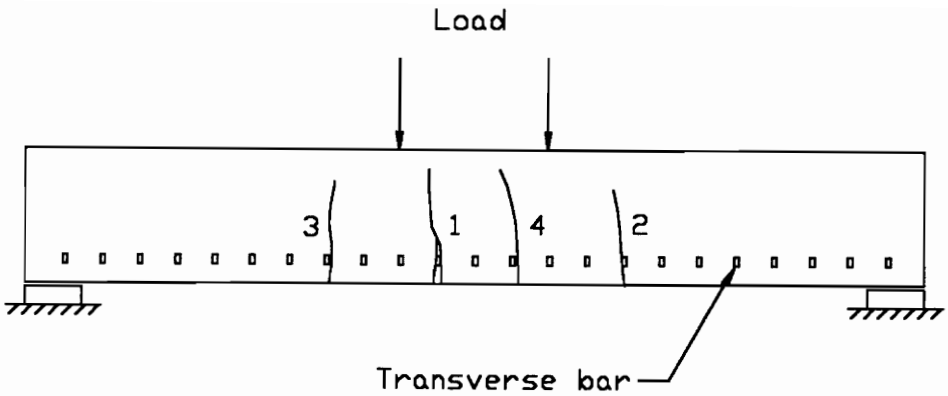

Figure 5.18 Cracking Pattern for Test MG-1

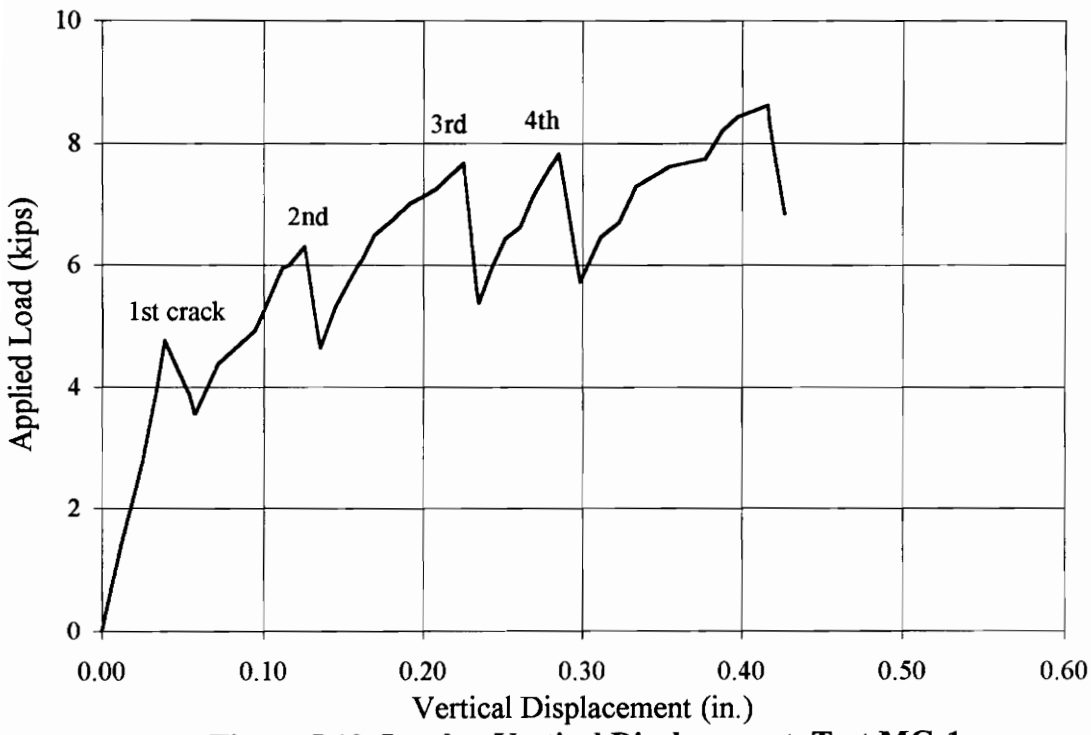

Figure 5.19 Load v. Vertical Displacement, Test MG-1

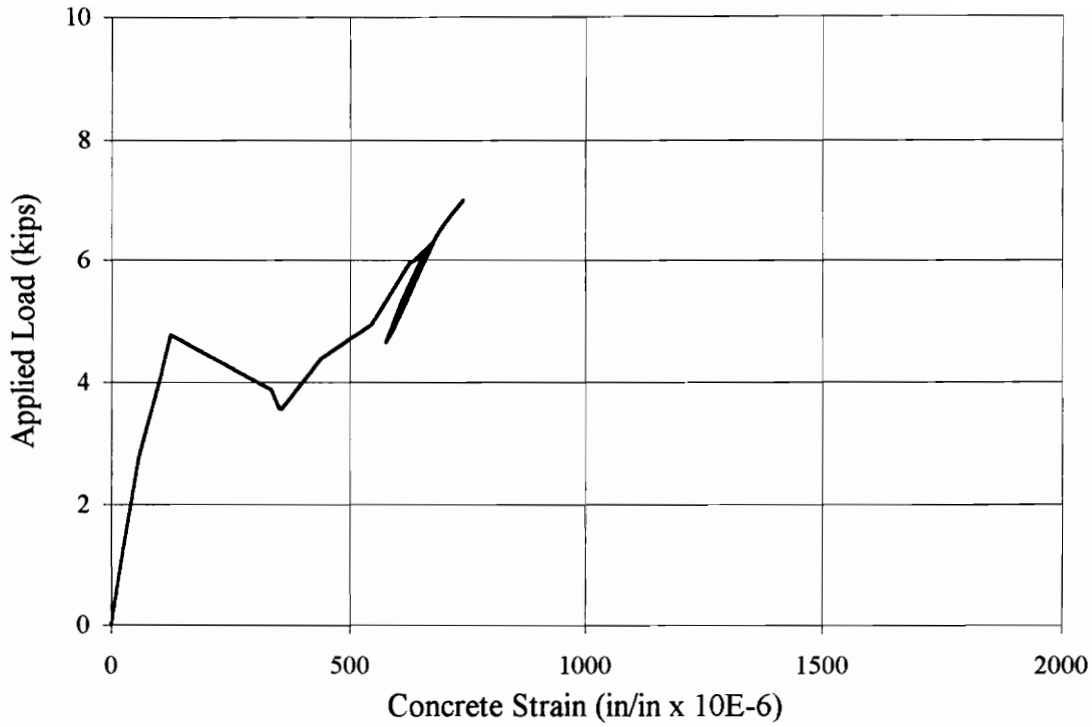

Figure 5.20 Load v. Concrete Strain, Test MG-1

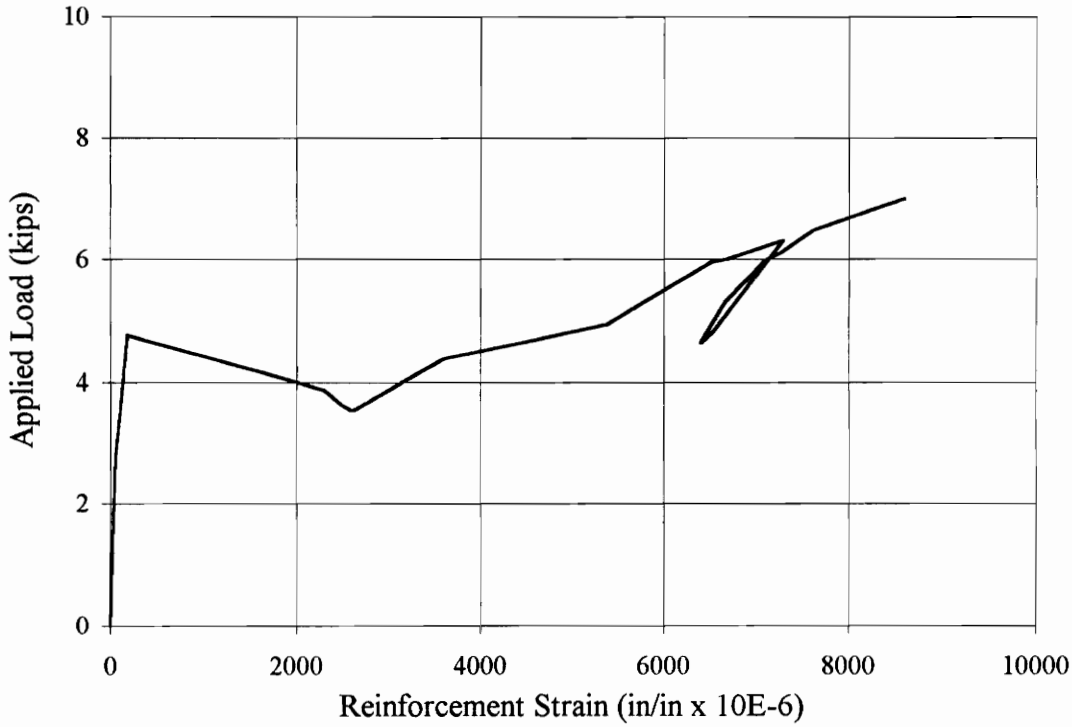

Figure 5.21 Load v. Reinforcement Strain, Test MG-1

Indicated bar strains were quite high at ultimate, almost 0.014 in./in. This corresponds to a bar force of approximately 2000 lb, which is equal to the tensile capacity determined from the tensile tests (Chapter 3). Figure 5.21 shows the bar strain behavior for this test.

5.3 Cyclic Tests

The second set of tests were loaded cyclically in increments of percent of the ultimate load determined from the first set (See Table 4.3 and Fig. 4.8). Seven cycles were performed to each load level. Following the last cycle, the beams were loaded monotonically to failure. Table 5.3 lists the load levels used for each cyclic test.

Table 5.3: Loading Levels for Cyclic Tests

	Applied Load - kips					
Test	Mono. Ult.	20%	35%	50%	65%	80%
ST-2	20.8	4	7	10	14	17
FR-2	18.8	3	6	9	12	15
D4-2	28.8	6	10	14	18	22
D6-2	19.9	4	7	10	13	16
MG-2	8.6	1.7	3	4.3	5.6	6.9

The data plots provided are simplified from the actual test data. Typically, only the peak values for the first and last cycle at each load level are plotted. This was done to clarify the plots by removing intermediate points.

The cyclic tests followed some general trends. The cycles at 20 percent of ultimate were typically below the first cracking load and so had little apparent effect on the beams and produced no obvious damage. Cycles at 20 percent, even after cracking had occurred, were essentially repetitive, with the displacement and strain values (at 20 percent and at zero load) returning to the same point on their respective curves. Load-displacement plots of the post-cracking 20 percent cycles show an obvious change in

stiffness from the pre-cracking cycles. Figure 5.22 shows a typical load-deflection plot for four successive cycles at 20 percent of ultimate.

Cycles at the higher load levels did not behave as uniformly. The peak and zero-load values of displacement and strain tended to increase slightly with each cycle in a series, though the difference appeared to decrease with each cycle. With each higher level, the permanent set (data readings at zero load) generally increased. Figure 5.23 shows a typical load-deflection plot for a cycle of 80 percent.

5.3.1 Test ST-2

Beam ST-2 was reinforced with two #4 steel bars. Load was cycled at the following levels: 4 kips, 7 kips, 10 kips, 14 kips, 17 kips. The first series of loads to 4 kips produced no cracking.

First cracking, a flexure crack at midspan, occurred at 6 kips, during the first loading to 7 kips. No further cracks occurred during the remaining cycles to 7 kips, nor during the following 4 kip cycle. A second crack formed 10 in. to the right of the first when the load first reached 10 kips. The remaining 10 kip cycles and the next series of 4 kip cycles proceeded without incident.

A third crack occurred on the other side of center from the second at 12 kips, during the first loading to 14 kips. No more cracks occurred during the rest of the test. The existing cracks continued to propagate during the remaining cycles. Figure 5.24 shows the crack pattern for this test.

Following the last 17 kip loading, the beam was unloaded and then loaded monotonically to failure. At a load of about 21 kips, it became apparent that the steel bars were beginning to yield, as the bar strains increased rapidly with little increase in applied load. The beam continued to carry load, although deflections increased significantly, until shear failure occurred. Ultimate load was 26.8 kips, with a deflection of 0.57 in.

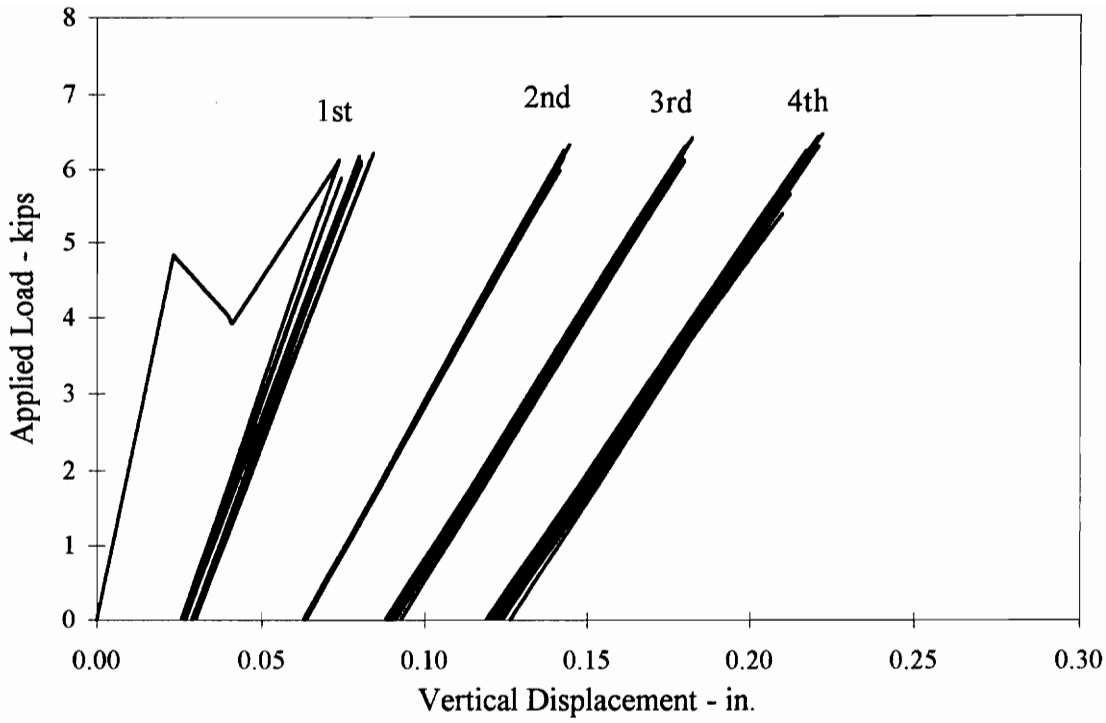

Figure 5.22 Typical Load-Deflection Behavior for Cycles at 20% of Ultimate

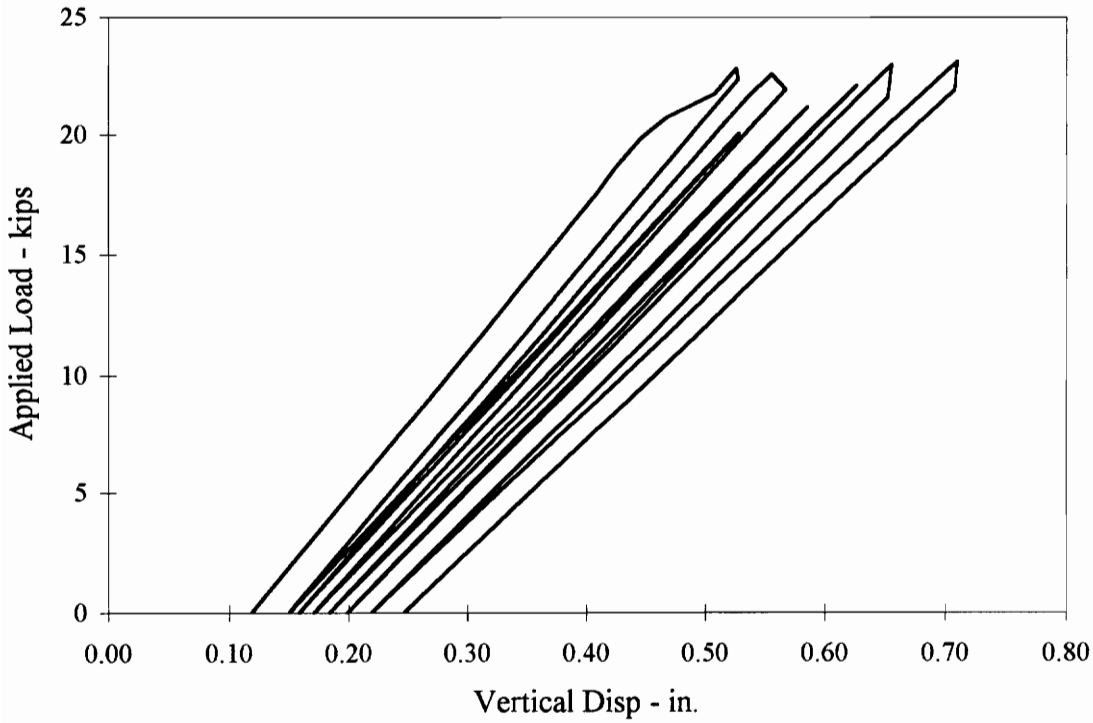

Figure 5.23 Typical Load-Deflection Behavior for Cycle to 80% of Ultimate

Capacity dropped to 7 kips, and further ram extension simply deflected the beam and increased the size of the shear crack, with no additional load capacity. A load-deflection plot is shown in Fig. 5.25.

Indicated concrete strain reached 0.0028 in./in. at ultimate load. It appeared that the concrete was just beginning to crush when the shear crack occurred. The concrete did crush extensively on top where the shear crack extended to the load point. Figure 5.26 shows the load-concrete strain curve for this test.

As stated above, the bar strains increased rapidly above an applied load of 21 kips. At ultimate, the indicated strains were 0.012 in./in., well above the expected yield point of 0.00207 in./in. A plot of load versus bar strain, Fig. 5.27, shows that the bars were into the yield plateau region when beam failure occurred.

5.3.2 Test FR-2

Beam FR-2 was reinforced with two #4 FRP bars. Load was cycled at levels of 3 kips, 6 kips, 9 kips, 12 kips and 15 kips.

The first series of 3 kip load cycles did not produce any cracks, nor any significant change in stiffness between the first and last loading. The first crack occurred during the fourth loading to 6 kips, when the applied load reached about 6.5 kips. The crack occurred below the left load point and corresponded with the location of a transverse bar. The remainder of the 6 kip cycles proceeded without incident.

The second series of 3 kip cycles proceeded normally, with no additional cracks forming. There was a distinct loss in stiffness (based on the slope of the load-deflection curve) between this and the first 3 kip series. The 9 kip and 12 kip series went normally as well, though there were small increases in strain and deflection at successive zero points. The intervening 3 kip series showed little change in beam behavior.

A second crack appeared at 14.5 kips, on the first loading to 15 kips. It was located under the right load point, at the location of another transverse bar. During the next loadings to 15 kips, there were small increases in strain and deflection at successive

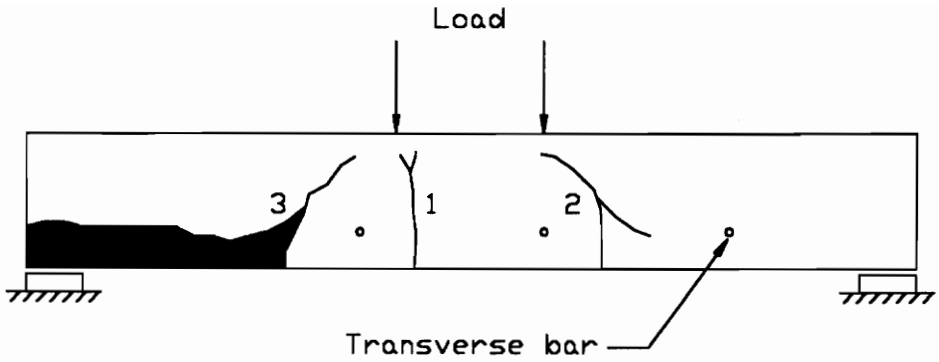

Figure 5.24 Cracking Pattern for Test ST-2

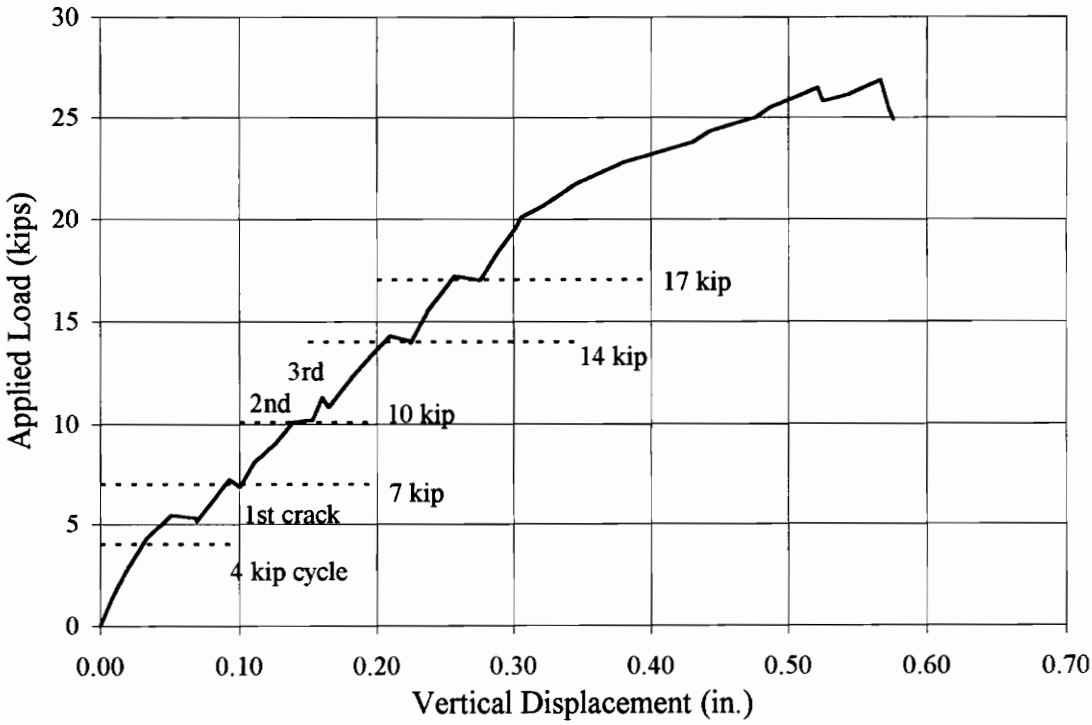

Figure 5.25 Load v. Vertical Displacement, Test ST-2

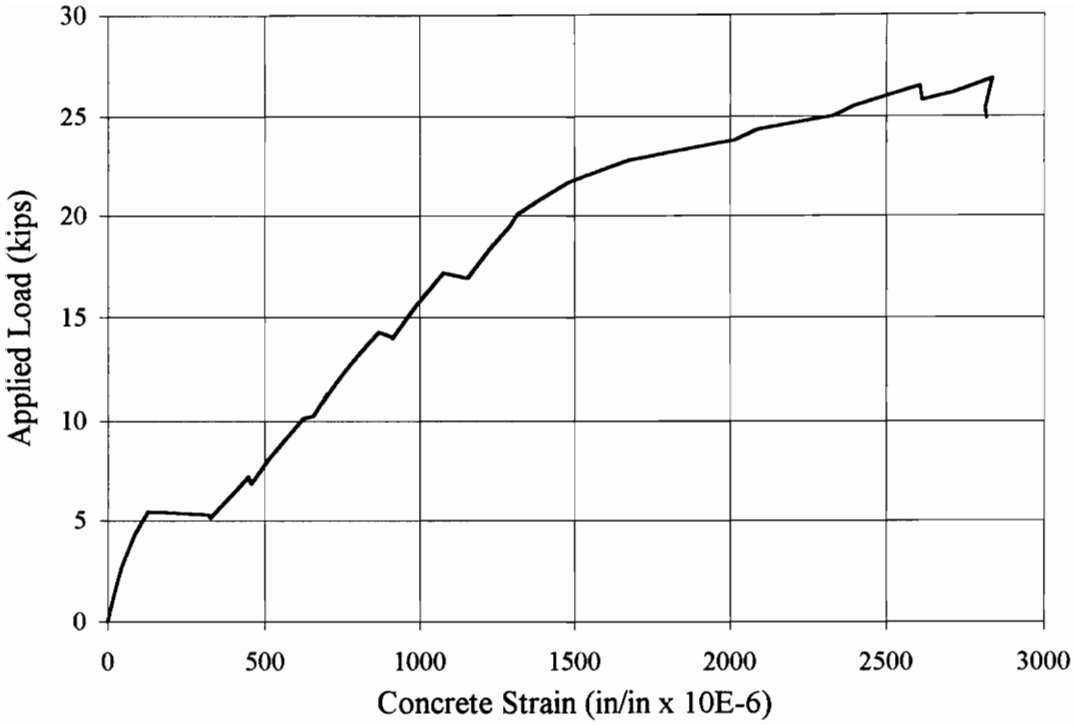

Figure 5.26 Load v. Concrete Strain, Test ST-2

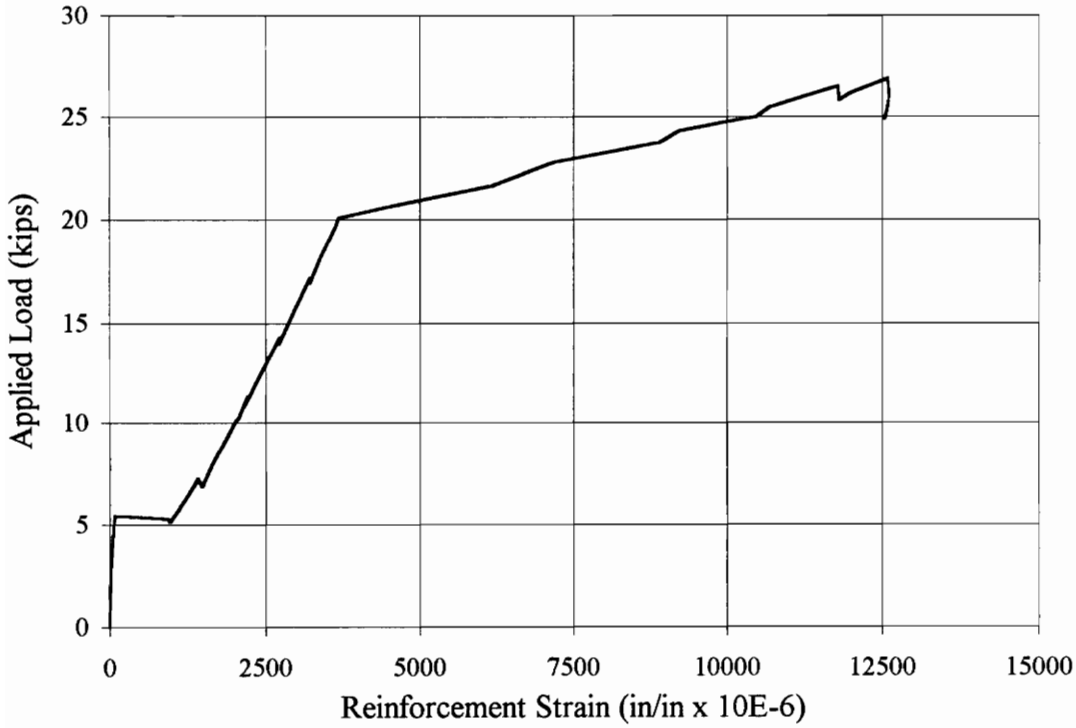

Figure 5.27 Load v. Reinforcement Strain, Test ST-2

zero points and larger increases in those values at maximum load. Also, after unloading for the third time, a crack was visible on top of the beam, running from the top of the first crack to the left support, on the back side only. Figure 5.28 shows the crack pattern.

Final loading followed the same initial stiffness as the 15 kip cycles. At 19.4 kips, it was observed that the concrete was beginning to crush slightly near the front left load point. The beam was loaded to 21.3 kips, the ultimate load reached. Load dropped slowly for about two minutes, during which faint cracking sounds were heard. When the load had decreased to 19.4 kips, there was a loud bang and the load dropped suddenly to about 12 kips. At this point, only the concrete on the front left had crushed.

The ram was extended further, although the post-peak load capacity was only 15 kips. Extension was halted when centerline deflection approached one inch. The concrete was crushed entirely across the top, and the flexure cracks had branched in several places, top and bottom. The load-displacement behavior is shown in Fig. 5.29.

Indicated strain in the concrete reached a maximum of 0.001 in./in., about a third of the strain expected before crushing. Obviously, since crushing did occur, the location of the gage did not correspond with the maximum strain, as with test D4-1 (Section 5.2.3). Figure 5.30 shows the concrete strain gage results for this test.

The bar gages indicated a stress of 70 ksi at ultimate applied load. The two gages on bar #4 (wired individually) performed flawlessly to just past ultimate, when their indicated strain exceeded 0.016 in./in. (equivalent to a stress of 77 ksi). The gages on bar #3 (wired in series) went offscale during the cycles of 9 kips, when indicated bar stress was only about 28 ksi. Up to that point, however, they had performed quite well. This problem was expected as bar #3 was only calibrated to 5 kip (tensile force) because of the gages' tendency to go offscale at high loads. A plot of strain data from bar #4 is shown in Fig. 5.31.

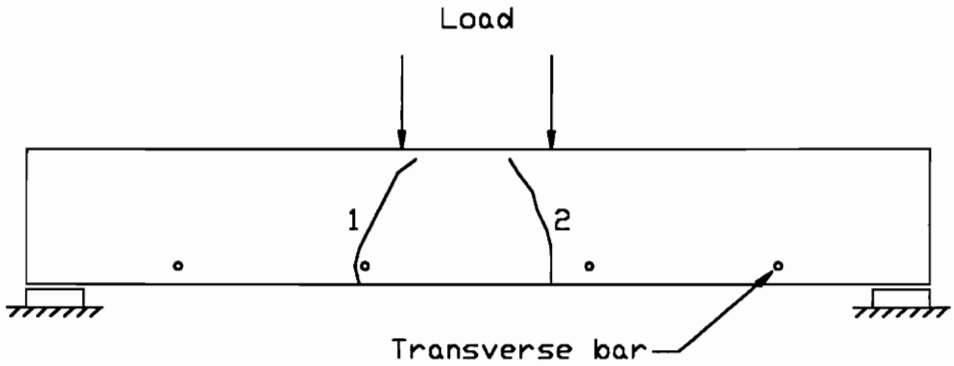

Figure 5.28 Cracking Pattern for Test FR-2

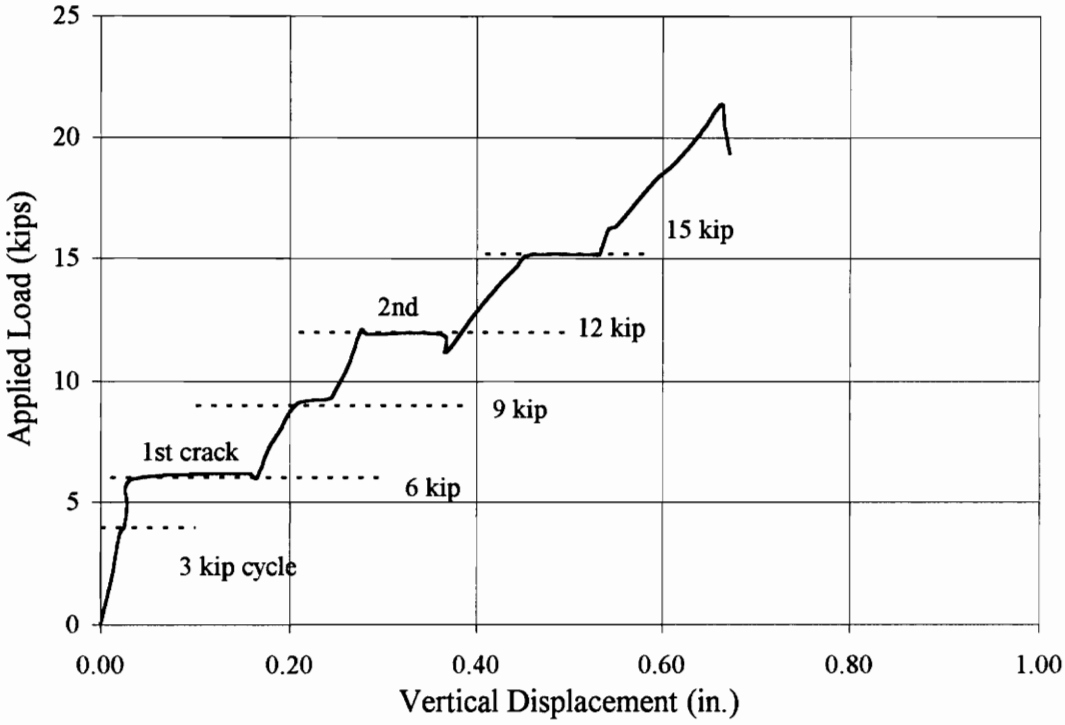

Figure 5.29 Load v. Vertical Displacement, Test FR-2

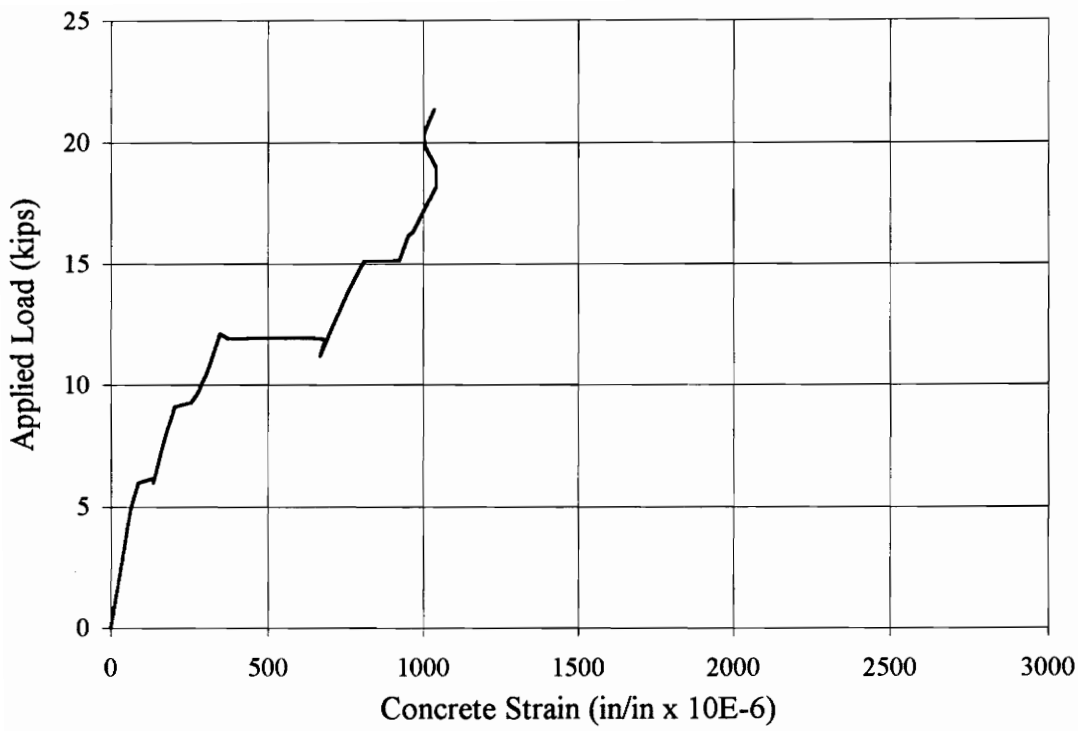

Figure 5.30 Load v. Concrete Strain, Test FR-2

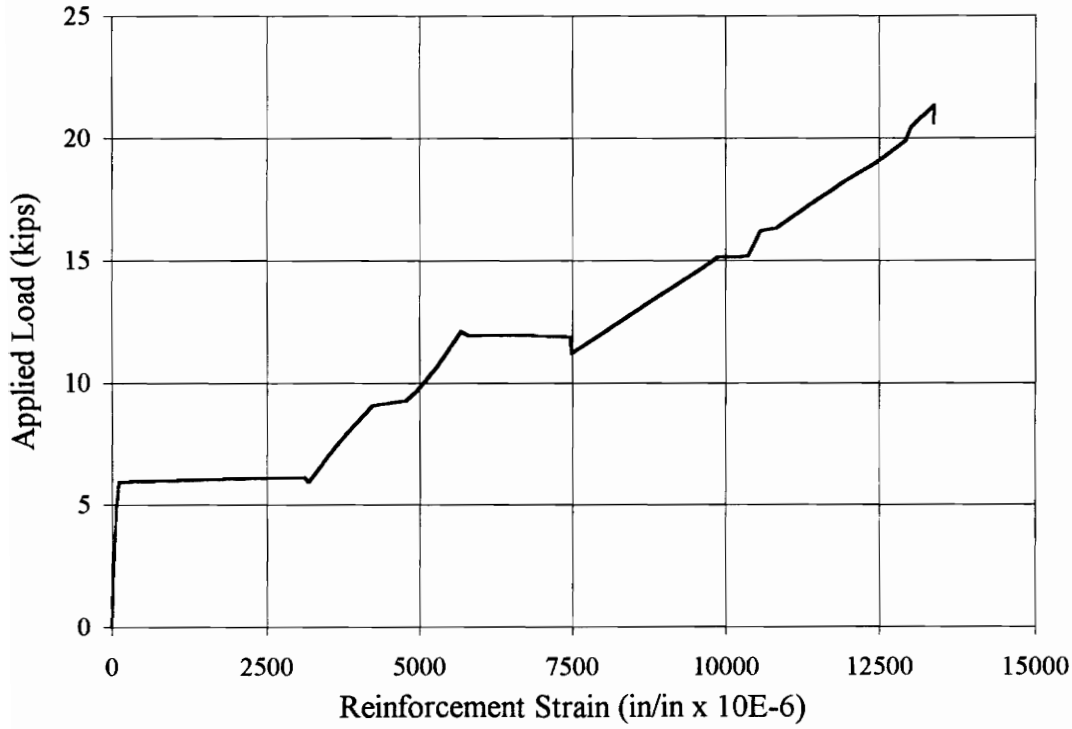

Figure 5.31 Load v. Reinforcement Strain, Test FR-2

5.3.3 Test D4-2

Beam D4-2 was reinforced with a single piece of Duragrid grating, with the main bars at 4.5 in. Load levels applied were 6 kips, 10 kips, 14 kips, 18 kips and 22 kips.

First cracking took place at 5.5 kips, at the location of the transverse bar near the left load point, during the first loading to 6 kips. Nothing further occurred during this first load series.

A second crack occurred 12 in. to the right of the first, at a load of 7 kips, during the first loading to 10 kips. A third crack appeared when load reached 10 kips for the first time, this one located 6 in. to the left of the first. The remaining cycles to 10 kips, as well as the following series of 6 kip loads proceeded without further incident. A fourth crack occurred at the transverse bar between the first and second cracks when the load reached 14 kips for the first time. The crack pattern is shown in Fig. 5.32.

The cycles prior to 22 kips all proceeded normally, with the load-deflection plots following essentially the same slope up and back. The cycles of 22 kips were not as consistent, however. Each successive loading resulted in larger displacements and strains. The permanent set (values at zero load) increased as well. After the first 22 kip loading, the zero-load deflection was 0.15 in., the peak-load deflection 0.53 in. After the last cycle, the deflections were 0.25 in. and 0.71 in., respectively.

The first sign of concrete crushing appeared by the left load point at about 18 kips, during the cycles of 22 kips. With the concrete crushing and deflections increasing, it was apparent that 22 kips was close to the ultimate load of the beam. During the re-loading after the cycles, the beam failed. Load reached about 23 kips, then slowly and steadily dropped off, accompanied by numerous cracking noises. At about 21 kips, a louder crack was heard, the load dropped to 16 kips and deflection increased sharply.

Further ram extension only increased deflection. Significant cracking noises were heard; it was believed that the bars were probably beginning to pull apart--as in D4-1--so extension was halted. Figure 5.33 shows the load-displacement plot for this test.

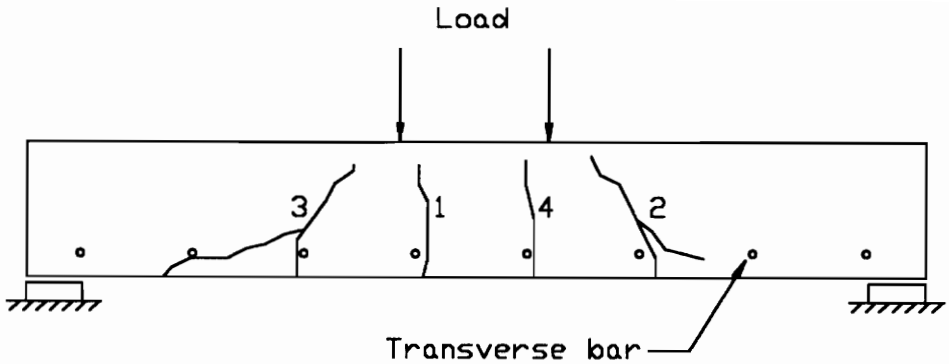

Figure 5.32 Cracking Pattern for Test D4-2

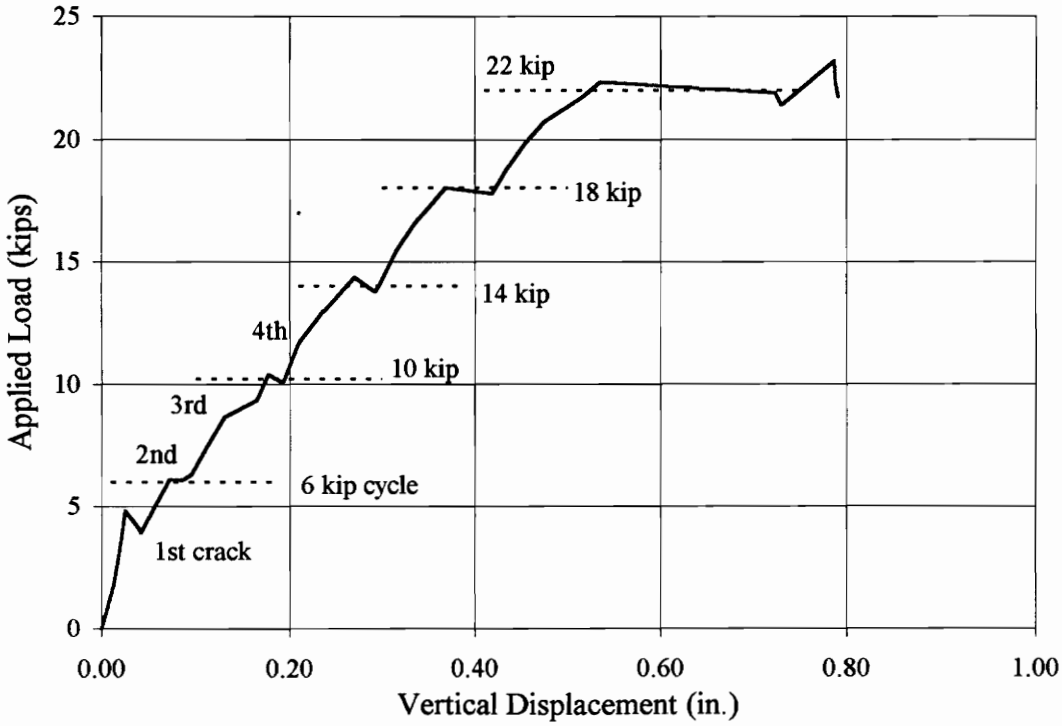

Figure 5.33 Load v. Vertical Displacement, Test D4-2

The peak strain indicated in the concrete (between the load points) was 0.0021 in./in., slightly less than the expected crushing strain. Figure 5.34 shows the concrete strain plot. Like the previous Duragrid tests, there was an obvious difference between strains in the top and bottom flanges of the bars. At ultimate, top strain was 0.006 in./in. (equivalent to a stress of 32 ksi) and bottom strain was 0.008 in./in. (43 ksi). Figure 5.35 shows the applied load versus bar strain relation for this test. None of the bars failed in tension.

5.3.4 Test D6-2

Beam D6-1 contained a Duragrid grating with two bars 6 in. on center. Load was cycled at levels of 4 kips, 7 kips, 10 kips, 13 kips and 16 kips.

Nothing happened during the first load cycle to 4 kips. First cracking occurred at 6 kips, while loading to the 7 kip stage for the first time. The crack lined up with the transverse bar closest to the right load point. A second crack occurred during the 7 kip cycle. While loading to that level for the fourth time, the load reached 7.7 kips before the crack formed, dropping the load to about 6 kips. This crack appeared two transverse bars to the left of the first. Figure 5.36 shows the crack pattern.

Nothing further happened during the remaining loadings to 7 kips, nor during the following cycles to 4 kips. The 10 kip, 13 kip, 16 kip and intervening 4 kip cycles all proceeded without further cracking. The strains and deflections returned to about the same point within each cycle, though there was some increase in permanent offset, especially in the higher load cycles.

After the final loading to 16 kips, it was observed that a crack had appeared across the top of the beam, near the location of the second crack. The second crack had developed into a diagonal crack, while the first remained essentially vertical. The top of the second had propagated horizontally near the surface, near the left load point.

Following the cycles, the beam was reloaded. Upon reaching 15 kips, numerous cracking sounds were heard and the load dropped off slowly to about 14 kips. It was

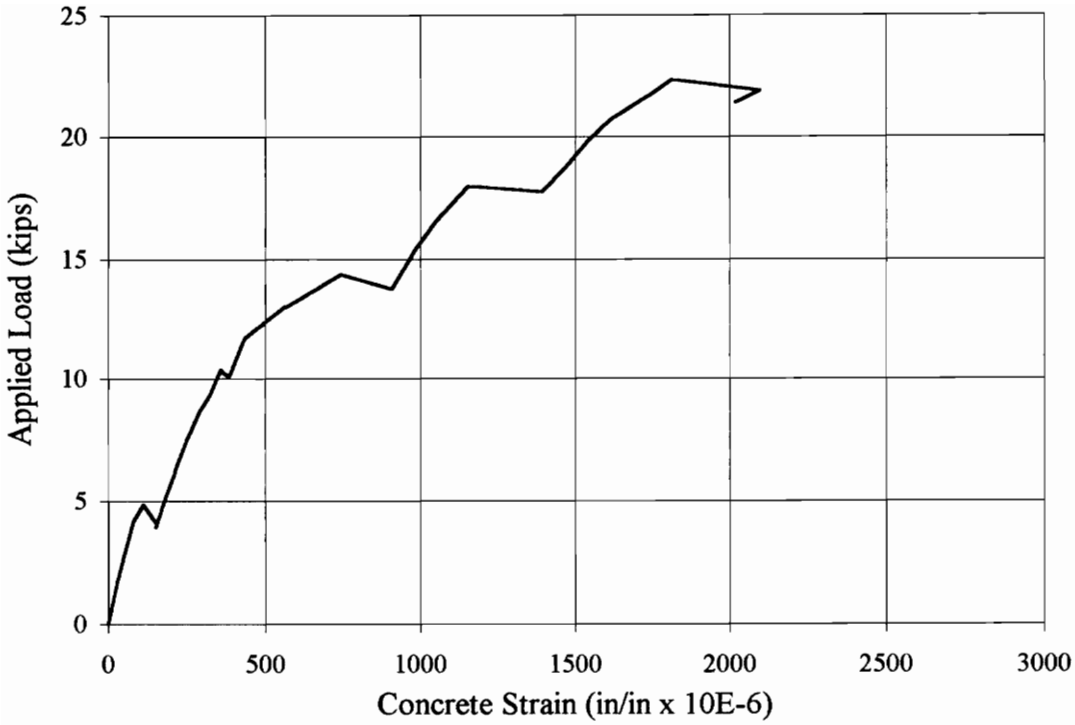

Figure 5.34 Load v. Concrete Strain, Test D4-2

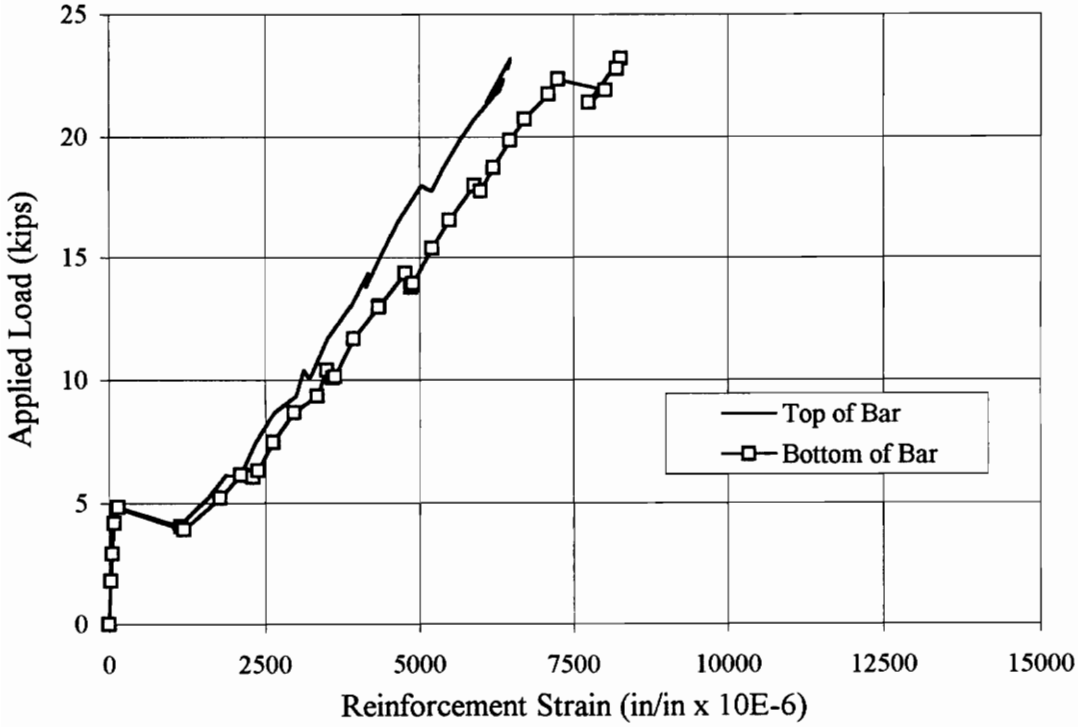

Figure 5.35 Load v. Reinforcement Strain, Test D4-2

observed that the concrete had begun crushing, on the front side of the left load point. At this point, the concrete strain gage indicated strains of about 0.0017 in./in., only slightly more than half the expected crushing strain.

Load was increased, in stages, to about 18 kips. Above that, if load was applied to about 19 kips, the load would drop off back to 18 kips, though strains and deflections increased. At a load of 18.6 kips, deflection was 0.67 in. Load was then increased to about 19.6 kips (ultimate load reached, though not sustained), with a deflection of 0.70 in. Figure 5.37 shows the load-deflection behavior of the beam.

Once loading stopped, repeated cracking noises were heard and it was presumed that failure was imminent. Load continued dropping as cracking sounds increased, until there was a loud bang and the load dropped to 14 kips. It was steady there for about two minutes, though more cracking noises were heard. There was loud bang and the load dropped to 6 kips. Crushing of the concrete was quite severe at this point. Figure 5.38 shows a plot of concrete strain for the entire test. On the back of the beam, the second crack had extended into more of a shear crack, like those observed on the other tests. The front part of the second crack did not form this shear crack, however. Further extension of the ram only increased deflection with no increase in load capacity.

Indicated strains in the bars at ultimate load were 0.009 in./in. (top) and 0.014 in./in. (bottom). These correspond to stresses of 48 ksi and 75 ksi, for an average bar stress of 62 ksi. Figure 5.39 shows the bar strain behavior for this test.

5.3.5 Test MG-2

Beam MG-2 was reinforced with a sheet of Multigrid grating. Load was cycled at levels of 1.7 kips, 3 kips, 4.3 kips, 5.6 kips and 6.9 kips.

The cycles of 3 kips, 4.3 kips and first three cycles of 1.7 kips proceeded without incident. The first three sets of 1.7 were virtually identical, the permanent set at the end of the third was only 0.01 in.

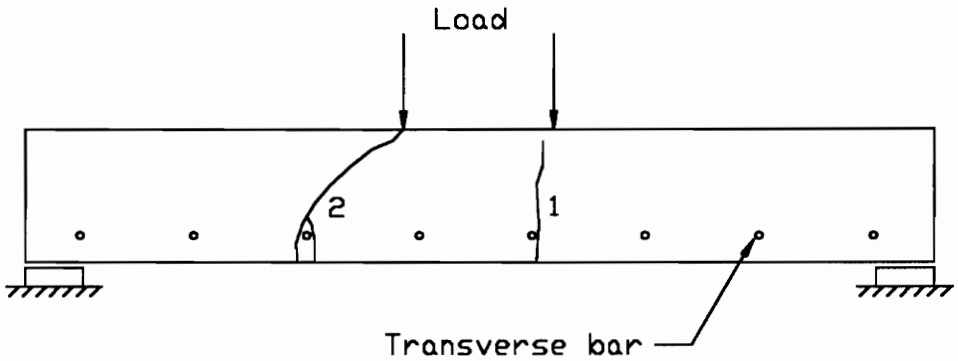

Figure 5.36 Cracking Pattern for Test D6-2

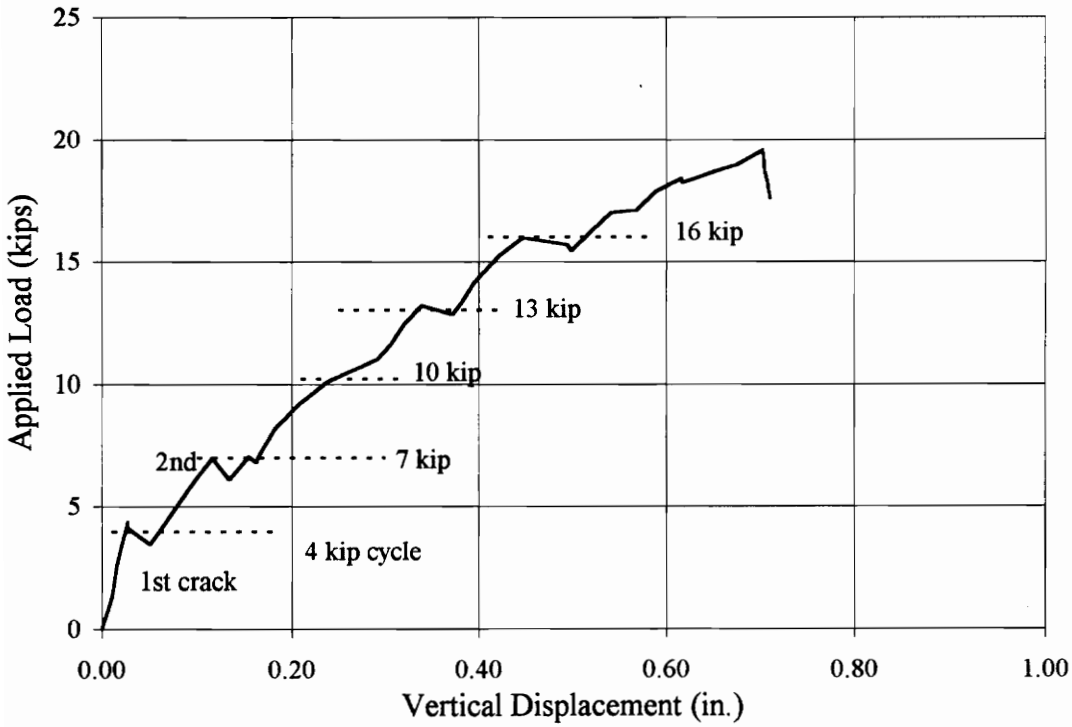

Figure 5.37 Load v. Vertical Displacement, Test D6-2

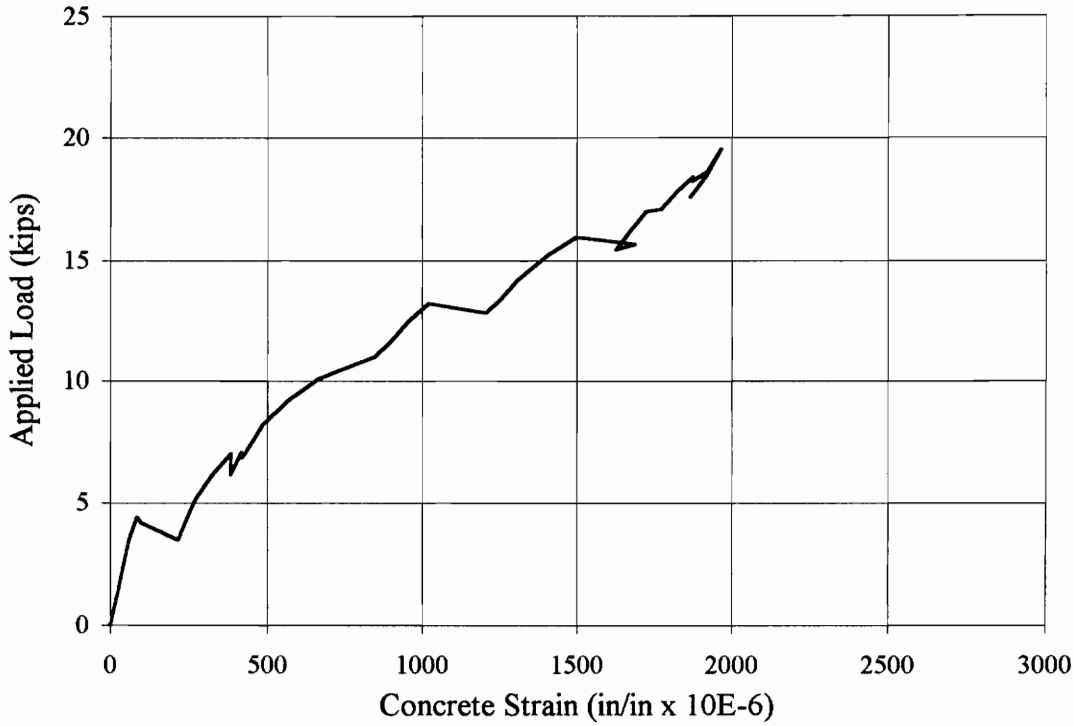

Figure 5.38 Load v. Concrete Strain, Test D6-2

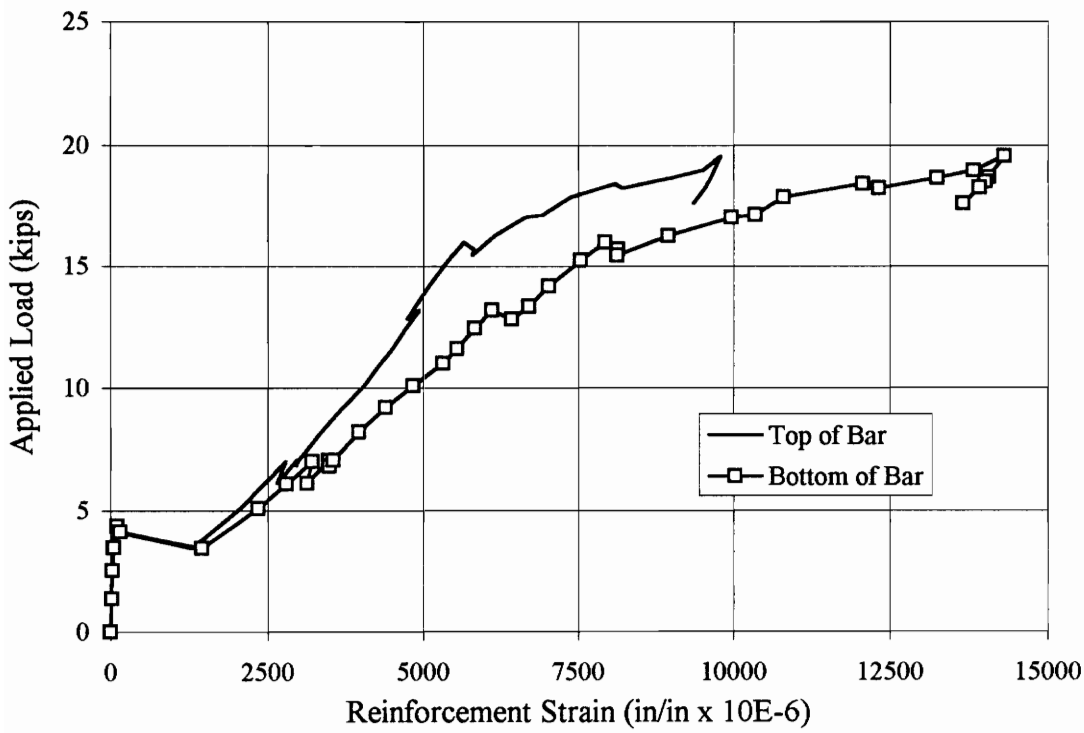

Figure 5.39 Load v. Reinforcement Strain, Test D6-2

The first crack appeared at 5.3 kips during the first loading to 5.6 kips. The crack was located near the right load point, at the location of a transverse bar. A second crack occurred on the same initial loading to 5.6 kips, at a load of 5.7 kips. This crack was located 8 in. to the left of the first.

After the fourth and fifth loading to 5.6 kips, a faint crack was observed between the first two cracks. On the sixth loading this grew to a full crack, at a load of 5.9 kips.

No further cracks occurred during the 5.6 kip cycles. The following 1.7 kip cycle went normally, although there was a noticeable loss in stiffness from the first cycles. Permanent set was about 0.08 in. at the end of this set.

A fourth crack occurred at 7.4 kips on the third loading to 6.9 kips. This was located to the left of the first. A fifth crack occurred at about 8 kips, during final loading. While waiting for the load to settle, further cracking noises were heard, though no new cracks appeared. The load dropped to 7.2 kips after this crack. Figure 5.40 shows the crack pattern for this test.

Continued loading reached 8.2 kips (ultimate), though this was not sustained and load dropped back to 7 kips. A load of 7.5 kips was sustained on the next step, though further cracking noises were heard. The next loading caused failure. About a minute after loading, several louder cracks were heard as the load dropped. In another minute, a loud bang was heard, deflection increased to about 0.6 in. and load dropped off to 1 kip. No further loading was performed, as it was presumed that several or all of the bars were broken. A load-deflection plot is shown in Fig. 5.41.

Indicated concrete strain was 0.0013 in./in. at ultimate load. No crushing of the concrete was evident. Figure 5.42 shows the concrete strain plot. Bar strains reached about 0.013 in./in. at ultimate. This corresponds to a bar force of 1900 lb, close to the ultimate bar force determined from tensile tests. A plot of the bar strain data is shown in Fig. 5.43.

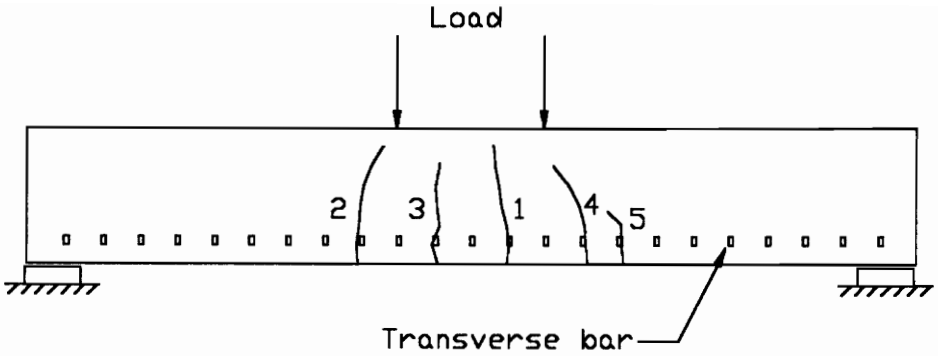

Figure 5.40 Cracking Pattern for Test MG-2

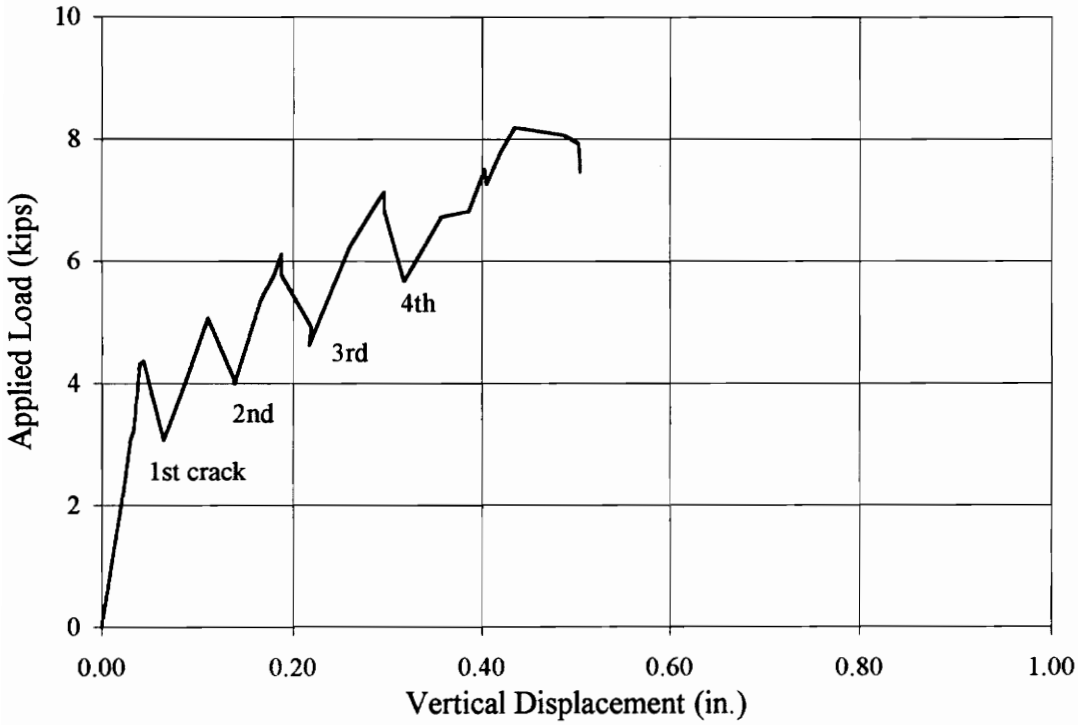

Figure 5.41 Load v. Vertical Displacement, Test MG-2

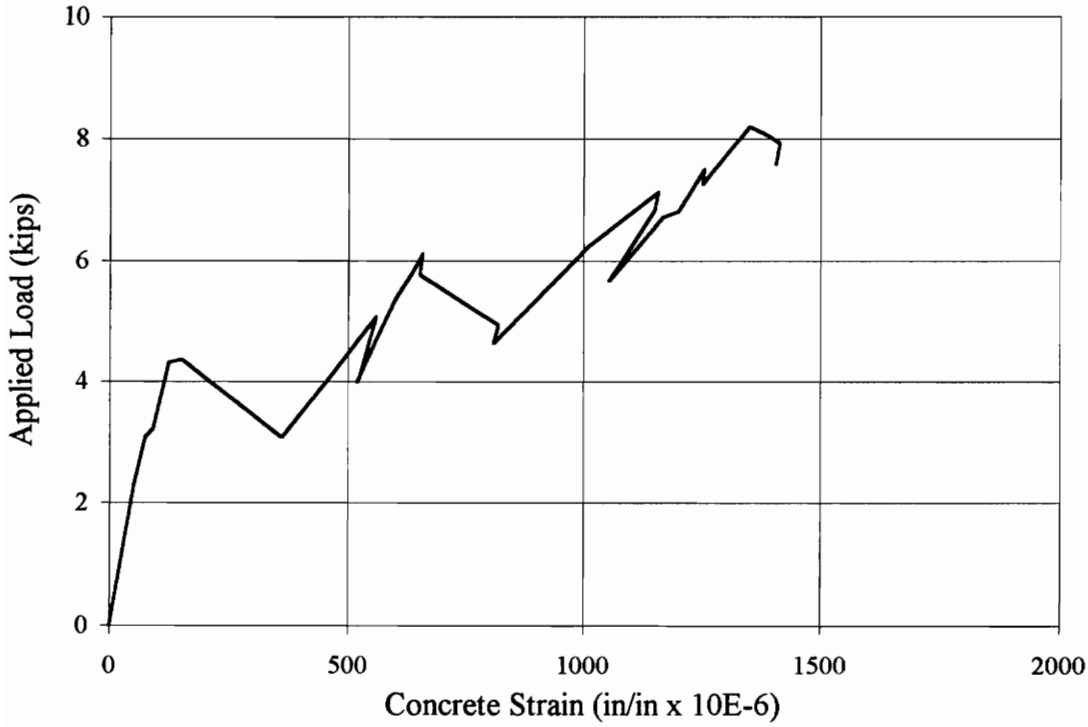

Figure 5.42 Load v. Concrete Strain, Test MG-2

Figure 5.43 Load v. Reinforcement Strain, Test MG-2

CHAPTER 6

ANALYSIS OF TEST RESULTS

In this chapter, the results of the beam tests are discussed further, analyzed and compared. Important observations are noted and possible explanations offered. Comparisons are made on several levels: with the work of others, between reinforcement types, with prediction calculations from Chapter 4, and between monotonic and cyclic tests within each reinforcing.

6.1 General Analysis

All of the beams, except those reinforced with Multigrid, had ultimate loads of about 20 kips. The Multigrid beams failed at less than 9 kips, due to tensile failure of the reinforcing grid. Figure 6.1 shows an ultimate load comparison for all of the tests.

In general, there was little difference between the first and second test of each reinforcing type. The steel and FRP bar tests increased in capacity, the Duragrid (4.5 in.) capacity decreased significantly, and the Duragrid (6 in.) and Multigrid tests remained essentially the same. While recognizing that a limited number of tests were run, it appears that the cyclic loading pattern had minimal effect on the performance of the beams.

Most tests ultimately failed in shear, although bar yielding or crushing of the concrete may have preceded that failure mode. Again, the Multigrid reinforced beams were significantly different, as those failed at less than half the ultimate load of the other tests, due to the low tensile strength of the Multigrid.

As expected, those beams that developed more cracks had smaller crack widths. The Multigrid and Duragrid (4.5 in.) beams developed the most cracks, four or five. Crack widths at ultimate for these tests were only about 0.06 in. The Duragrid (6 in.) and steel bar reinforced beams produced two or three cracks, with typical maximum crack

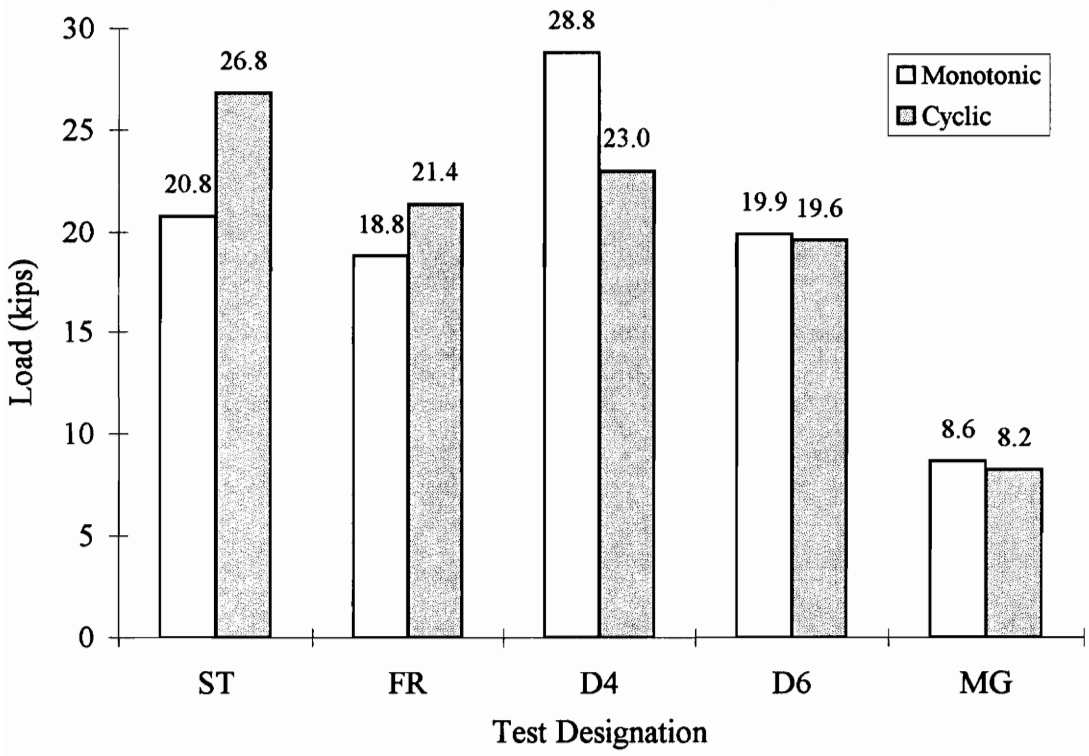

Figure 6.1 Ultimate Load Values for All Tests

widths of 0.10 in. The beams reinforced with FRP bars produced just two cracks, with a maximum crack width of nearly 0.20 in.

6.2 Comparison with Previous Work

In this section, the test results and observations from this project are compared with previous reported work. The behavior of steel-reinforced concrete beams is well documented and will not be discussed here, but rather only compared with prediction calculations in Section 6.5.1

6.2.1 FRP Bar Reinforced Beams

As reported by others who tested FRP bar reinforced concrete beams, the deflections were larger than in steel reinforced beams, and the strength of the FRP forced the failure in the concrete before the reinforcement failed.

GangaRao and Faza (1991) reported sudden crack formation and propagation, similar to that noted in Chapter 5. They attributed this abrupt cracking to a weak bond of the bar with the concrete. Large crack widths were also reported by these researchers.

6.2.2 Grating Reinforced Beams

All cracks that appeared in the Duragrid and Multigrid reinforced beams corresponded with the location of a transverse bar. Bank (1992) and Goodspeed (1991) both reported similar happenings in tests of grating reinforced concrete members. As mentioned in Chapter 2, the grid's transverse bars provide anchorage for the main bars and push against the concrete, placing it in horizontal shear and causing a crack. The steel and FRP bars are able to provide their own bond along their entire length and so do not involve the transverse bars.

The bar failure in test D4-1 appears to have been caused by the transverse bar simply pushing down on the main bar, causing the main bar to split lengthwise. The transverse bar pulled away from the top part of the main bar (Fig. 5.11). Bank (1992)

reported the same type of grid failure in beams which failed in shear. He concluded that the failure was the result of stress concentrations caused by the transverse bar bearing on the main bar. According to Bank, the transverse bars must transfer all of the load from the concrete to the main bars. As with Bank's tests, the Duragrid bar failures occurred during post-ultimate loading of the beams, and therefore did not limit the beam strength.

Unlike several other reports on the use of grating reinforcement, no horizontal delamination at the level of the gratings was observed. The delamination was felt to be a result of the grid creating a discontinuity between the concrete below the grating and the concrete above. The lack of such delamination in these tests may be a result of the short span not allowing the beams to undergo large displacements. Based on previous work, delamination had been expected, especially with the close spacing of the Multigrid.

No evidence of previous work using Multigrid as reinforcement was found. Other experiments have been performed using molded gratings, though these gratings were typically larger than the Multigrid, with 1 in. or 1.5 in. deep bars. The weakness of the Multigrid in tension forced the end of the tests before any concrete failure could occur, thus the shear failures and crushing of concrete that occurred with the Duragrid beams were not observed.

6.3 Comparisons Between Tests

In this section, general comparisons are made among all of the tests. Comparisons are based on data trends and observations.

6.3.1 Load-Deflection Behavior

Figures 6.2 and 6.3 show the load-deflection plots for the two series of tests. The plots reveal that the tests can be divided into three distinct groups, based on their relative stiffness. The steel (ST) and Duragrid 4.5 in. (D4) tests were similar and had the highest stiffness. Significantly less stiff were the tests of Duragrid 6 in. (D6) and FRP bar (FR). Finally, the Multigrid (MG) tests were the lowest of the group.

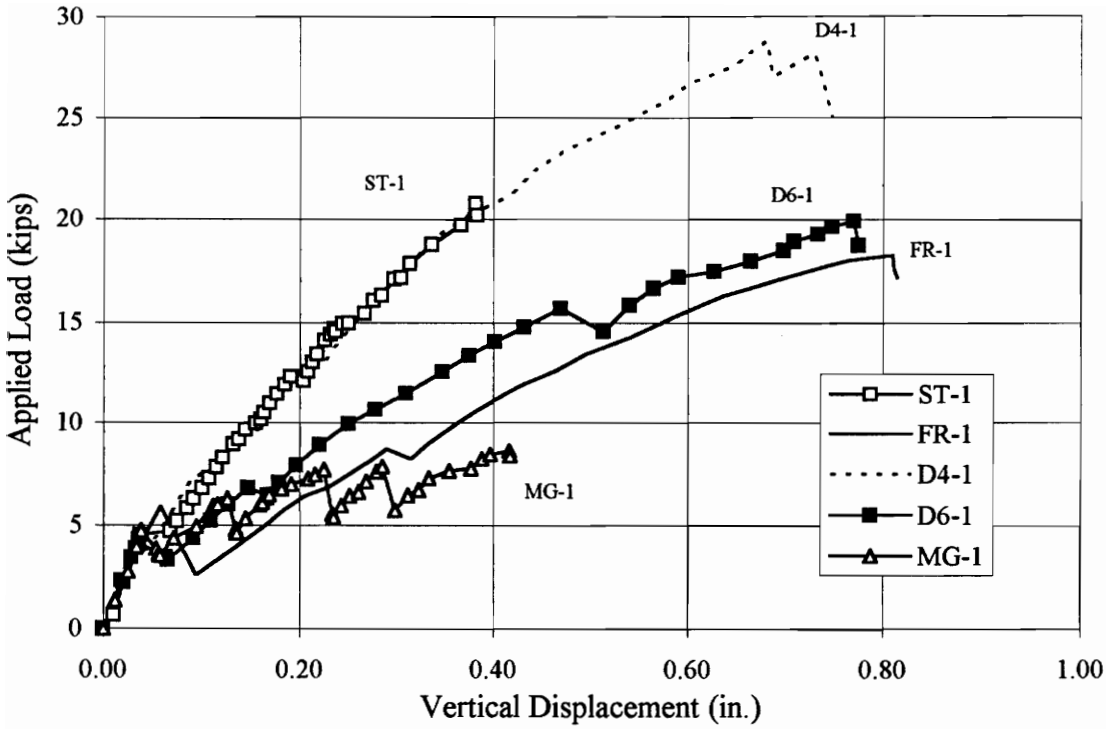

Figure 6.2 Load v. Vertical Displacement Comparison, Monotonic Tests

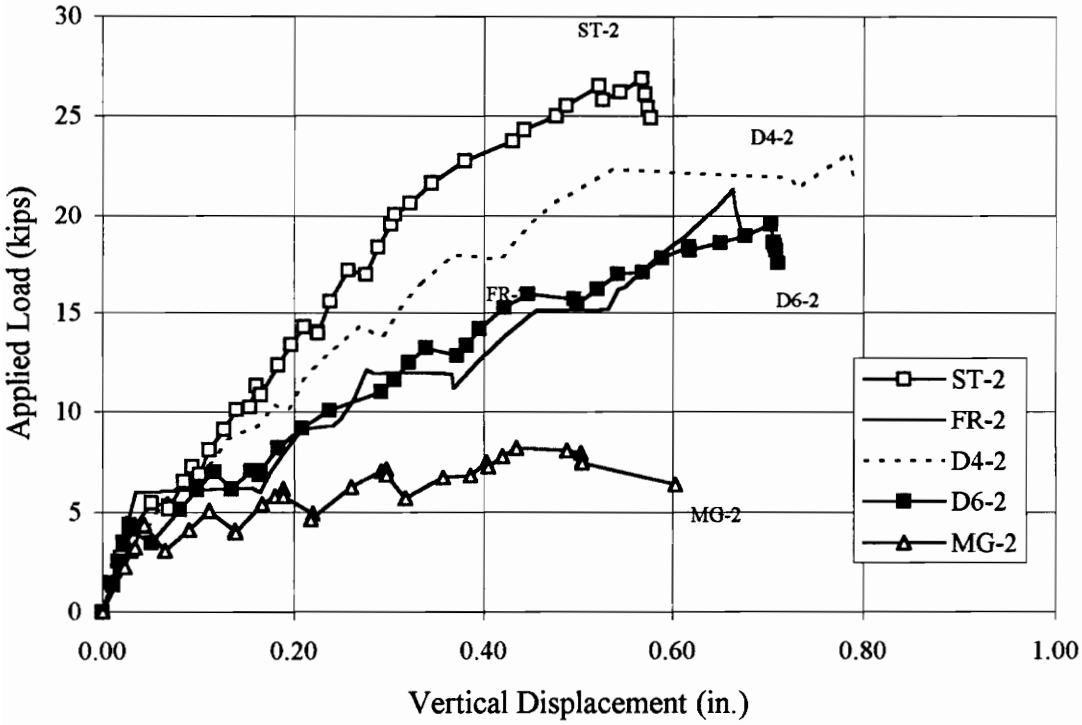

Figure 6.3 Load v. Vertical Displacement Comparison, Cyclic Tests

The pre-cracking behavior of all the tests was essentially the same. First cracking occurred at about 5 kips. Cracking was accompanied by a drop in load and an increase in deflection, though the magnitude of these changes varied for each test.

In the first series of tests, the steel and Multigrid reinforced beams had ultimate deflections of about 0.40 in. The other tests reached at least 0.70 in. before failure, as shown in Fig. 6.2. The small deflections of ST-1 and MG-1 occurred for different reasons, however. The steel reinforced beam was stiff and failed in shear, while the Multigrid beam had very low stiffness and failed because of bar failure.

In the second series of tests, all of the beams deflected at least 0.50 in. before failure (Fig. 6.3). The steel reinforced beam increased ultimate deflection over ST-1 because bar yielding prior to shear failure provided some ductility.

The plateaus on the second test series load-deflection plots are due to the cyclic loading, and show the increase in deflection which each additional cycle. To generate the curves, the first and last points for each cycle were plotted, showing the deflection at the beginning and end of each load level.

6.3.2 Bar Strain

Because all of the reinforcements had a different composition, it was expected that the indicated bar strains would vary widely, as shown in Fig. 6.4. The only direct comparison which can be made from the bar strains is between the two types of Duragrid. Higher strains were indicated in the bars in beams D6 than those in D4, mainly because D4 had three bars carrying the tensile load, while D6 had only two.

A general comparison can be made based on bar force, as calculated from the calibration factors for each reinforcement type. To make this a valid comparison, one needs to determine the total force in the reinforcement, rather than just the force in the gaged bar, because the bars all had different cross-sectional areas. The total force in the reinforcement is calculated by multiplying the measured strain by the calibration factor (to get individual bar force), then multiplying by the number of bars. The total force in the

reinforcement at a given load should be (assuming all the internal moment arms are equal) the same for all tests, as shown in Fig. 6.5. Averages of the bar strains and calibration factors were used to generate Figs. 6.4 and 6.5.

The Duragrid bars indicated a distinct difference in strain between the two gages on each bar. On the Duragrid, the gages were placed on the top and bottom flanges of the I-bars. With the steel and FRP bars, it is not known which way the gages were oriented in the beams--top and bottom or on the sides--just that they were on opposite faces of the bars. The Multigrid gages were located on the sides of the bars.

The gages on the top flanges typically indicated lower strains than the gages on the bottom flanges (Chapter 5). This suggests that the Duragrid acts in bending as well as in tension. Therefore, to model the action of Duragrid as reinforcing, one could consider both its tensile and flexure capacities.

6.3.3 Concrete Strain

Comparisons between concrete strain should be made cautiously, as the placement of the gage plays an important role. The maximum strain may occur at any point between the load points, and the gage location--always at midspan--may not correspond to that maximum strain location. For this reason, the concrete data for each test was presented in Chapter 5, but no comparisons or analyses are attempted here.

6.4 Comparison with Predictions

In this section, prediction results--specifically ultimate load and load-deflection behavior--are compared with the test results. Details on the prediction methods are given in Section 4.5.

6.4.1 Steel Bar Reinforced Beams

Shear strength calculations underestimated the actual shear capacity of both beams, as shown in Table 6.1. The yield point of the bars was correctly predicted for both

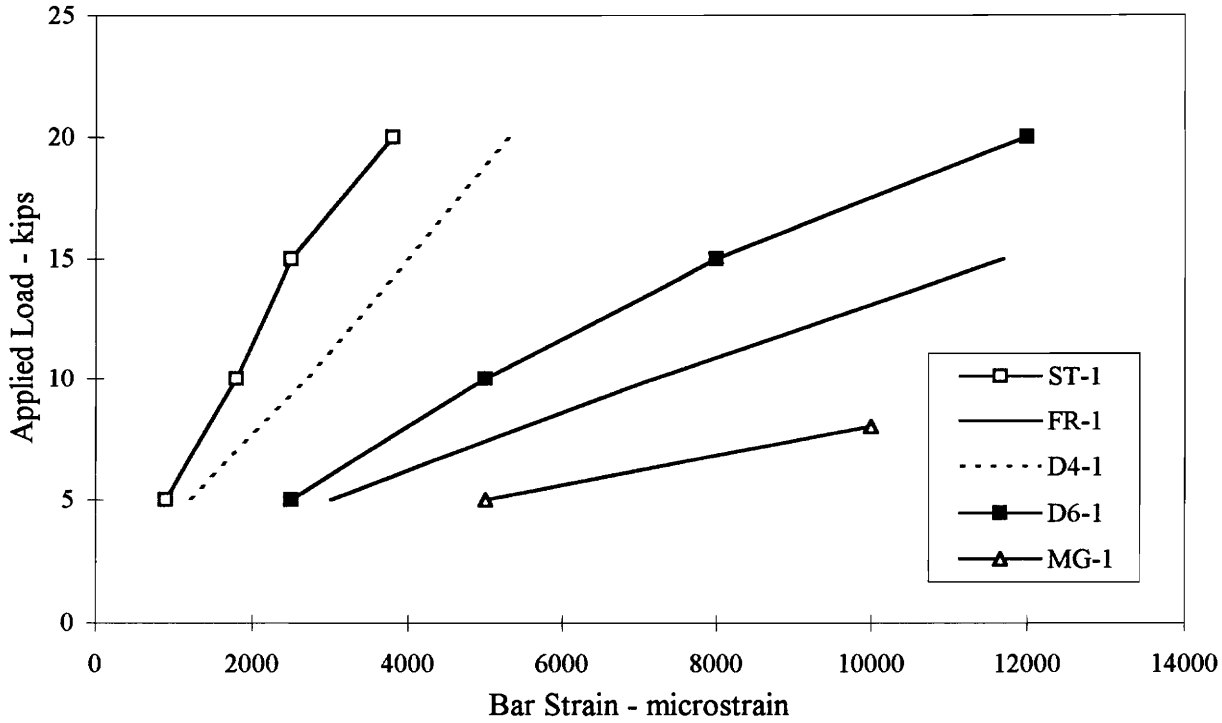

Figure 6.4 Comparison of Reinforcement Strains

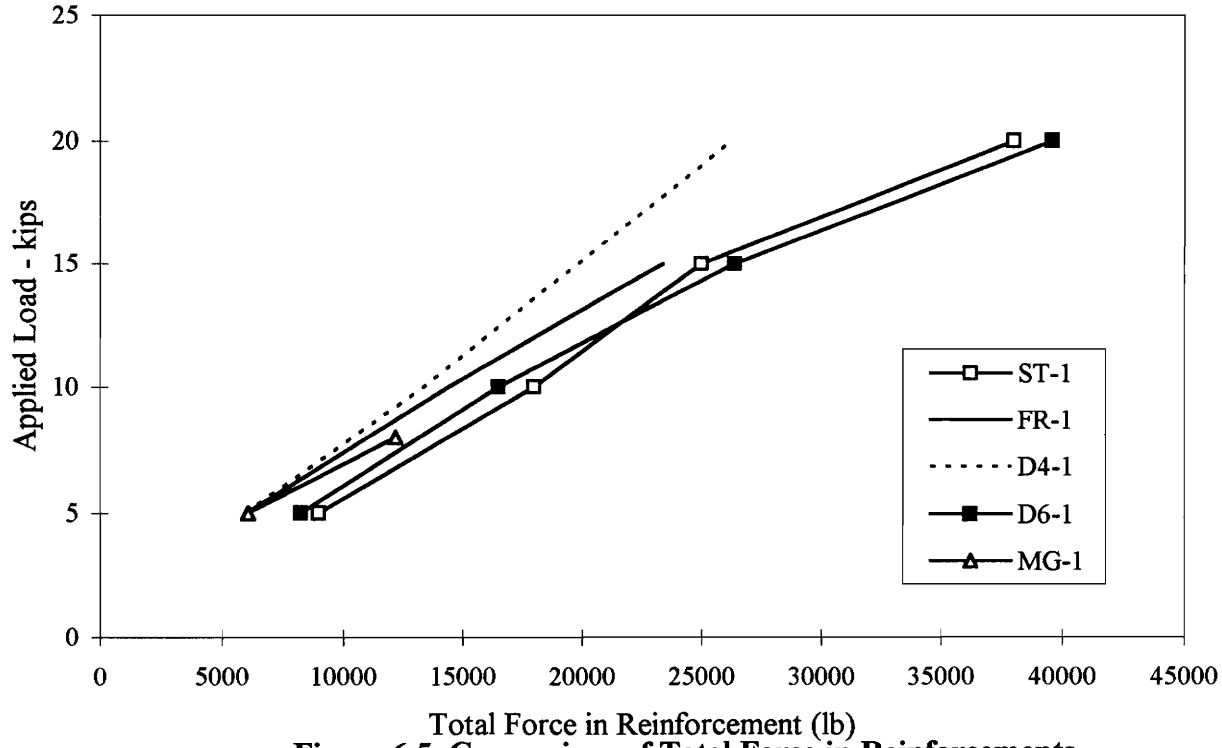

Figure 6.5 Comparison of Total Force in Reinforcements

tests. A comparison of the RESPONSE-generated load-deflection curves and the actual test data are shown in Figs. 6.6 and 6.7. The post-cracking behavior of the test beams was significantly less stiff than predicted.

Because of the small span-to-depth ratio of the beams (L/d = 6), they were close to being considered deep beams. This may have resulted in shear deformations or behavior other than pure flexure, making incorrect Eq. 4-9 which was used to estimate deflection.

Table 6.1 Predicted and Observed Data, Steel Bar Tests

ST-1	Failure Mode	Load (kips)	Defl. (in.)
Prediction	Shear	17.5	0.13
Test Results	Shear	20.8	0.38

ST-2	Failure Mode	Load (kips)	Defl. (in.)
Prediction	Shear	18	0.14
Test Results	Flexure, bars	26.8	0.57

6.4.2 FRP Bar Reinforced Beams

Calculations did not correctly predict the ultimate load, deflection or failure mode, as shown in Table 6.2. A comparison of the load-deflection predictions and the test data, shown in Figs. 6.8 and 6.9, indicates that the prediction greatly overestimated the stiffness of the members.

Table 6.2 Predicted and Observed Data, FRP Bar Tests

FR-1	Failure Mode	Load (kips)	Defl. (in.)
Prediction	Shear	21	0.32
Test Results	Flex., concrete	18.8	0.75

FR-2	Failure Mode	Load (kips)	Defl. (in.)
Prediction	Shear	22	0.31
Test Results	Flex., concrete	21.3	0.66

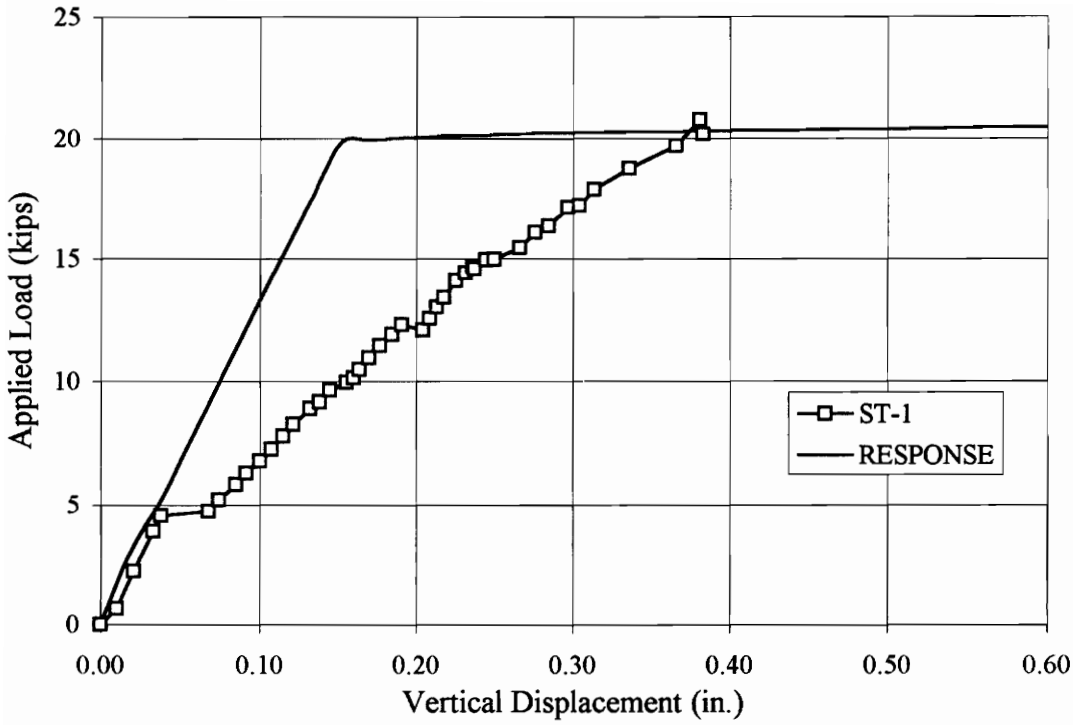

Figure 6.6 Displacement Comparison, ST-1 v. Prediction

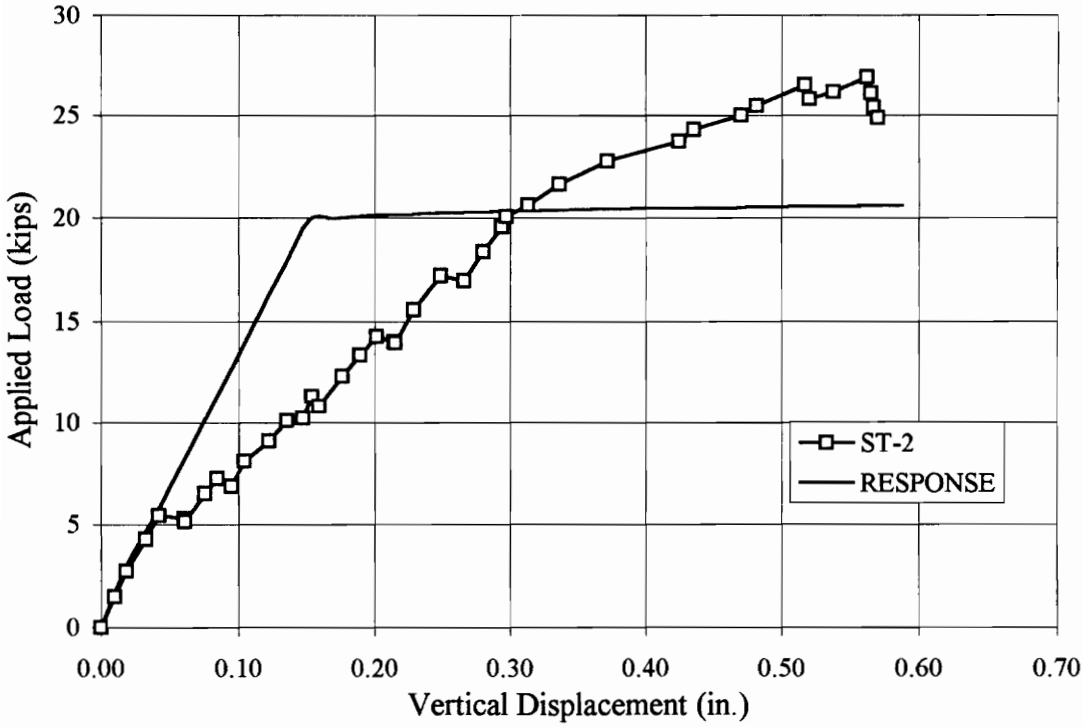

Figure 6.7 Displacement Comparison, ST-2 v. Prediction

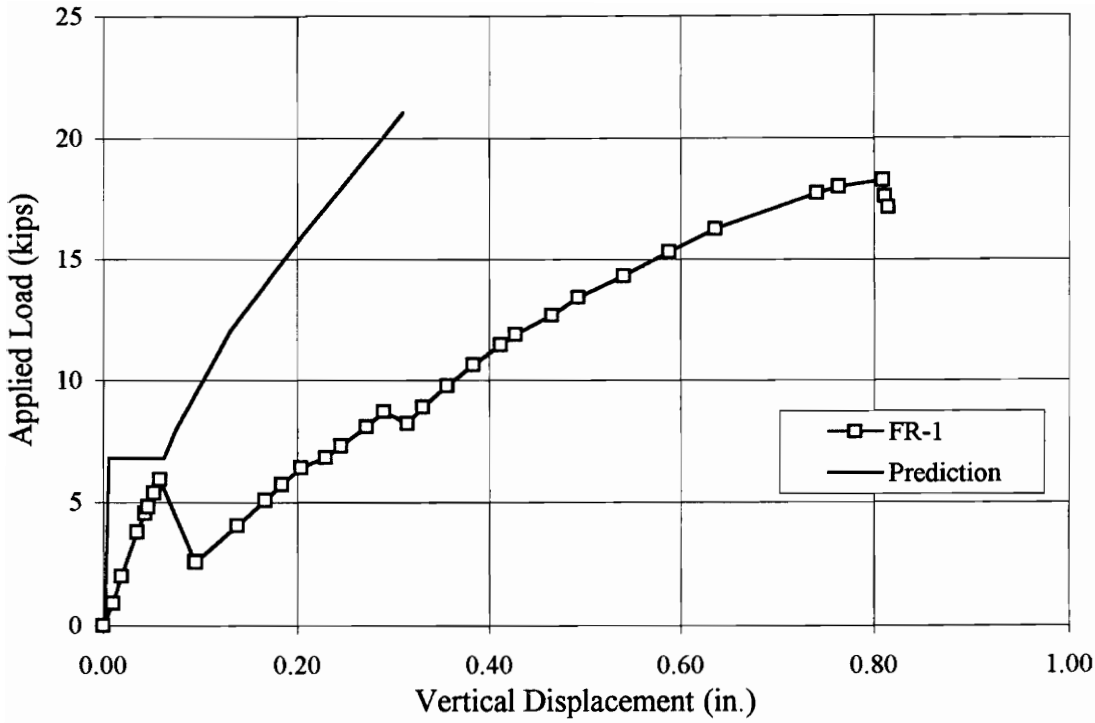

Figure 6.8 Displacement Comparison, FR-1 v. Prediction

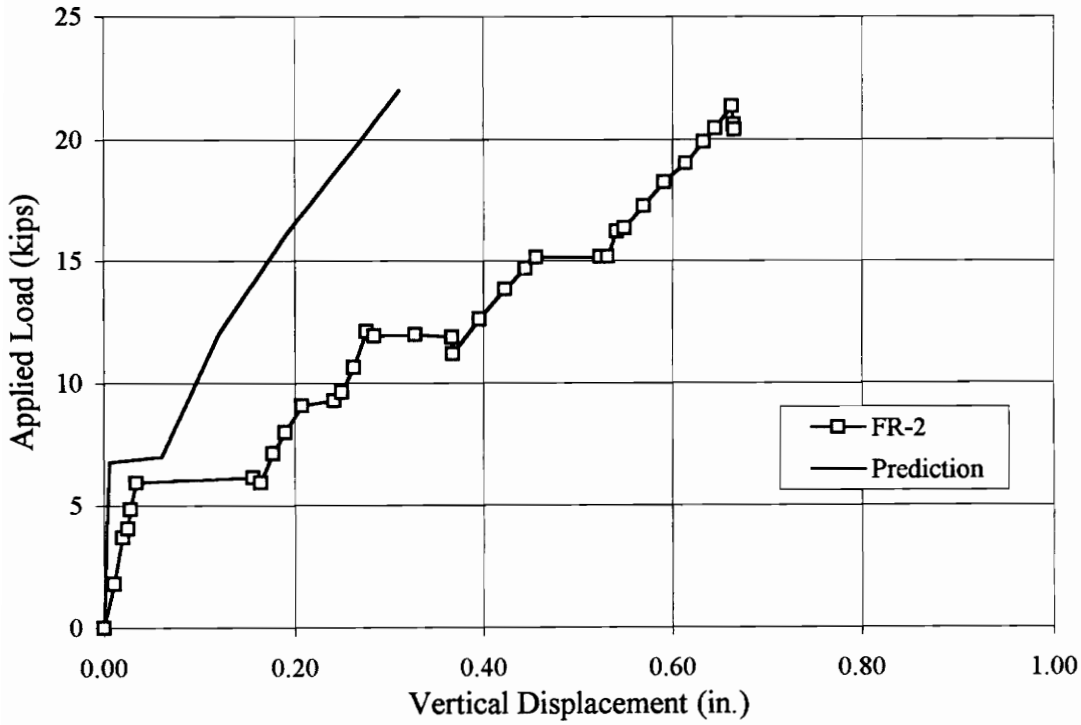

Figure 6.9 Displacement Comparison, FR-2 v. Prediction

The crack patterns and observed behavior of the test beams offer some explanation for the inaccuracy of the predictions. In both FR-1 and FR-2, only two cracks appeared. The uncracked sections of beam seemed to act as rigid members and rotate around the cracks, with little or no actual bending behavior. Figure 6.10 shows beam FR-1 after failure; the rigid body rotation about the center crack is clearly visible. This action probably caused the higher than expected deflections and low apparent stiffness. Because of this unexpected behavior, the test results neither verify nor refute GangaRao and Faza's (1991) modified deflection expressions.

6.4.3 Duragrid (4.5 in.) Reinforced Beams

The ultimate load of test D4-1 was the highest recorded for all the tests. This capacity greatly exceeded the predicted shear capacity. The ultimate load for test D4-2 was closer to the predicted failure load. For both tests, deflections were significantly underestimated, as shown in Table 6.3.

Figure 6.11 shows a comparison between the predicted and observed load-deflection of test D4-1. The prediction curve, based on the moment of inertia of the cracked section, is close to the actual data, up to the predicted failure load.

A plot of predicted and observed load-deflection data for test D4-2 is shown in Fig. 6.12. The test data matches the prediction up to a load of 10 kips, before becoming considerably less stiff.

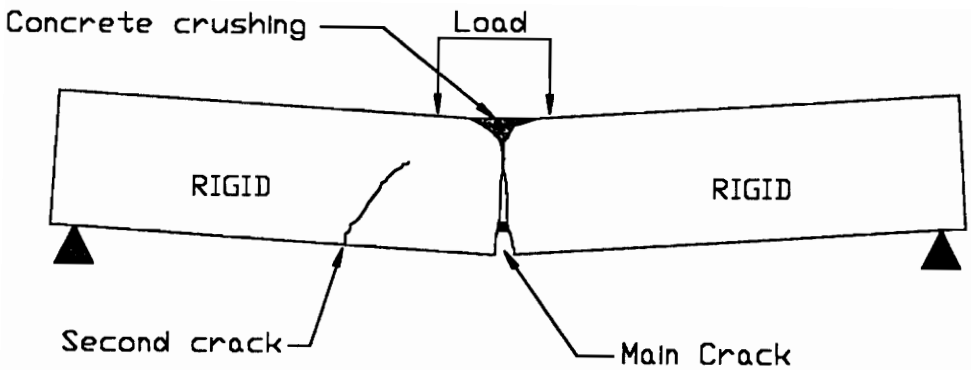

Figure 6.10 Failure of Test FR-1, Showing Rigid Body Rotation

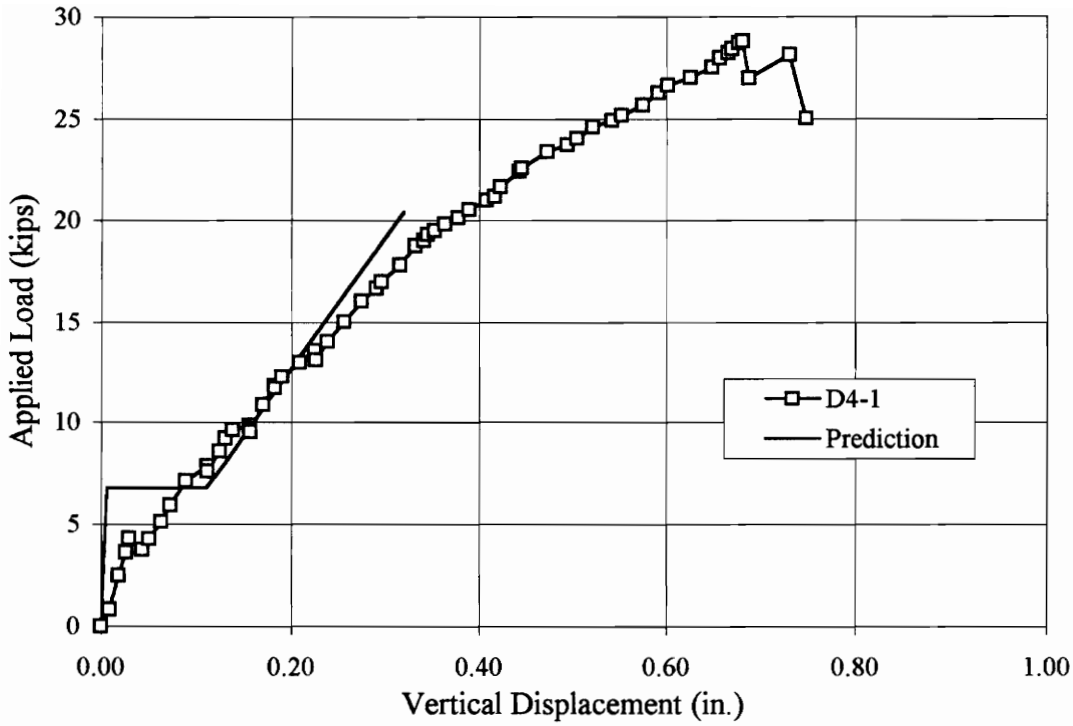

Figure 6.11 Displacement Comparison, D4-1 v. Prediction

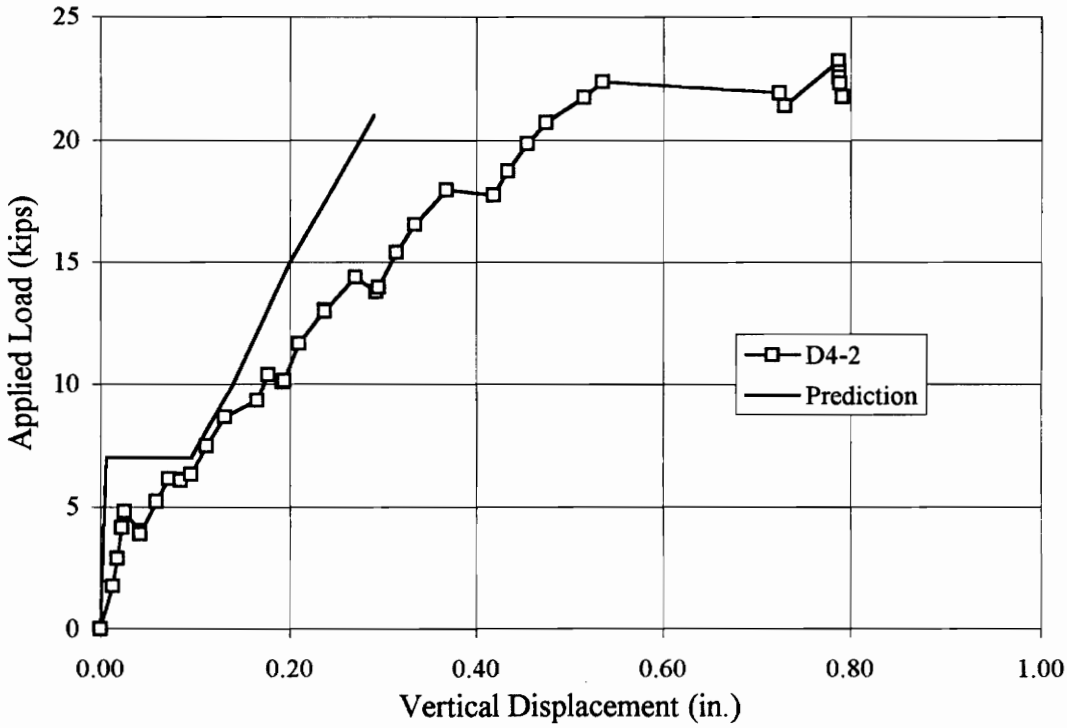

Figure 6.12 Displacement Comparison, D4-2 v. Prediction

Table 6.3 Predicted and Observed Data, Duragrid (4.5 in.) Tests

D4-1	Failure Mode	Load (kips)	Defl. (in.)
Prediction	Shear	20.4	0.32
Test Results	Shear	28.8	0.67

D4-2	Failure Mode	Load (kips)	Defl. (in.)
Prediction	Shear	21	0.29
Test Results	Shear	23	0.73

6.4.4 Duragrid (6 in.) Reinforced Beams

Calculations correctly predicted the shear capacity of both D6 tests, as shown in Table 6.4. The deflections at ultimate, however, were underestimated.

Figures 6.13 and 6.14 show comparisons of the predicted and observed load-deflection behavior for tests D6-1 and D6-2, respectively. In both cases, the predictions overestimated the stiffness of the sections. It appeared that the same type of rigid body action noticed in FR-1 may have been occurring, as the beam appeared to be divided by the cracks into three rigid members and simply rotated about those cracks.

Table 6.4 Predicted and Observed Data, Duragrid (6 in.) Tests

D6-1	Failure Mode	Load (kips)	Defl. (in.)
Prediction	Shear	20.6	0.41
Test Results	Shear	19.9	0.77

D6-2	Failure Mode	Load (kips)	Defl. (in.)
Prediction	Shear	21.2	0.42
Test Results	Shear	19.6	0.70

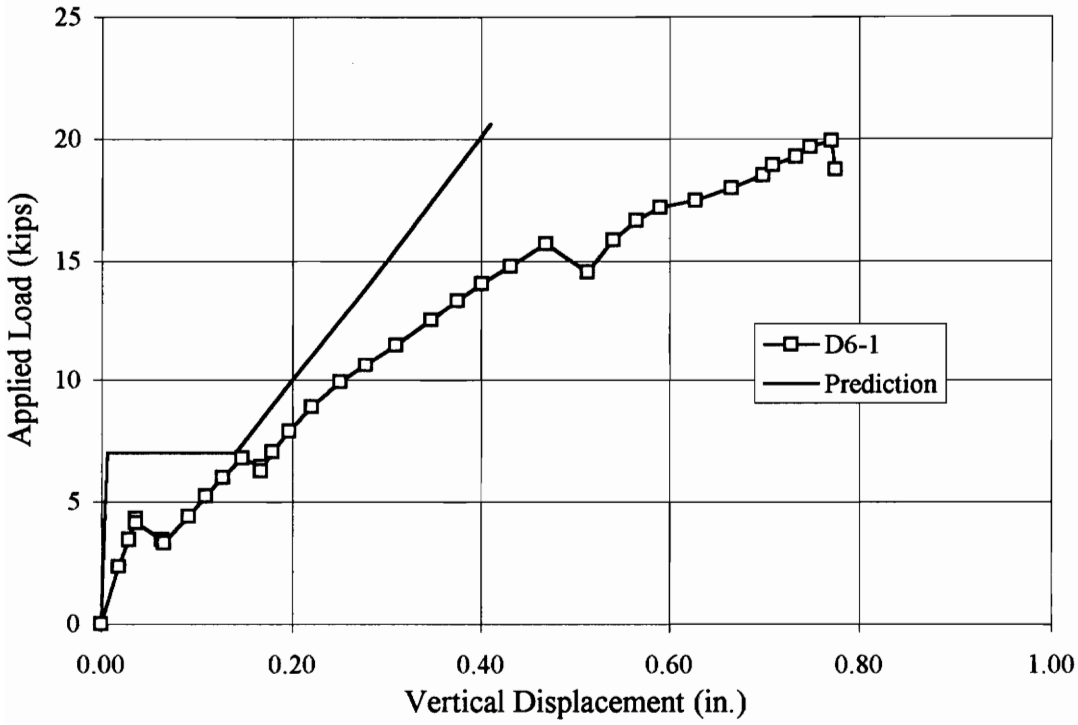

Figure 6.13 Displacement Comparison, D6-1 v. Prediction

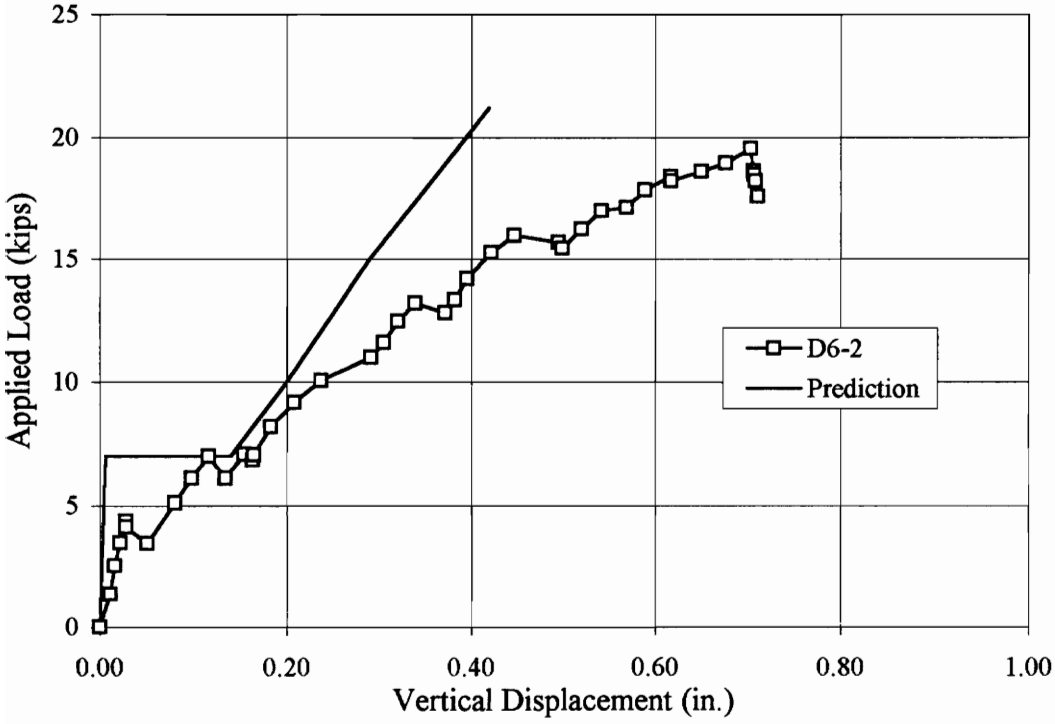

Figure 6.14 Displacement Comparison, D6-2 v. Prediction

6.4.5 Multigrid Reinforced Beams

The ultimate loads for tests MG-1 and MG-2 were essentially the same as the predicted ultimate loads for bar failure, as shown in Table 6.5. Comparisons of the load-deflection predictions and actual results are shown in Figs. 6.15 and 6.16. The load-deflection predictions were based on the moment of inertia of the cracked, transformed section. The overall stiffness was less than predicted, though the tests did appear to have the same load-deflection slope as that predicted, but only between cracking loads.

Table 6.5 Predicted and Observed Data, Multigrid Tests

MG-1	Failure Mode	Load (kips)	Defl. (in.)
Prediction	Flexure, bars	8.4	0.26
Test Results	Flexure, bars	8.6	0.42

MG-2	Failure Mode	Load (kips)	Defl. (in.)
Prediction	Flexure, bars	8.4	0.26
Test Results	Flexure, bars	8.2	0.43

6.5 Comparison Between Monotonic and Cyclic Loading

Figure 6.1 shows a comparison of the ultimate loads for all of the tests. In general, the two tests for each reinforcement were very similar with respect to ultimate load, stiffness and crack pattern. Each of the following sections describes the similarities and differences within each pair of tests.

The only physical difference between the first and second tests was the age of the concrete; both contained the same reinforcement in the same position. With respect to testing, the only variation was the monotonic versus cyclic loading.

6.5.1 Steel Bar Reinforced Beams

The load-deflection behavior of tests ST-1 and ST-2 was essentially the same up to 15 kips. At that point ST-1 became less stiff than ST-2 and failed at 21 kips. Test ST-2

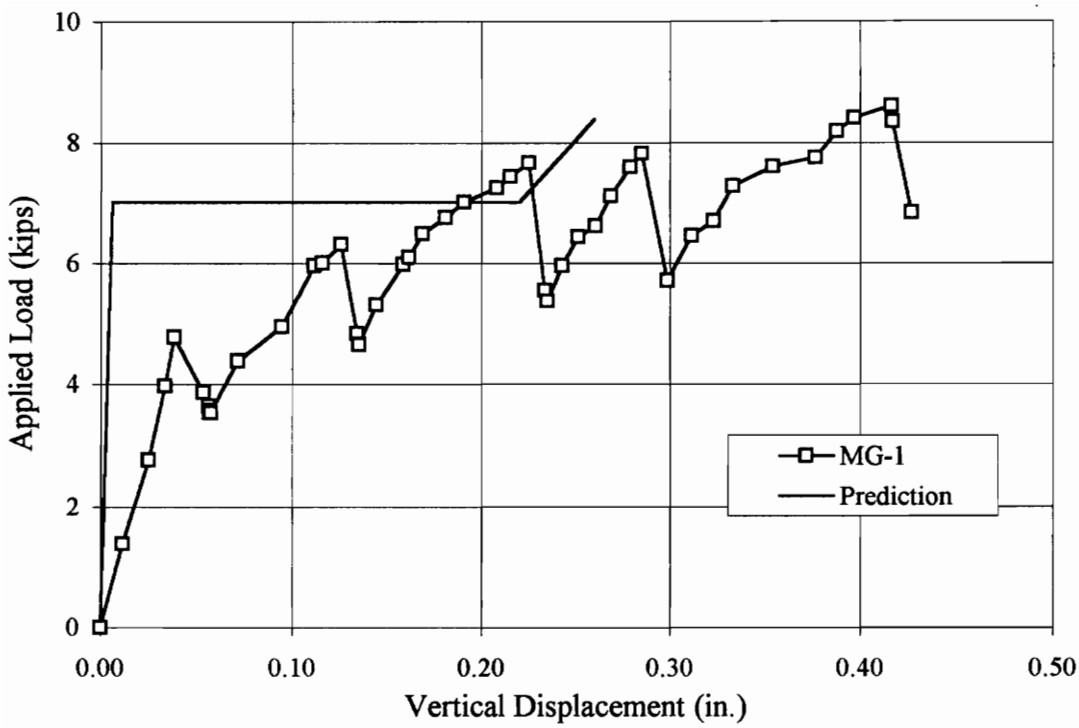

Figure 6.15 Displacement Comparison, MG-1 v. Prediction

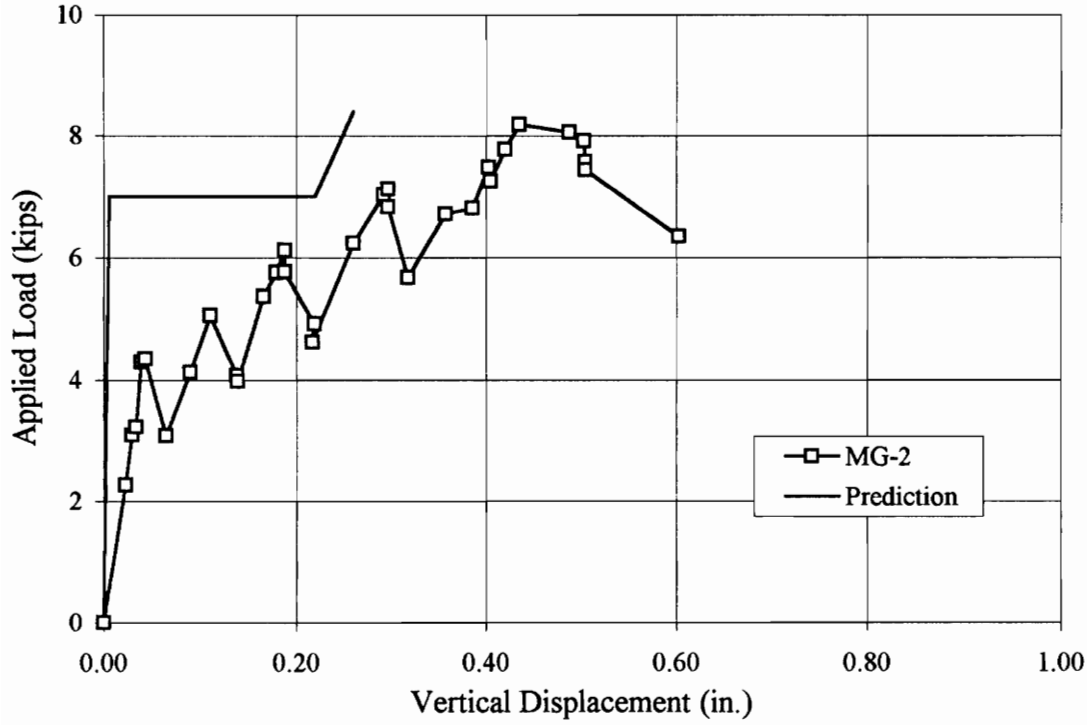

Figure 6.16 Displacement Comparison, MG-2 v. Prediction

continued at the same slope up to 21 kips, when the bars yielded. Figure 6.17 shows a comparison of load-deflection behavior. Beam ST-1 failed suddenly in shear, while beam ST-2 showed some ductility prior to shear failure.

In test ST-1, the bars appeared to yield just before shear failure occurred, while in ST-2 the bars were well beyond the yield point at beam failure. Concrete strains were virtually the same for both tests, up to the failure point of ST-1. The cracking patterns for the two tests were similar.

6.5.2 FRP Bar Reinforced Beams

Failure occurred at a higher load in FR-2, but with less deflection than FR-1, indicating that FR-2 was stiffer. Figure 6.18 shows a comparison of load-deflection behavior for the tests.

The indicated concrete strain in FR-2 was much less than FR-1, although concrete crushing was the initial failure mode for both tests. The ultimate indicated strain for FR-2 was only 0.001 in./in., compared with 0.0027 in FR-1. As noted before, the location of the concrete strain gage may not always coincide with the location of maximum strain.

Each test produced two cracks with similar cracking loads. FR-1 typically indicated higher bar strains than FR-2 for a given load.

6.5.3 Duragrid (4.5 in.) Reinforced Beams

Compared to D4-1, test D4-2 had only a slight decrease in stiffness. At 20 kips, D4-1 had a deflection of about 0.40 in., while D4-2's deflection was 0.48 in. Ultimate load for D4-2 was about 15 percent less than for D4-1 (23 kips v. 28 kips). The 23 kip value is more in the range of the other tests, as the ultimate shear capacity of the section. It is unknown why D4-1 achieved such a high load--whether it was due to the reinforcement or simply an anomaly in the test. Figure 6.19 shows the load-deflection data for the two D4 tests.

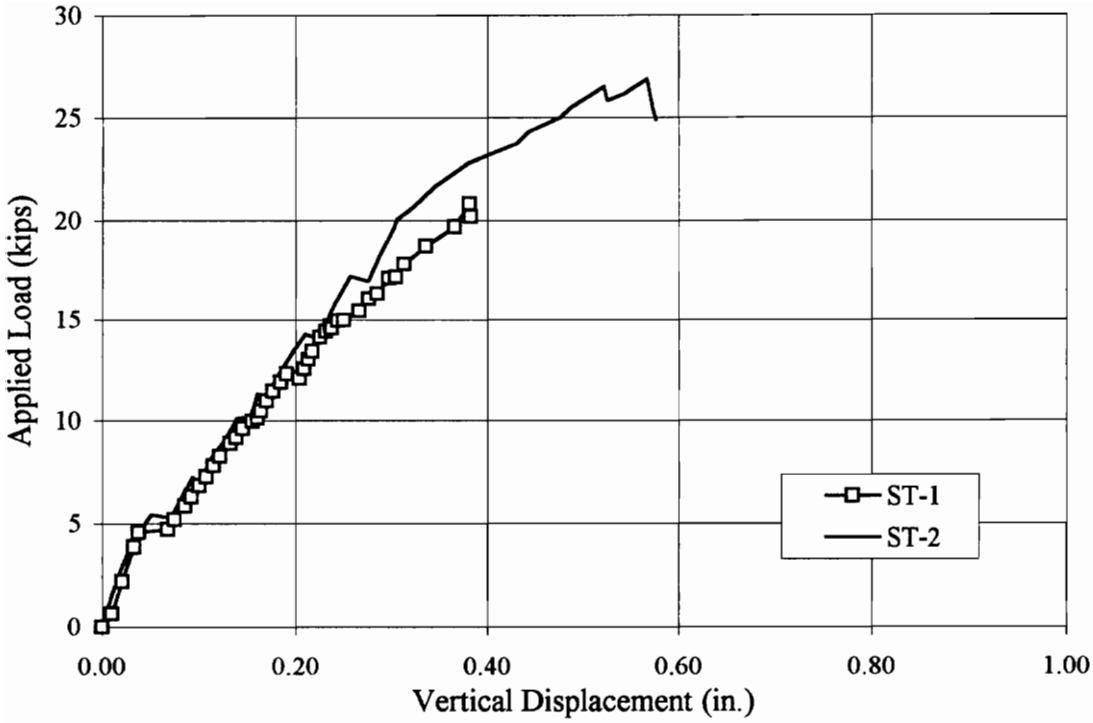

Figure 6.17 Displacement Comparison, ST-1 v. ST-2

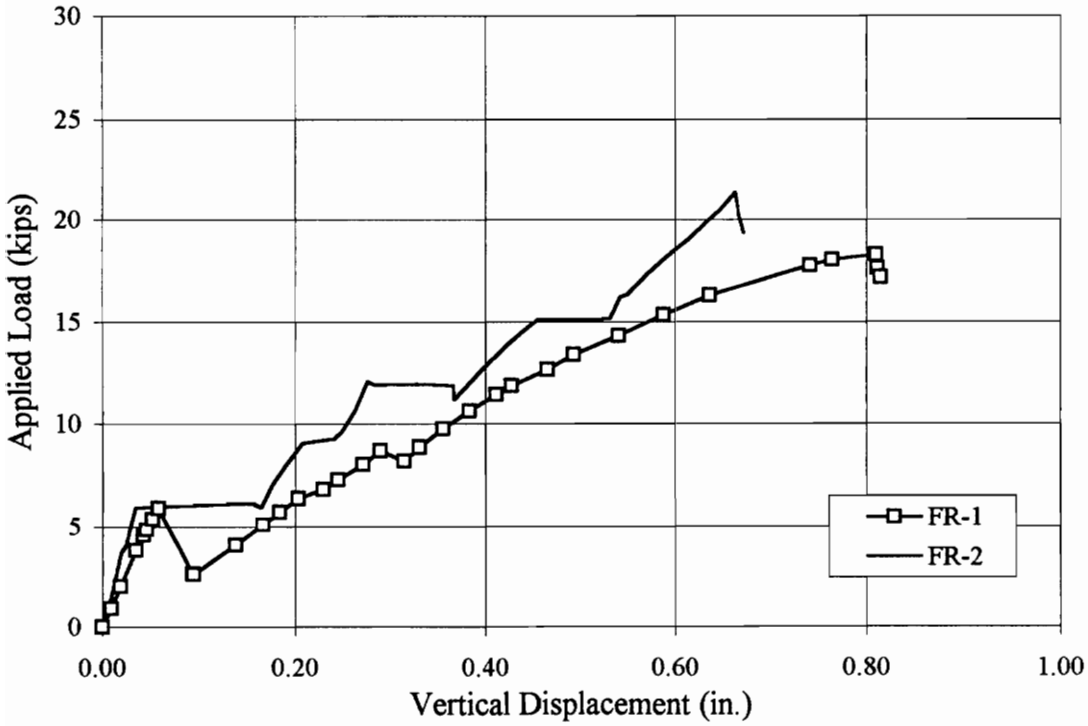

Figure 6.18 Displacement Comparison, FR-1 v. FR-2

Indicated concrete strains were significantly lower in the first test. Bar strains were only slightly less in D4-1. In both tests, the concrete began crushing first, followed by complete beam failure in shear.

6.5.4 Duragrid (6 in.) Reinforced Beams

The behavior of D6-2 was virtually identical to D6-1. The ultimate loads differed by only 300 lb, and deflection at ultimate was just 0.07 in. greater in D6-2, although that test had the lower ultimate capacity. Figure 6.20 shows a comparison between the two load-displacement behaviors.

Overall, the cyclic loading pattern had little noticeable effect on ultimate strength, stiffness or failure mechanism. The only major difference was that D6-1 developed three flexure cracks while D6-2 developed only two. Both beams experienced some concrete crushing before shear failure.

6.5.5 Multigrid Reinforced Beams

The performance of MG-1 and MG-2 were virtually the same. Ultimate load decreased by only 400 lb from MG-1 to MG-2. Displacements at ultimate were both about 0.42 in. Figure 6.21 shows the load-displacement behavior of the two tests. Both beams failed due to rupture of the reinforcing grid. No signs of concrete crushing were evident in either test. The cyclic pattern had no significant effect on the failure load or mechanism of the Multigrid reinforced beams.

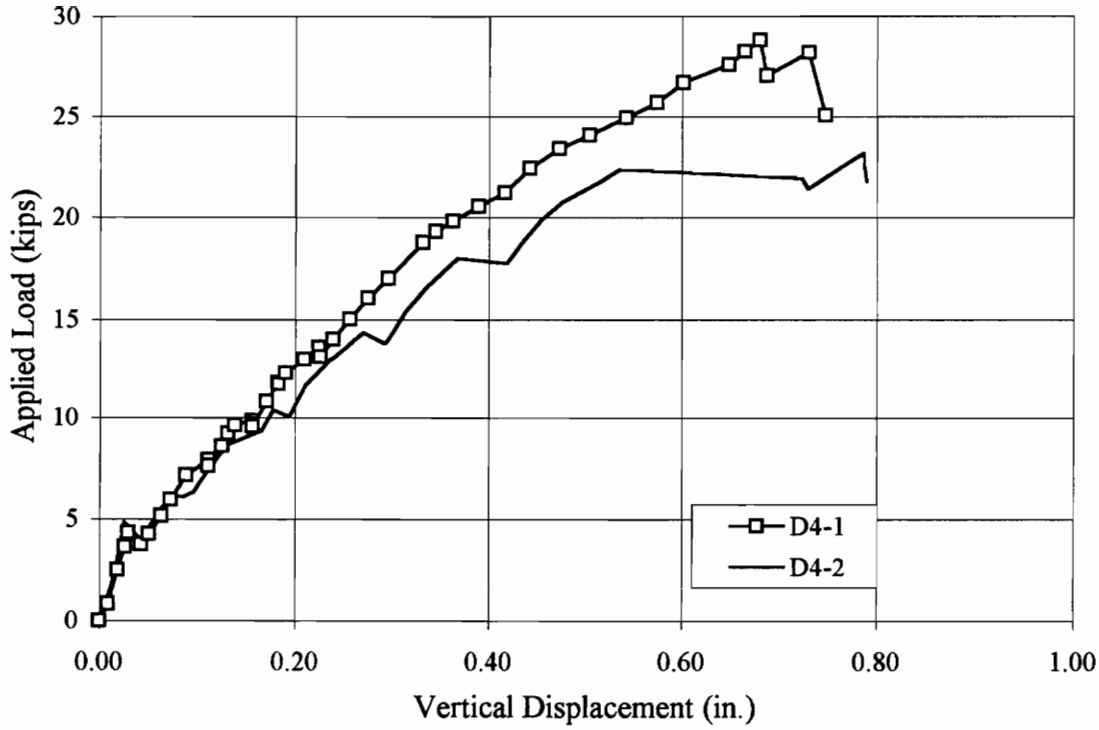

Figure 6.19 Displacement Comparison, D4-1 v. D4-2

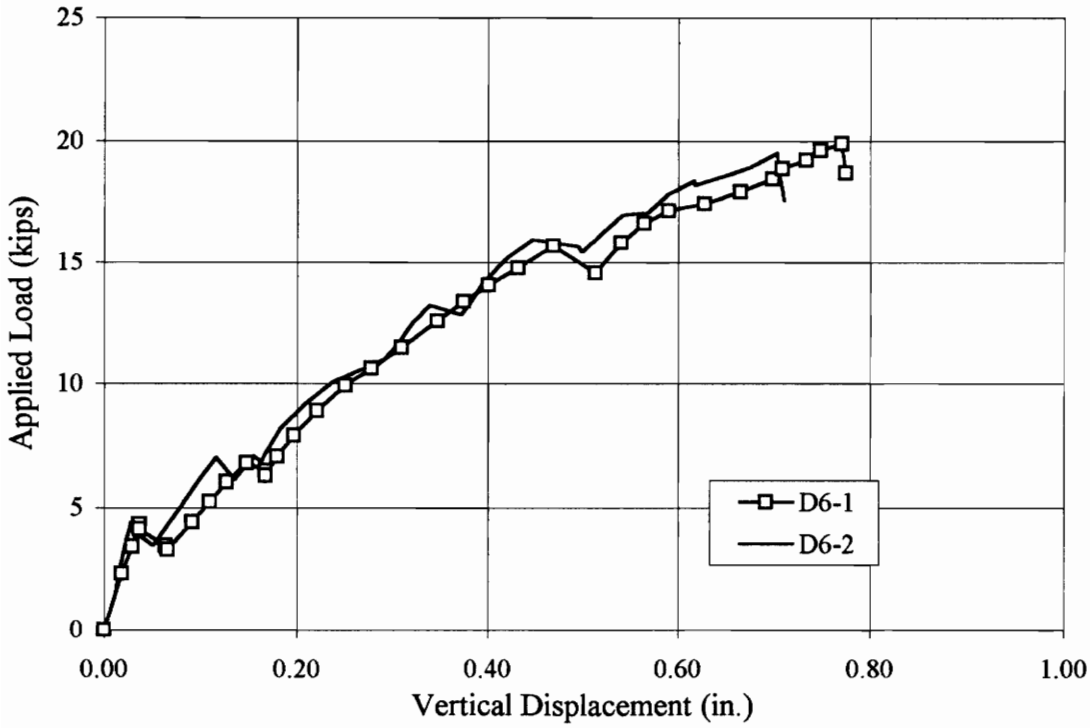

Figure 6.20 Displacement Comparison, D6-1 v. D6-2

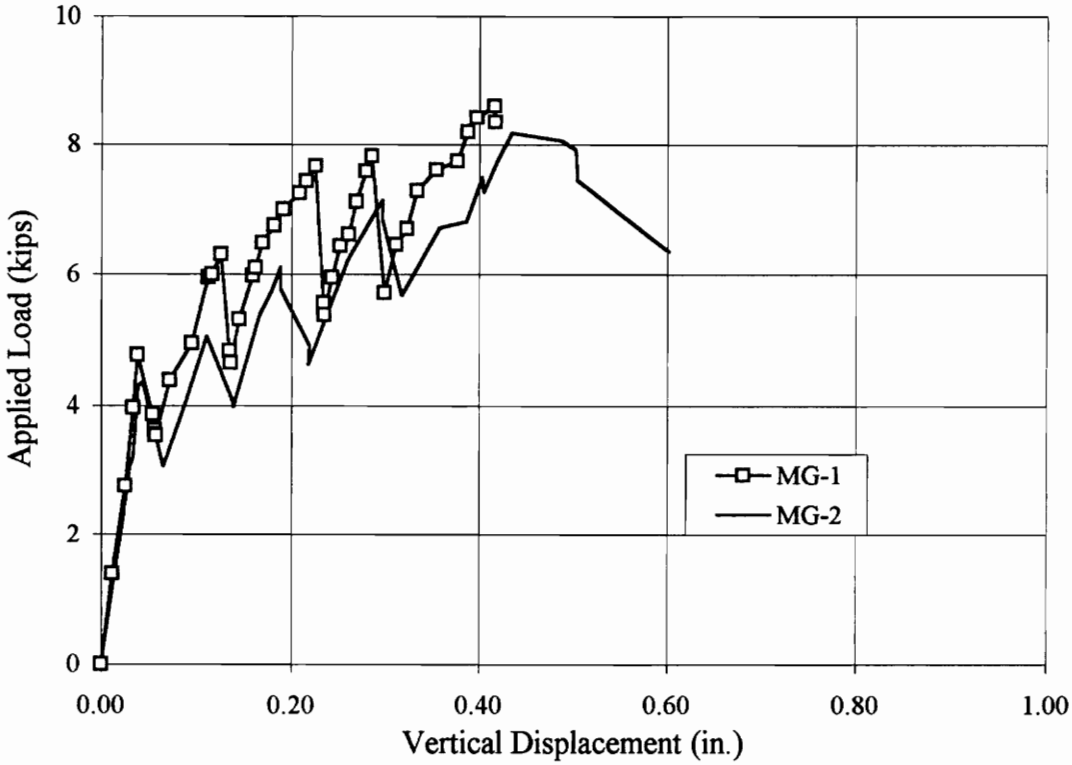

Figure 6.21 Displacement Comparison, MG-1 v. MG-2

CHAPTER 7

SUMMARY, CONCLUSIONS, AND RECOMMENDATIONS

This chapter provides a summary and conclusions based on the testing program described in Chapter 4, the test results presented in Chapter 5 and the comparisons and analysis of Chapter 6. Several recommendations for future work are presented.

7.1 Summary

This report describes the preparation, performance and results of research on the use of fiberglass-reinforced plastic materials as reinforcement for concrete. This study is a preliminary investigation into the use of such materials, and is intended to serve as a basis for future work at Virginia Polytechnic Institute and State University. The ultimate goal of the research is incorporation of fiberglass materials as reinforcement for concrete bridge decks.

The objective of research into FRP reinforcement materials is a solution to the problem of damage caused by the corrosion of steel reinforcement. Fiberglass materials are non-corroding, but their use as reinforcing for concrete requires additional research. Problems include lack of ductility, cost and a shortage of design guidelines.

For this project, ten concrete beams were constructed and tested. Steel bars and four fiberglass reinforcement arrangements were used, with two test beams for each reinforcement material. The simple-span beams were tested in bending to failure. One set of tests was loaded monotonically, the second set cyclically.

Prediction calculations were made based on both current reinforced concrete theory and on the work of others. Experimental results were analyzed and compared on several levels.

7.2 Conclusions

Based on the results of this study, the following conclusions are drawn:

(1) This study confirms that steel reinforcing bars set the standard with respect to providing ductility and stiffness for reinforced concrete. The steel bars created the stiffest beams with the least amount of reinforcing. Steel's widespread use and acceptance, along with proven design methods, create strong barriers against its being completely replaced as the primary reinforcement for concrete. The only apparent weakness of steel is its susceptibility to corrosion damage.

(2) Fiberglass reinforcing materials, primarily because of their low elastic modulus, should not be substituted for steel on a one-to-one ratio, as demonstrated by a comparison of the FRP bar and steel bar reinforced beams. To achieve the stiffness of steel reinforcement, members need to be over-reinforced with FRP, which makes concrete compressive strength the limiting factor.

(3) The pultruded fiberglass gratings have potential for use as concrete reinforcement. They were able to provide the same strength as the steel bar reinforcement, although deflections were typically larger. The gratings offer savings in construction cost, as they provide reinforcement in both directions, eliminating the need for field cutting and tying of bars.

(4) The Multigrid adds little strength to the concrete beams, with ultimate loads only slightly above the first cracking load. Due to the Multigrid's poor performance as a reinforcing and its small grid openings, which make concrete placement difficult, this material is not recommended for future investigation.

(5) The cyclic loading pattern of the second series of tests had no significant effect on the performance of the reinforcements. Ultimate load, load-deflection behavior and failure mechanism were essentially the same for each pair of tests.

(6) The span of the test beams was too short to produce a flexural failure in all cases. Shear failure tended to control, prohibiting examination of the true flexure capacity of the reinforcing materials.

(7) In general, the observations of others were confirmed in these tests. Similar trends in behavior were noticed, especially crack patterns and locations, deflections and failure modes.

7.3 Recommendations

Based on the results and the experience gained during this study, the following recommendations are made for future work in this area:

(1) If the focus of future investigation is the performance of fiberglass-reinforced plastic materials as the top reinforcing in bridge decks, effort should be placed on modeling that situation accurately. The ultimate goal of research should be the construction and testing of a full scale, multi-span slab with double reinforcing.

(2) A larger number of tests need to be performed in order to make statistically sound judgments and conclusions. Focusing on one or two reinforcing materials would make this more feasible.

(3) Further investigations should concentrate on using Duragrid or a similar pultruded grating. Of all the materials tested, it appears that the Duragrid with 4.5 in. bar spacing provided the best alternative to steel, based on stiffness and strength. Further

work needs to be done to find the optimal bar spacing. Ultimately, to facilitate acceptance by the construction industry, design equations need to be developed so a designer can select any grid that fits the design requirements.

(4) Further examination of the behavior of fiberglass reinforcement under fatigue or dynamic loading is needed. Loading histories should be developed which better simulate traffic loads on a bridge deck.

(5) It has been mentioned that the gratings provide reinforcing in both directions; however no examination has been done on the performance of the transverse bars as reinforcement. To verify the gratings' capabilities, transverse direction testing of slabs reinforced with gratings is necessary.

REFERENCES

ACI Standard for Bridge Deck Construction, ACI 345-82 (1982). American Concrete Institute, Detroit, MI.

ACI Building Code Requirements for Reinforced Concrete, ACI 318-89 (1989). American Concrete Institute, Detroit, MI.

ASTM D3916, "Standard Test Method for Tensile Properties of Pultruded Glass-Fiber-Reinforced Plastic Rod."

ASTM A370, "Standard Test Methods and Definitions for Mechanical Testing of Steel Products."

Bank, L.C. and Mosallam, A.S. (1991). "Experimental Study of FRP Grating Reinforced Concrete Slabs," *Advanced Composite Materials in Civil Engineering Structures*, ASCE, pp. 111-122.

Bank, L., Xi, Z. and Munley, E. (1992). "Tests of Full-Size Pultruded FRP Grating Reinforced Concrete Bridge Decks," *Proceedings of the Materials Engineering Congress*, ASCE, pp. 618-631.

Bank, L. and Xi, Z. (1993). "Pultruded FRP Gratings as a Reinforcement for Concrete," *Proceedings of the 48th Annual Conference,* Composites Institute and Society of the Plastics Industry, Inc.

Bank, L. and Xi, Z. (1993). "Pultruded FRP Grating Reinforced Concrete Slabs," *Fiber-Reinforced-Plastic Reinforcement for Concrete Structures - International Symposium, 1993.* ACI SP-138, pp. 561-583.

Bedard, C. (1992). "Composite Reinforcing Bars: Assessing Their Use in Construction," *Concrete International*, Vol. 14, No. 1, pp. 55-59.

Collins, M.P. and Mitchell, D. (1991). "RESPONSE computer program," *Prestressed Concrete Structures*, Prentice-Hall.

"Deck Built Minus Top Steel." (1994). *Engineering News Record,* Vol. 232, No. 25, pp. 18.

EXTREN Design Manual. (1989). Morrison Molded Fiberglass Company, Bristol, VA.

GangaRao, H.V.S. and Faza, S.S. (1991). "Bending and Bond Behavior and Design of Concrete Beams Reinforced with Fiber Reinforced Plastic Rebars," West Virginia University, Constructed Facilities Center.

Goodspeed, C., Schmeckpeper, E., Henry, R., Yost, J. and Gross, T. (1990). "Fiber Reinforced Plastic Grids for the Structural Reinforcement of Concrete," *Procedings of the First Materials Engineering Congress*, ASCE, pp.593-604.

Goodspeed, C., Schmeckpeper, E., Gross, T., Henry, R., Yost, J. and Zhang, M. (1991). "Cyclical Testing of Concrete Beams Reinforced with Fiber Reinforced Plastic Grids," *Advanced Composite Materials in Civil Engineering Structures*, ASCE, pp. 278-287.

Kodiak Fiberglass-Reinforced Plastic Rebar. (1988). International Grating, Inc., Houston, TX.

Fiberglass Grating Catalog. (1993). McNichols Co., Tampa, FL.

Nawy, E.G., Neuwerth, A.M. and Phillips, C. (1971). "Behavior of Fiber Glass Reinforced Concrete Beams," *Journal of the Structural Division*, ASCE, Vol. 97, No. ST9, pp. 2203-2215.

Nawy, E.G. and Neuwerth, A.M. (1977). "Fiberglass Reinforced Concrete Slabs and Beams," *Journal of the Structural Division*, ASCE, Vol. 103, No. ST2, pp. 421-440.

Porter, M.L. and Barnes, B.A. (1991). "Tensile Testing of Glass Fiber Composite Rod," *Advanced Composite Materials in Civil Engineering Structures*, ASCE, pp. 123-131.

Tarricone, P. (1993). "Plastic Potential," *Civil Engineering*, Vol. 63, No. 8, pp. 62-63.

APPENDIX A

REINFORCEMENT CALIBRATION DATA

The results of the individual reinforcement calibrations are presented in this section. For each material, a summary is provided which shows the important results of the regression analyses of the calibration data. Following the summary, the actual data from the calibration exercises is provided.

The two important regression analysis results are the slope of the load-strain plot and the "R-squared" value for that plot. The slope is the slope of the best-fit line to the data, while the R-squared value indicates how close to that line the data is. An R-squared value of 1.0 indicates that the data exactly fits the line; values of 0.99 are considered acceptable.

Descriptions of the calibration procedures and analysis of the results are given in Chapter 4.

Also included is a stress-strain curve for the steel reinforcing bars, as recorded from the tensile tests of those bars (Chapter 3).

A1 Steel Bars

A1.1 Tensile Test Stress-strain Curve

0.2% Offset Yield = 92 ksi

Ultimate Strength = 147 ksi

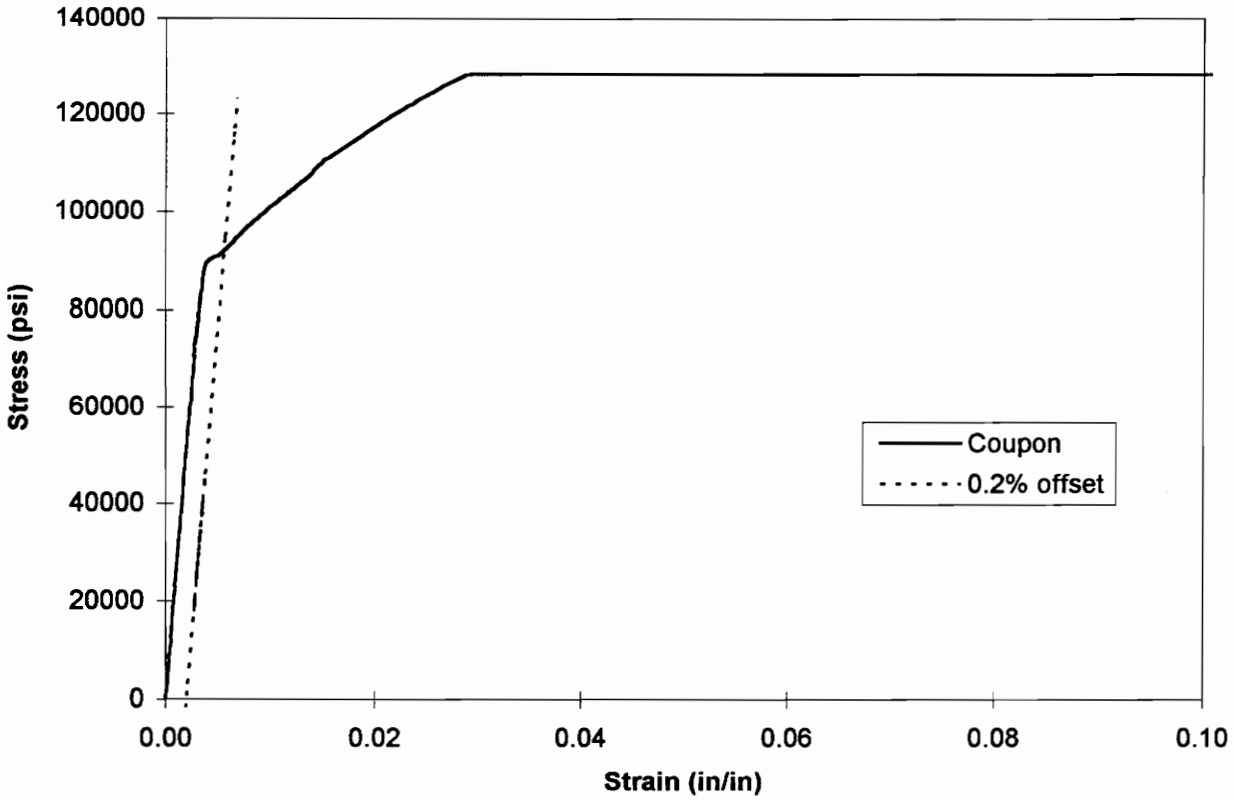

A1.2 Summary

Slopes of Load-Strain Plots

Bar #	Gage A	Gage B
S1	5.031	4.843
S2	5.255	5.083
S3	5.335	4.489
S4	4.837	5.236

R-squared Values

Bar #	Gage A	Gage B
S1	0.9990	0.9997
S2	0.9996	0.9976
S3	0.9997	0.9977
S4	0.9994	0.9998

A1.3 Steel Bar #1

Bar label: S1
Date: 9/14/94
Load to: 5000 lbs

Calibration Data

	Gage A	Gage B
Load (#)	Microstrain	Microstrain
0	0	0
510	121	118
1050	214	218
1660	334	342
2150	433	443
2630	522	541
2990	593	615
3490	689	721
4000	790	826
4500	889	931
5020	990	1041
4080	807	843
3540	703	732
3010	601	621
2500	503	515
1990	403	406
1500	310	305
1000	214	200
500	117	94
0	17	-15

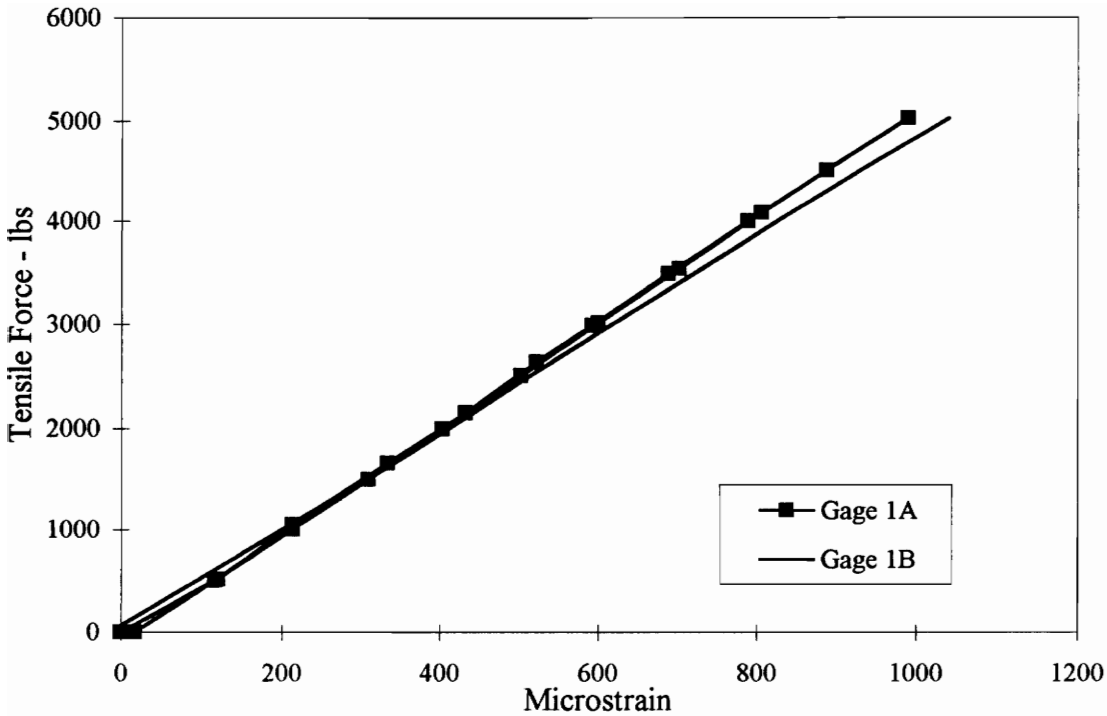

Tensile Force v. Strain, Calibration of Steel Bar #1

Regression Analysis Results

Bar S1	Slope	R-squared
Gage A	5.031	0.9990
Gage B	4.843	0.9997

A1.4 Steel Bar #2

Bar label: S2
Date: 9/17/94
Load to: 5000 lbs

Calibration Data

	Gage A	Gage B
Load (#)	Microstrain	Microstrain
0	0	0
1540	277	290
1580	289	310
2280	437	458
3060	583	604
3580	685	705
4060	772	793
4580	872	894
5030	960	982
4600	878	899
4000	762	783
3470	661	682
3000	570	592
2470	470	492
1970	374	400
1470	278	307
960	178	212
500	91	130
0	-10	41

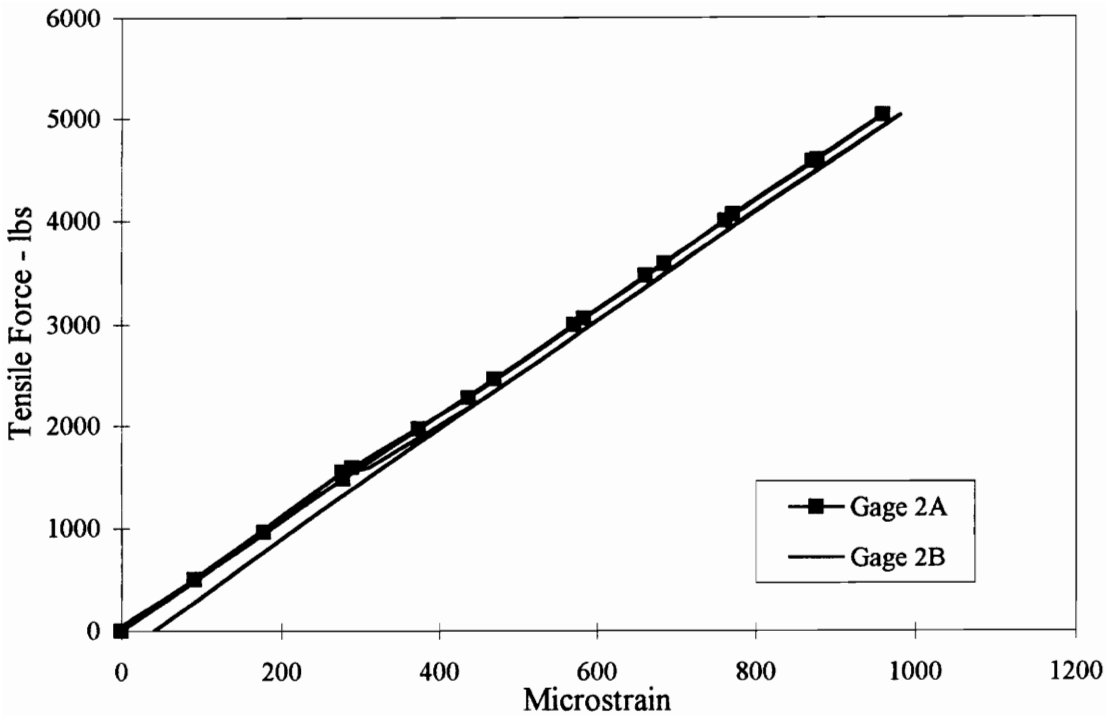

Tensile Force v. Strain, Calibration of Steel Bar #2

Regression Analysis Results

Bar S2	Slope	R-squared
Gage A	5.255	0.9996
Gage B	5.083	0.9976

A1.5 Steel Bar #3

Bar label: S3
Date: 9/16/94
Load to: 5000 lbs

Calibration Data

	Gage A	Gage B
Load (#)	Microstrain	Microstrain
0	0	0
470	76	128
1880	344	434
2770	514	625
3550	662	789
4060	762	898
4580	863	1007
5010	946	1096
4520	852	995
4010	755	890
3520	659	785
3000	560	676
2460	458	563
1970	363	457
1470	268	351
900	163	228
430	80	122
50	7	40
0	0	30

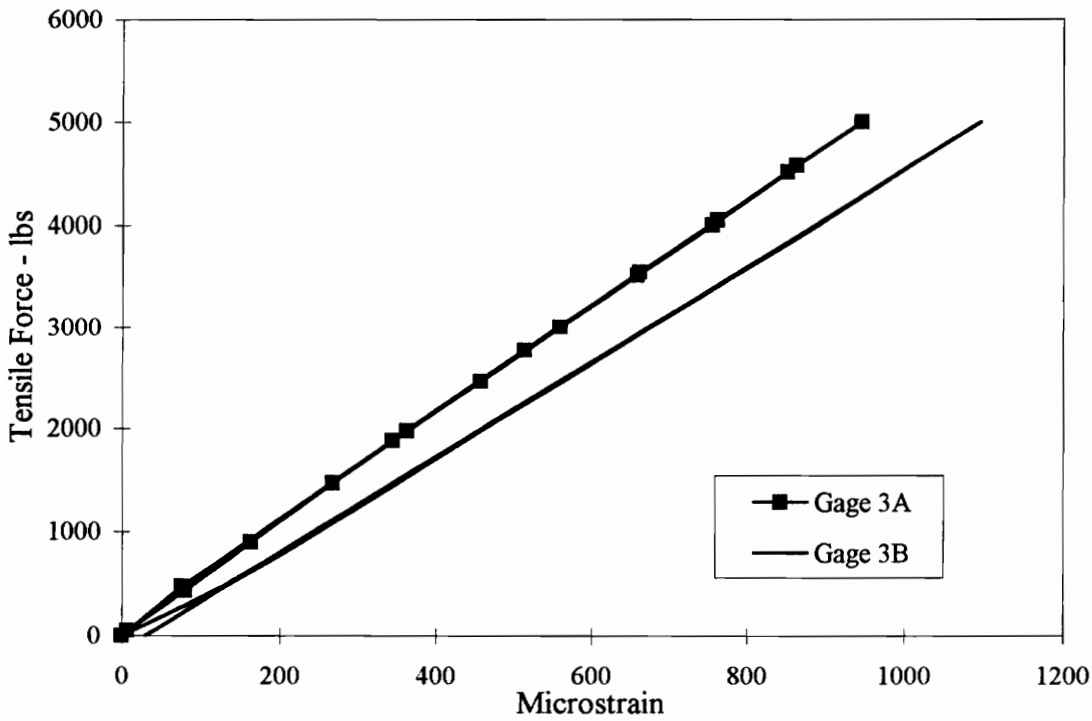

Tensile Force v. Strain, Calibration of Steel Bar #3

Regression Analysis Results

Bar S3	Slope	R-squared
Gage A	5.335	0.9997
Gage B	4.489	0.9977

A1.6 Steel Bar #4

Bar label: S4
Date: 9/16/94
Load to: 5000 lbs

Calibration Data

	Gage A	Gage B
Load (#)	Microstrain	Microstrain
0	0	0
750	160	140
1200	254	222
1500	315	283
2750	569	523
3440	708	655
4040	831	772
4600	945	883
4970	1020	955
4530	931	867
4020	830	770
3470	720	661
2970	620	566
2470	518	470
2000	422	378
1480	317	277
960	211	177
480	114	83
0	16	-10

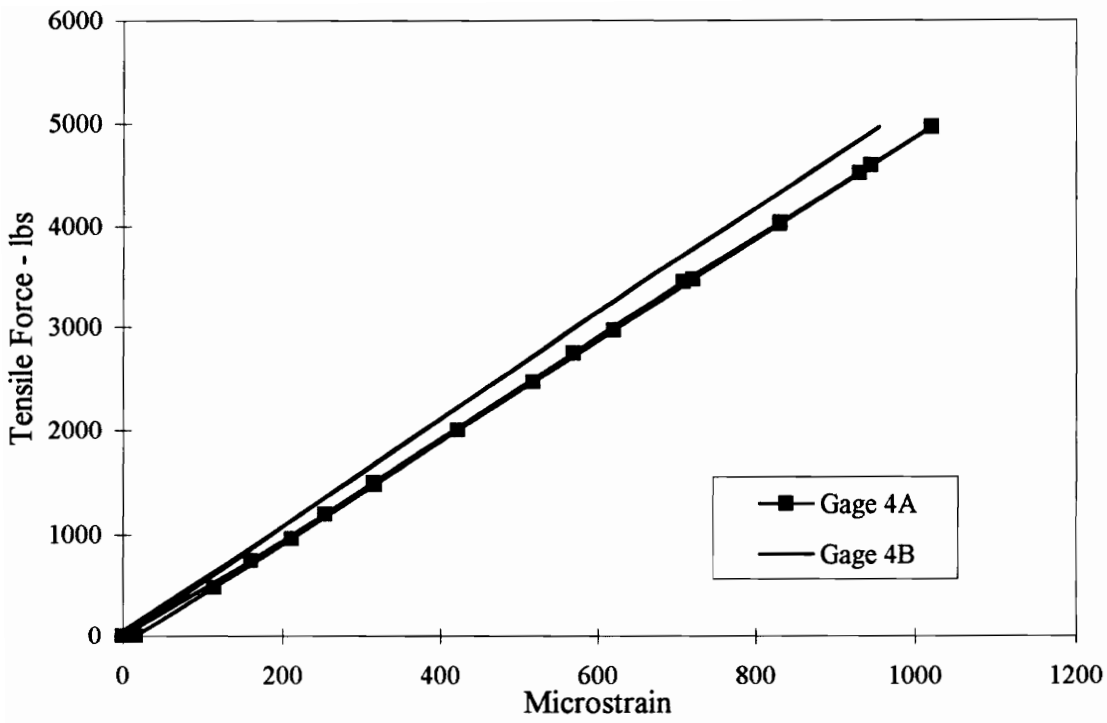

Tensile Force v. Strain, Calibration of Steel Bar #4

Regression Analysis Results

Bar S4	Slope	R-squared
Gage A	4.837	0.9994
Gage B	5.236	0.9998

A2 FRP Bars

A2.1 Summary

Slopes of Load-Strain Plots

Bar #	Gage A	Gage B
F1	0.690	n/a
F2	0.920	0.944
F3	1.321	n/a
F4	1.015	0.923

R-squared Values

Bar #	Gage A	Gage B
F1	0.9796	n/a
F2	0.9969	0.9977
F3	0.9931	n/a
F4	0.9975	0.9915

A2.2 FRP Bar #1

Bar label: F1
Date: 11/17/94
Load to: 5000 lbs
Gages: Wired in series

Calibration Data

Load (#)	Microstrain
0	0
1260	2420
2090	3830
3170	5410
4170	6420
5140	7095
3960	5770
2870	4410
1920	3085
860	1520
0	65

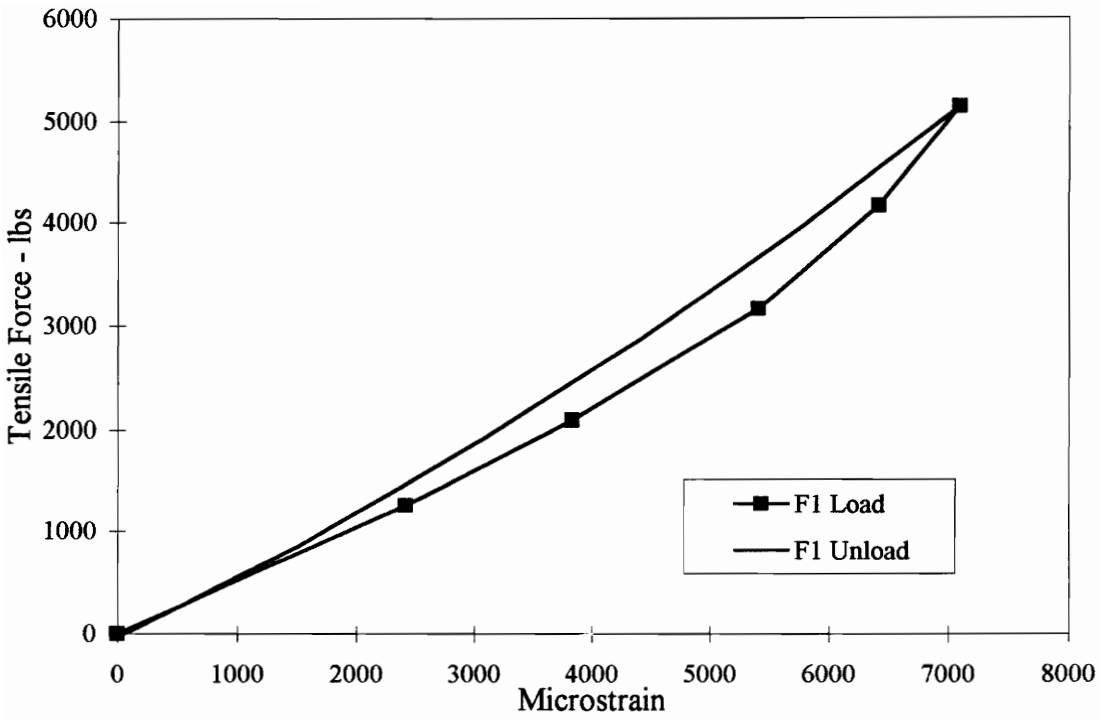

Tensile Force v. Strain, Calibration of FRP Bar #1

Regression Analysis Results

	Slope	R-squared
Bar F1	0.690	0.9796

A2.3 FRP Bar #2

Bar label: F2
Date: 10/24/94
Load to: 10,000 lbs
Gages: Wired individually

Calibration Data

	Gage A	Gage B
Load (#)	Microstrain	Microstrain
0	0	0
2250	2448	2204
3140	3414	3150
4050	4405	4105
5050	5518	5187
6000	6600	6190
7050	7822	7346
8180	9163	8590
9000	10190	9600
9050	9530	9545
8000	8437	8497
6850	7220	7353
5880	6214	6365
5000	5300	5469
4000	4290	4450
2970	3195	3325
2020	2236	2320
1100	1280	1340
0	34	140

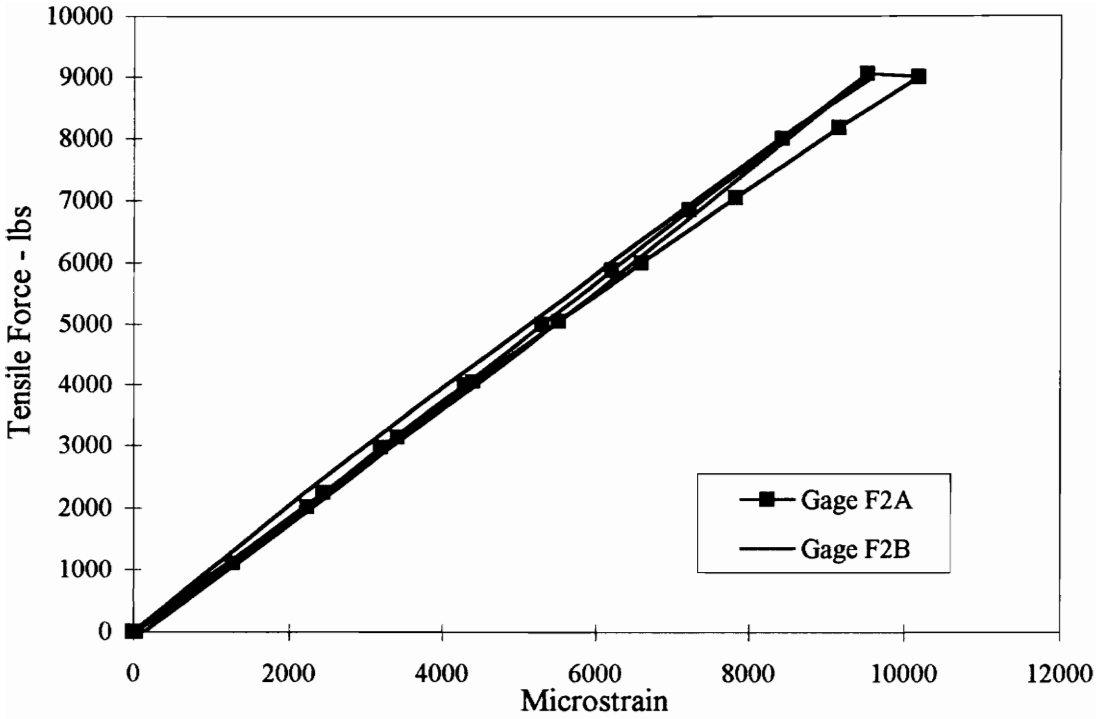

Tensile Force v. Strain, Calibration of FRP Bar #2

Regression Analysis Results

Bar F2	Slope	R-squared
Gage A	0.9202	0.9969
Gage B	0.944	0.9977

A2.4 FRP Bar #3

Bar label: F3
Date: 11/13/94
Load to: 5000 lbs
Gages: Wired in series

Calibration Data

Load (#)	Microstrain
0	0
1370	1075
2160	1640
3180	2385
4150	3085
5090	3815
3940	2810
2890	1930
1900	1180
920	520
0	-77

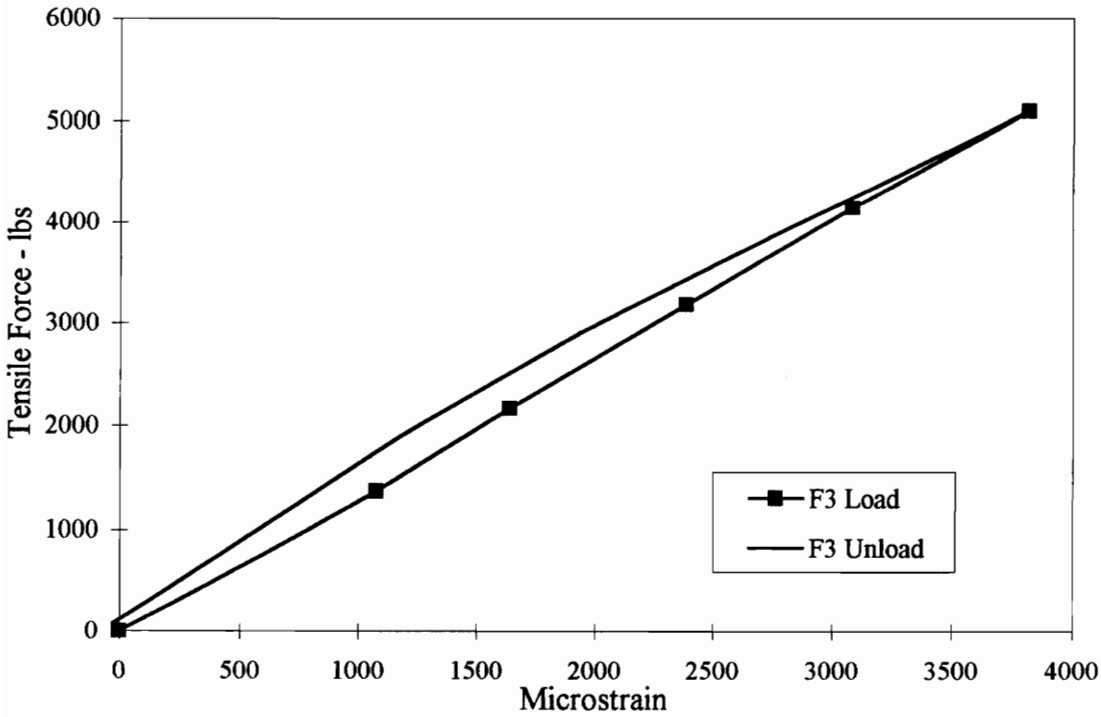

Tensile Force v. Strain, Calibration of FRP Bar #3

Regression Analysis Results

	Slope	R-squared
Bar F3	1.321	0.9931

A2.5 FRP Bar #4

Bar label: F4
Date: 10/16/94
Load to: 10,000 lbs
Gages: Wired individually

Calibration Data

	Gage A	Gage B
Load (#)	Microstrain	Microstrain
0	0	0
2150	2095	2069
3150	3042	3100
4150	3985	4135
5100	4884	5121
6050	5807	6156
7040	6787	7287
8100	7843	8505
9080	8869	9705
10000	9783	10851
9000	8880	9892
7920	7854	8785
6900	6904	7740
5900	5955	6690
4950	5066	5700
4020	4178	4710
2980	3156	3556
1950	2184	2460
950	1202	1384
60	265	489
0	145	426

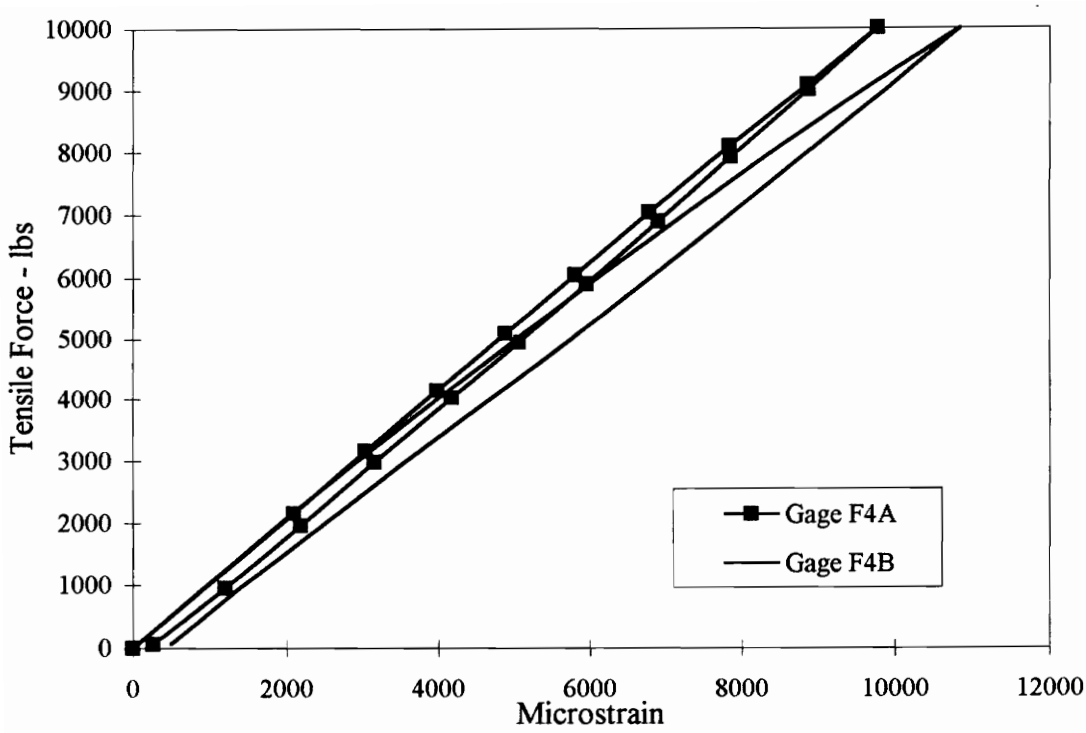

Tensile Force v. Strain, Calibration of FRP Bar #4

Regression Analysis Results

Bar F4	Slope	R-squared
Gage A	1.015	0.9976
Gage B	0.923	0.9915

A3 Duragrid Grating

A3.1 Summary

The same grating bar was used for all of the calibration experiments. Trials #1 and #2 had the two gages wired individually, while trials #3 and #4 had the gages wired in series.

Slopes of Load-Strain Plots

Trial #	Gage A	Gage B
1	1.795	1.518
2	1.787	1.527
3	1.646	n/a
4	1.646	n/a
Average slope:		1.65

R-squared Values

Trial #	Gage A	Gage B
1	0.9999	0.9988
2	0.9998	0.9996
3	0.9994	n/a
4	0.9999	n/a

A3.2 Duragrid Trial #1

Date: 11/2/94
Pull to: 4000 lb
Gages: Wired individually

Calibration Data

Load (lb)	Gage A Microstrain	Gage B Microstrain
0	0	0
750	406	512
2510	1405	1646
3420	1908	2242
3980	2220	2613
3000	1673	1974
1920	1065	1281
900	478	629
0	5	83

Gage A on top flange
Gage B on bottom flange

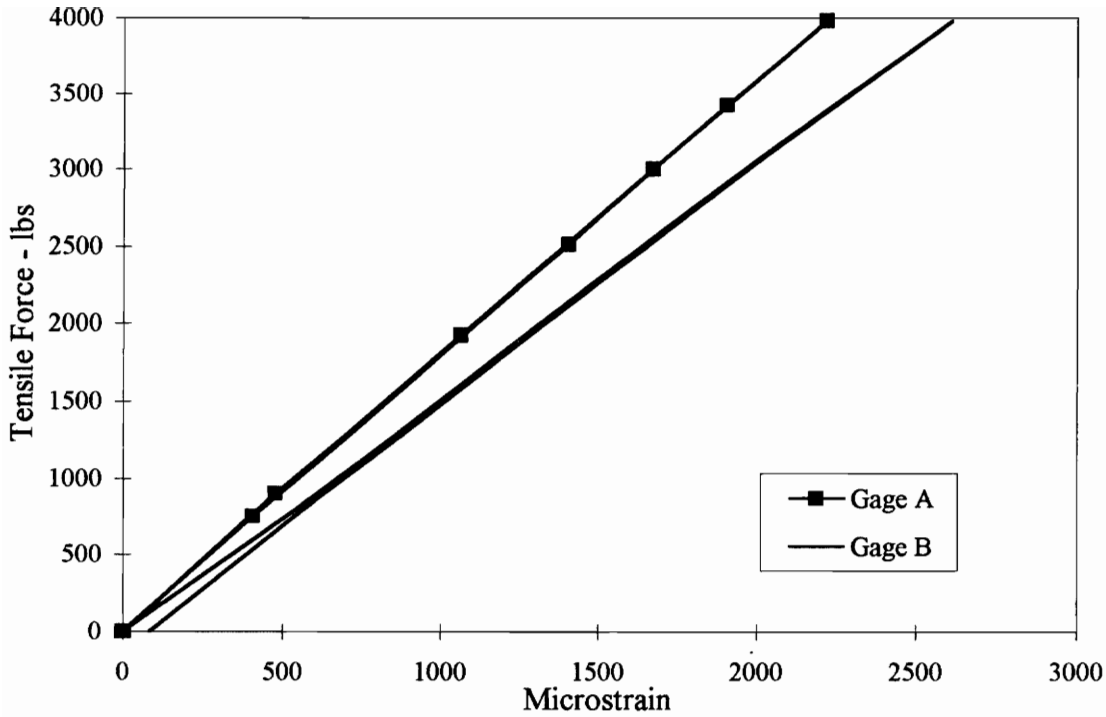

Tensile Force v. Strain, Calibration of Duragrid, Trial #1

Regression Analysis Results

Trial 1	Slope	R-squared
Gage A	1.795	0.9999
Gage B	1.518	0.9988

A3.3 Duragrid Trial #2

Date: 11/2/94
Pull to: 4000 lb
Gages: Wired individually

Calibration Data

Load (lb)	Gage A Microstrain	Gage B Microstrain
0	0	0
770	420	522
1750	967	1150
2610	1455	1708
3560	1996	2327
4000	2244	2608
3010	1693	1967
1920	1071	1266
900	486	619
0	14	45

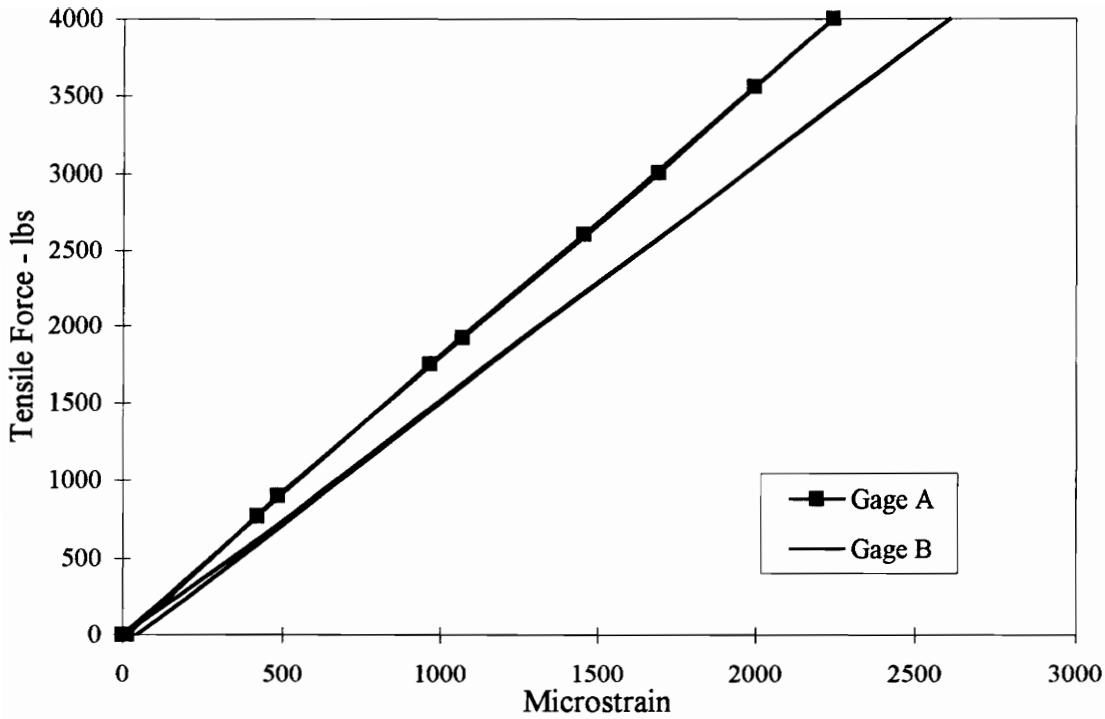

Tensile Force v. Strain, Calibration of Duragrid, Trial #2

Regression Analysis Results

Trial 2	Slope	R-squared
Gage A	1.787	0.9998
Gage B	1.527	0.9996

A3.4 Duragrid Trial #3

Date: 11/10/94
Pull to: 4000 lb
Gages: Wired in series

Calibration Data

Load (#)	Microstrain
0	0
1460	918
1510	960
3970	2446
3190	1970
1930	1232
910	617
0	61

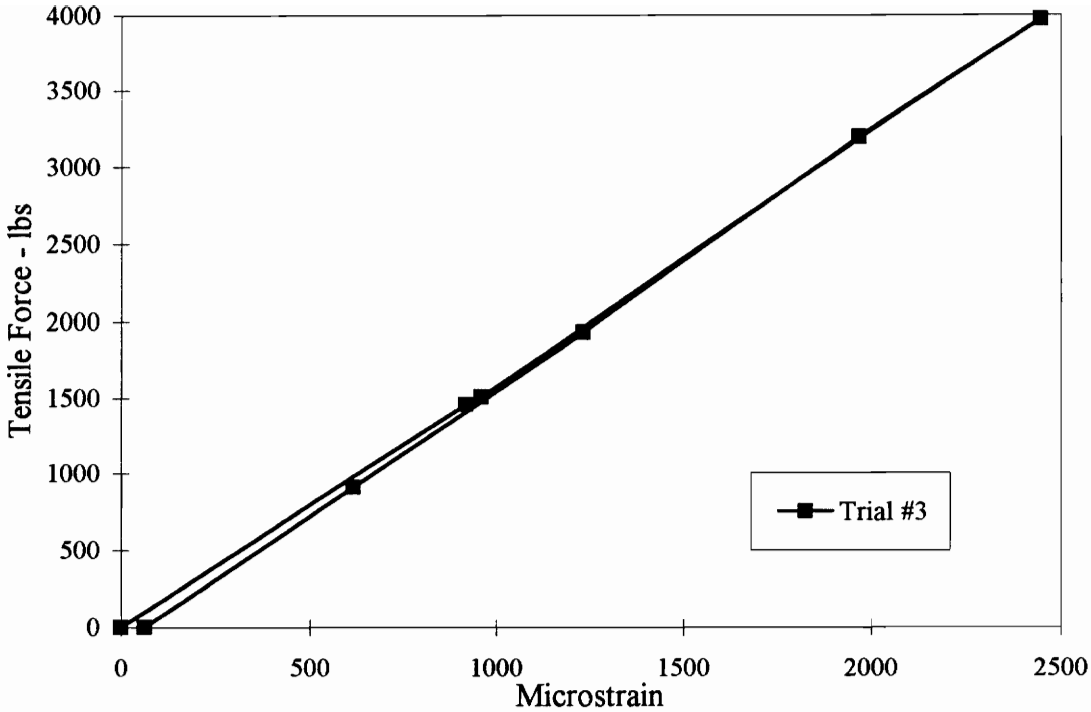

Tensile Force v. Strain, Calibration of Duragrid, Trial #3

Regression Analysis Results

	Slope	R-squared
Trial 3	1.646	0.9994

A3.5 Duragrid Trial #4

Date: 11/10/94
Pull to: 4000 lb
Gages: Wired in series

Calibration Data

Load (#)	Microstrain
0	0
1110	680
2050	1243
3150	1920
4030	2452
2980	1806
1980	1218
870	542
0	24

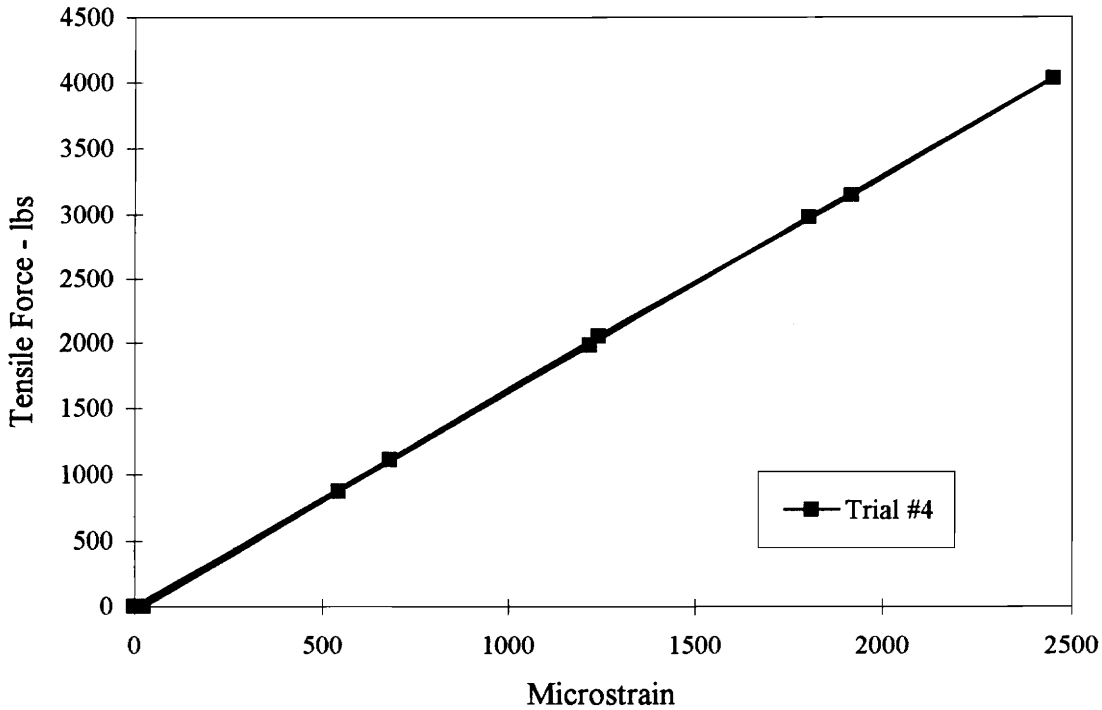

Tensile Force v. Strain, Calibration of Duragrid, Trial #4

Regression Analysis Results

	Slope	R-squared
Trial 3	1.654	0.9999

A4 Multigrid Grating

A4.1 Summary

The same grating bar was used for all of the calibration experiments. Trial #1 had the gages wired individually, while trial #2 had the gages wired in series.

Slopes of Load-Strain Plots

Trial #	Gage A	Gage B
1	0.203	n/a
2	0.214	0.196

R-squared Values

Trial #	Gage A	Gage B
1	0.9981	n/a
2	0.9940	0.9918

A4.2 Multigrid Trial #1

Date: 11/2/94
Pull to: 700 lb
Gages: Wired individually

Calibration Data

Load (lb)	Gage A Microstrain	Gage B Microstrain
0	0	0
220	1151	1100
520	2550	2580
700	3450	3730
630	3115	3370
510	2604	2800
370	1960	2085
240	1355	1440
100	760	750
0	318	247

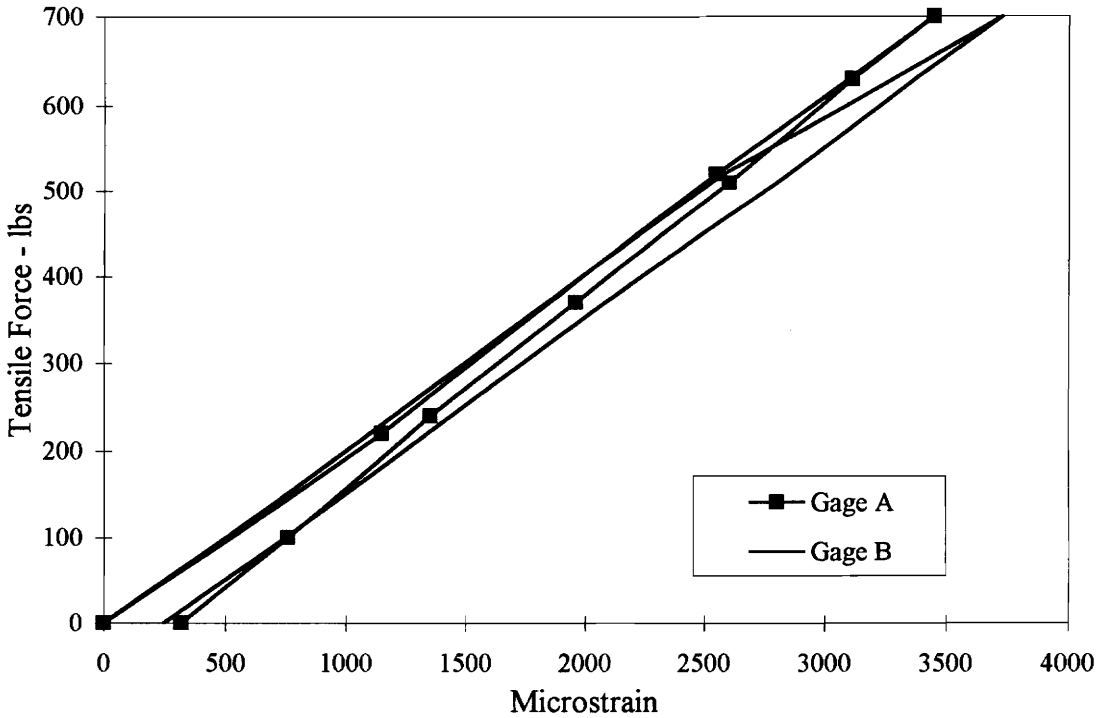

Tensile Force v. Strain, Calibration of Multigrid, Trial #1

Regression Analysis Results

Trial 1	Slope	R-squared
Gage A	0.214	0.9940
Gage B	0.196	0.9918

A4.3 Multigrid Trial #2

Date: 11/13/94
Pull to: 500 lb
Gages: Wired in series

Calibration Data

Load (lb)	Microstrain
0	0
150	830
300	1545
490	2452
440	2240
250	1350
150	830
0	110

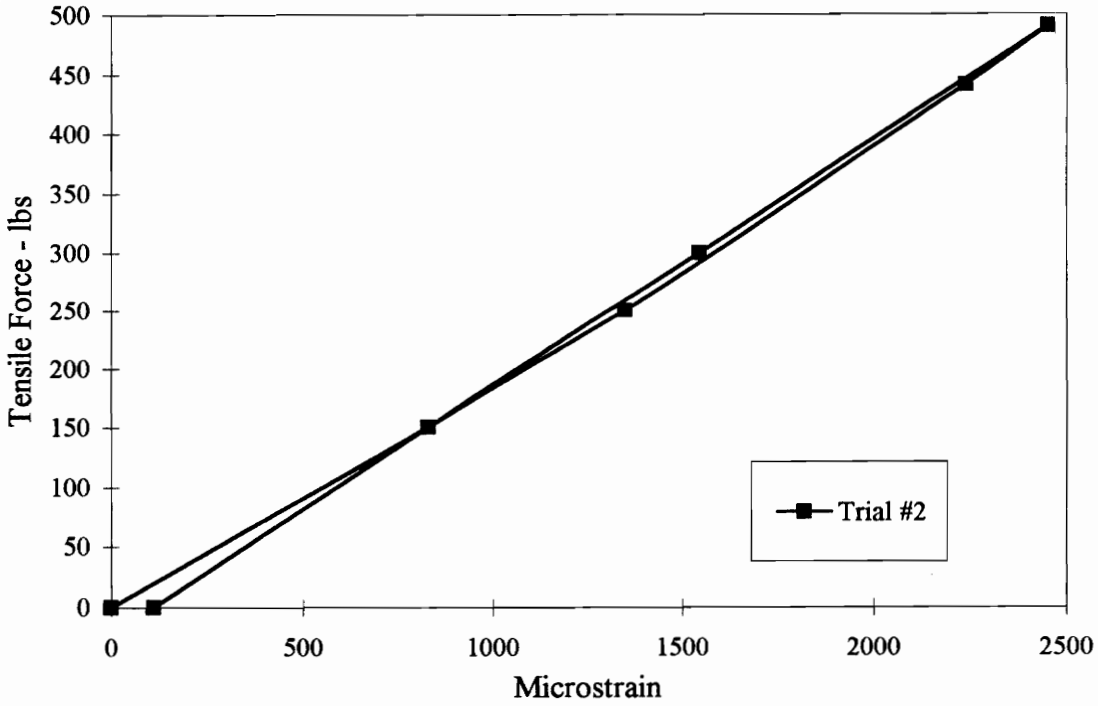

Tensile Force v. Strain, Calibration of Multigrid, Trial #2

Regression Analysis Results

	Slope	R-squared
Trial #2	0.203	0.9981

VITA

Peter A. Allen, son of Roy and Jerolyn Allen, was born on September 29, 1971, in Greenville, South Carolina. He grew up in Scotia, New York, graduating from Scotia-Glenville High School in 1989. He graduated with a Bachelor of Science in Civil Engineering from Lafayette College, Easton, Pennsylvania, in May, 1993. In August, 1993, he enrolled in the graduate program in the Structures Division of the Via Department of Civil Engineering at Virginia Polytechnic Institute and State University.